POLITECNICO DI TORINO

Master's Degree in

AUTOMOTIVE ENGINEERING

Master's Degree Thesis

A.Y. 2023/2024

The modeling and simulation on electrothermal characteristics of electric vehicle lithium-ion battery

Supervisors

Prof. Papurello Davide

Candidate

Benbo Zhang

July 2024

Index

Abstract

The rising trend in global average temperatures has become difficult to ignore. Therefore, many countries around the world have proposed various plans to deal with the unrestrained use of fossil fuels and formulated roadmaps to wean themselves off fossil energy. In the field of automotive production design, many companies have begun to focus on the use of renewable energy. Therefore, the presence of electric vehicles in the market has gradually increased in recent years. Usually, the energy of electric vehicles comes from the chemical energy in the battery, so the battery management system (BMS) effectively evaluates and monitors the battery, which is the key to ensuring the safe and smooth running of electric vehicles. However, the car will face various complex conditions on the actual road, and the parameters of the battery such as voltage, soc, current and so on show nonlinear changes. Therefore, it is urgent to establish a mathematical model in BMS to reflect the dynamic characteristics of batteries under complex conditions accurately. This thesis uses the experimental data of an 18650 ternary Li-ion battery to build an electrothermal coupling model, whose parameters can be updated according to the soc, current, and temperature, so as to accurately reflect the voltage and temperature variation of the battery, and improve the ability of BMS to evaluate and predict the state of the battery. The main contents are as follows: Firstly, the working principle of the battery is analyzed, and the second-order RC equivalent circuit model is selected as the basis of the electrical characteristic model. Using the experimental data in the HPPC test, the model's parameters are identified based on the least squares algorithm. After building the model in Matlab Simulink, error verification was performed to confirm the accuracy of the electrical characteristic model. Then, the experimental data of lithium batteries, which are the same type and have similar specifications, are used to verify the migration of the model parameters, and prove that the model parameters have good adaptability. The Bernadi heat generation model and lumped parameter model based on the equivalence principle are used as the basis of the battery thermal model. Finally, the two models are fused into an electrothermal coupling model, and the model architecture is established on Matlab. In the end, a simple longitudinal motion model of the vehicle is established according to the kinematics principle of the vehicle, and the current curve of the automotive lithium battery pack under specific driving conditions (NEDC, WLTC, etc.) is obtained. Using this as the current command input of the electrothermal coupling model, the terminal voltage, soc, temperature, and other data for a single lithium battery are collected to study the electrothermal characteristics of the lithium battery. This study

will help us to build a more powerful BMS system in the future.

Nomenclature

BMS	Battery Management System
CC-CV	Constant current and constant voltage discharge process
DST	Dynamic stress test
HPPC	Hybrid Pulse Power Characterization test
LFP	Lithium Iron Phosphate
NCA	Nickel Cobalt Aluminium
NCM	Nickel Manganese Cobalt Oxide
NEDC	New European Driving Cycle
OCV	open-circuit voltage
PNGV	The Partnership for a New Generation of Vehicles battery equivalent model
RMS	Root mean square
SOC	State of charge of the battery
WLTC	World Light Vehicle Test Cycle
WLTP	World Light Vehicle Test Procedure
τ_1/τ_2	Time constants in the equivalent circuit model
C_1/C_2	The capacitance for polarization effect in the equivalent circuit model
C_c	The equivalent capacitance in the lumped parameter model, which represents the heat capacity of the battery material
C_d	Coefficient of air resistance
C_p	Battery specific heat capacity
C_s	The equivalent capacitance in the lumped parameter model, which represents the heat capacity of the battery surface
F_a	The air drag of vehicle
F_{acc}	Accelerating resistance of vehicle
F_i	Resistance caused by the slop
F_r	Rolling Resistance
F_t	Vehicle traction force
P_e	The engine power output
Q_C	The present battery capacity consumption
Q_{all}	The total heat generate by battery Bernardi equation
Q_b	The heat absorbed by the battery
Q_{ir}	Irreversible heat of reaction
Q_j	Joule heat of battery
Q_p	The heat caused by polarization reaction
Q_r	Rated capacity of battery
Q_r	Reversible heat of reaction

Q_s	Heat of self-discharging reaction of battery
R_0	The ohm internal resistance in the equivalent circuit model
R_1/R_2	The resistance for polarization effect in the equivalent circuit model
R_c	The equivalent resistance in the lumped parameter model, which represents the thermal resistance between core and surface of battery
R_s	The equivalent resistance in the lumped parameter model, which represents the thermal resistance between battery surface and air
T_a	Ambient temperature
T_b	The surface temperature of battery
T_e	Vehicle engine torque
U_{oc}	open-circuit voltage
U_t	Terminal voltage of battery
f_0	Coefficient of rolling resistance
i_0	Ratio of reducer
q_e	Heat exchange between the battery surface and the air
q_{radio}	Thermal radiation conducts heat
q_x	The rate of heat transfer along the x axis
r_w	Radius of wheel
η_t	Transmission efficiency
h	Convective heat transfer coefficient
E	Terminal voltage of battery
I	Current of discharging/charging
T	The engine torque
n	The rotation speed of engine
v	Vehicle speed
λ	Thermal conductivity
ρ	Density of battery
σ	Steffan-boltzmann constant

1 Introduction

1.1 Background and context of study

With the rapid development of the economy and technology, the environmental pollution caused by traditional fossil fuels has become increasingly severe. Moreover, due to the non-renewable nature of traditional energy sources, many countries have been embroiled in conflicts over these resources, which are becoming increasingly scarce. As an unconventional energy source, new energy has significant advantages over traditional energy. New energy can be reproduced in a shorter time and produces fewer harmful substances such as nitrogen oxides and sulfides during utilization. To effectively address the problems of energy shortages and environmental pollution, countries worldwide have focused on exploring and researching new energy. From a global perspective, new energy encompasses many subfields. Among these, new energy electric vehicles are a particularly important part of the new energy sector. Currently, many automotive manufacturing companies in various countries are placing great emphasis on the research and design of these environmentally friendly vehicles. As a result, the global automotive industry is transitioning from traditional fuel vehicles to new energy vehicles, adopting various alternative methods to effectively address global environmental and resource issues[1]. Based on the classification of automotive power sources, new energy vehicles can be divided into three categories: pure electric, hybrid, and fuel cell vehicles. Among these, pure electric vehicles are currently a hot direction in the rapid development of automotive technology.

To promote the development of new energy electric vehicles and further reduce global carbon emissions, many countries and regions have introduced plans to encourage the use of new energy in recent years. For example, Hainan Province in China plans to achieve the goal of using only pure electric vehicles across the province by 2030. Japan has announced that it will stop selling fuel vehicles after 2035, with many government agencies encouraging their employees to use electric vehicles and issuing administrative orders to prevent purchasing fuel vehicles for official use. The United Kingdom plans to ban the sale of fuel vehicles by 2030, similar to the plans of China and other Asian countries. Meanwhile, within the European Union, countries such as France have also announced plans to gradually phase out traditional fuel vehicles between 2030 and 2040. It is evident that countries around the world are progressively implementing stricter environmental requirements and emission policies, which has become an unstoppable trend.

For electric vehicles, the battery is the primary energy source. Compared to other types of batteries, lithium-ion power batteries have superior characteristics such as high safety and high energy density, making them widely researched and applied. Lithium-ion power batteries are currently considered the most suitable energy supply method for new energy electric vehicles [2]. Currently, ternary lithium batteries (e.g., NCA, NCM) are used in some high-performance electric vehicles due to their high energy density per unit weight and the ability to discharge at high currents even in low-temperature environments. Conversely, lithium iron phosphate (LFP) batteries are typically used in lower-end vehicles because of their lower production costs, despite their lower energy density, which results in reduced driving range for these models. Additionally, many consumers are concerned about the safety of the battery pack. LFP batteries have a higher thermal runaway temperature threshold compared to ternary lithium batteries, making them safer and promoting their widespread use. Figure 1.1.1 shows a simplified structural of the lithium battery and power train of an electric vehicle.

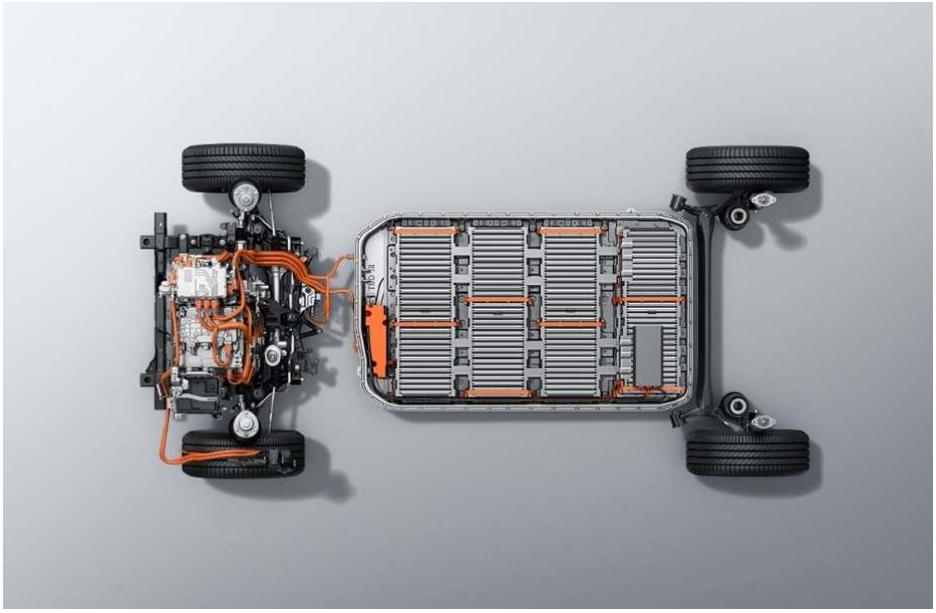

Figure 1.1.1 Simple structure of lithium battery and powertrain[5]

For electric vehicles, the safety of the power battery is the fundamental guarantee for its performance. To safely and fully utilize the power battery's performance and meet the power demands of electric vehicles under various operating conditions, effective monitoring, efficient management and control of the power battery are essential. The Battery Management System (BMS) is the key technology for managing and integrating the power batteries of electric vehicles. An advanced BMS not only ensures the safe use of power batteries but also optimizes the charging strategy, effectively enhancing the driving range, power output, and battery life of electric vehicles [3]. To

implement the functions of a BMS, it is first necessary to establish an accurate and efficient battery model. This model, combined with parameters such as load current and temperature, simulates the external characteristics of the battery. The management of the power battery is then achieved based on the output results of the battery model [4]. By thinking the complex chemical reactions within the power battery and the varied driving conditions of electric vehicles, modeling the battery requires considering the combined effects of external load and temperature. So this approach helps to develop a more accurate battery model that reflects the performance of the battery effectively.

The modeling of lithium-ion batteries involves two main aspects: the electrical model and the thermal model. The electrical model reflects the changes in voltage, current, and state of charge (SoC). The SoC is an important parameter indicating the remaining energy of battery and is crucial parameter for the BMS. Accurate SoC estimation can provide drivers with references to optimize driving strategies and is key to energy distribution and maximizing battery performance [6]. Since SoC cannot be directly obtained through sensors and must be estimated from voltage and current data, one technical challenge is to accurately estimate SoC and the terminal voltage of the battery based on current loads. The intensity of the internal electrochemical reactions in lithium batteries is closely related to temperature. When a lithium-ion battery is in operation, reversible redox reactions occur internally, generating heat, which is typically related to the entropy change of the chemical reactions. The lithium-ion battery also exchanges heat with its surroundings. When the heat generation rate exceeds the heat dissipation rate, the battery temperature rises. If the battery remains in this state for an extended period, the core temperature will incrementally increase step by step, potentially leading to electrolyte decomposition, battery swelling, internal separator dissolution, and eventually internal short circuits. Internal short circuits exacerbate chemical reaction rates and increase heat generation power. Once the battery core reaches the thermal runaway threshold temperature, the battery materials can spontaneously combust, causing explosions and thermal runaway [7]. If a single cell in the battery pack enters thermal runaway, it generates significant heat, potentially heating adjacent cells to their thermal runaway threshold, leading to the burning or explosion of the entire battery pack and causing thermal propagation [8]. Thermal runaway typically occurs due to the failure to monitor and predict the internal temperature of the battery, resulting in continuous temperature rise and eventual thermal runaway. With the widespread use of lithium batteries, the difference between surface and internal temperatures has become a critical issue due to varying battery shapes. Currently, Battery Management Systems usually monitor the battery surface temperature as a basis for thermal management control strategies and safety temperature warnings [9]. However, using some technical means to estimate and predict the internal temperature of the battery can significantly

enhance the effectiveness of the battery management system. Therefore, modeling the electro-thermal characteristics of the battery and integrating these models into the battery management system can achieve efficient prediction and management of battery operating states.

1.2 State of art

The modelling of automotive power lithium batteries is the premise of designing, manufacturing and managing batteries, and it is also the mathematical basis of battery condition estimation. At present, the lithium-ion battery model mainly includes electrical characteristics model, thermal model, electrothermal coupling model and aging model. The electrothermal coupling model describes the relationship between the electrical and thermal performance of the battery which because the strength of internal chemical reactions is related to temperature. And the terminal voltage of a battery is an extrinsic manifestation of its internal chemical reactions, so developing the electrothermal coupling model helps us to build a more efficient and reliable battery management system.

1.2.1 Model of electrical properties

In recent years, in order to study the electrical characteristics of the battery, many researchers have proposed three types of models to reflect the voltage change of the battery under the current load: the equivalent circuit model, the black box model and the electrochemical model. The equivalent circuit model is used to analyse the physical features of the battery and characterize the electrical characteristics of the battery by establishing a circuit network composed of circuit components such as resistors, capacitors, inductors and voltage sources. This kind of model has a simple structure and easy-to-calculate parameters and is widely used in real-time scenarios. Yann Liaw et al.[10] from Idaho National Laboratory proposed the first-order resistor-capacitance (RC) model and the second-order RC equivalent circuit model, which are characterize by the use of an RC loop to simulate the internal electrochemical and concentration polarization effect of the battery. These two models have high accuracy, easy-to-drive formulas, and have been applied in some BMS systems. Andre et al.[11] used an equivalent circuit model containing three RC loops, combined with Electrochemical

Impedance Spectroscopy and EIS data to test the performance of the model. Typical equivalent circuit models include Rint model, Thevenin model[12], PNGV model[13] and GNL model[14]. The Rint model simply equates the battery to the series combination of voltage source and resistance, ignores the polarization effect and concentration effect of the battery, but has poor accuracy.

Based on the Rint model, Thevenin model adds a series of RC networks to simulate the polarization effect of the battery, which can better reflect the nonlinear response of the battery terminal voltage under different current loads. The first-order RC model simulates lithium-ion batteries' charging and discharging behaviour by using an RC loop in series with a resistance. The experimental results show that the model can better simulate the external characteristics of the battery, but the disadvantage is that it cannot reflect the polarization effect of the battery. The second-order RC model approximates the battery dynamic performance by connecting two RC loops and a resistor in series. Compared with the first-order RC model, this model can better reflect the polarization effect inside the battery, so it is often applied to estimate the battery state. Studies have shown that increasing the number of RC networks of the Thevenin model can improve the model's accuracy. Still, when there are more than 3 RC networks, the model accuracy is not greatly improved, but the computation amount is significantly improved[15].

Compared with the first-order RC model, the PNGV model added a series capacitor, which was used to simulate the changing trend of the battery's open circuit voltage affected by the cumulative current. As the simulation time grows, the accumulation impact of current-voltage causes a decline in model accuracy. Therefore, this model is suitable for transient analysis of the battery, but not for long-term simulation using this model.

GNL model based on PNGV model adds a resistor in parallel, to reflect the self-discharge of the battery. The calculation of the Rint model is simple, but the accuracy is poor. The PNGV and GNL models have high accuracy, but the model is more complex, and there are too many parameters that need to be identified. Thevenin model has no obvious accuracy loss compared with the PNGV model and GNL model, but the calculation amount is much less, and now it is used in some on abord BMS. Qian Neng et al.[16] improved Thevenin model by increasing the number of RC circuits. According to the HPPC test experiment, the model parameters were identified and calibrated based on the least square method, and the equivalent circuit model was established according to the obtained parameters. Finally, the improved model has higher accuracy by comparing with the original Thevenin model. Ding X.F. et al.[17] improved Thevenin model without increasing the RC circuit number. Based on the HPPC test and open-circuit voltage experiment results, the battery model parameters

were identified by genetic algorithm and polynomial fitting, respectively. The accuracy of open circuit voltage calculation is improved. Therefore, the order of the RC model needs to be determined according to the working environment and state of the specific lithium battery. It is not the higher the order, the better, and we need to take into account the accuracy and calculation difficulty.

The black-box model is focused on the battery current and voltage data, which is completely based on the training data and does not reflect the internal chemical reactions of the battery, and does not depend on the accurate input-output mapping equation. Currently, the three most commonly used models are the neural network model, support vector machine model and genetic algorithm. The black-box model can effectively reflect the dynamic characteristics of the battery without relying on the accurate battery parameters, but the model's simulated precision is sensitive to the accuracy of the original data. Although a large amount of data samples can improve the accuracy of the black-box model, the overall training time will become longer[18]. In this research field, some researchers have made much progress. Wang et al.[19] proposed a thermoelectric coupling model based on neural network, and verified the effectiveness of the model through different battery tests. The model's accurate prediction ability will enable precise and effective battery condition monitoring in the BMS. Li et al.[20] established a lithium-ion battery model based on deep learning method and combined with data preprocessing to train the model, and the estimation error was within 3%. If the amount of data used by the black-box model is not large, the accuracy of the model will be reduced. Because there are many unpredictable factors in the actual use of vehicles, the training data cannot cover all the driving conditions, which also limits the application of black-box models in BMS.

The white box model, which is opposite to the black box model, is also a research hotspot in recent years. The electrochemical model is a kind of white-box model. This kind of model describes the distribution and evolution of parameters such as ion concentration and electrochemical reaction rate in the battery by establishing a kinetic partial differential equation to reveal the internal chemistry reaction principle of the battery. At present, the commonly used electrochemical models are mainly the Peukert equation model, Shepherd model and Nerst model. Theoretically, the electrochemical model can achieve high accuracy, but it is difficult to obtain model parameters and the overall calculation is complex, which has great limitations in real-world applications[21]. Newman et al.[22] from the University of California who first proposed the establishment of a porous electrode model and applied it to batteries. Doyle et al.[23] proposed Pseudo Two-dimensional (P2D) model based on the principles of electrochemical reaction kinetics, concentrated solution and porous electrode, which has been widely concerned and applied. Subsequently, some

researchers also proposed some simplified models to reduce the amount of calculation and ensure the accuracy of results, such as the Parabolic Polynomial Approximation (PP) Model[24] and the Single Particle Model (SP) model[25]. These simplified models can improve the efficiency of calculation, save the computing power of vehicles, and have the potential to be applied to BSM systems in the future.

1.2.2 Model of thermodynamic

The lithium-ion battery is also accompanied by the release and absorption of heat when it is working (charging and discharging), and its internal temperature is a value that is closely related to the safety, life and performance of the battery. Although it is very important to estimate the electrical parameters of the battery, it is also of great significance to study the changes in the internal temperature to evaluate the state of the battery. Currently, the commonly used thermodynamic models are divided into lumped parameter thermal models and distributed parameter thermal models. The lumped parameter thermal model is a thermal behaviour model that combines an equivalent circuit model with Joule's law and heat transfer principle. This kind of model ignores the electrochemical process, so the complexity of the thermal model is low. The earliest thermal model was proposed by Bernardi et al.[26] in 1985. This model combined electrochemical reaction, phase transition and thermal mixing process, which could effectively calculate and analyse the heat generation rate of batteries and provide a model basis for subsequent research on battery heat transfer. Forgez et al.[27] verified the difference between the core and surface temperature of the battery by using a simplified heating equation based on the two-state lumping-parameter thermal model. The model has a simple structure and can simulate the internal temperature directly by measuring the current and voltage of the battery. Allafi et al.[28] incorporated thermal convection, thermal radiation and other factors into the lumped model, thereby establishing a new type of battery thermal model and increasing the accuracy of the simulation. The lumped parameter model considers the battery as a whole, and the heat source comes from the battery core, but this will increase the temperature estimation error. In fact, there are multilayer film structures inside the battery, and the temperature distribution is not uniform. This uneven temperature distribution also affects the battery lifetime. Therefore, in order to estimate the battery temperature distribution more accurately, some researchers have proposed the distributed parameter thermal model. Richardson et al.[29] proposed a low-order two-dimensional thermal model of 18650 battery, and compared it with the finite element method simulation result. The results

show that the proposed model has similar computational efficiency and higher accuracy than the previous model. At present, the thermal model of battery has evolved to more dimensions, including considering the density distribution of current and so on, which is beneficial to improve the accuracy of simulation.

1.2.3 Electrothermal coupling model

At present, many researchers model the features of the battery, in addition to studying the electrical model, and take the influence of battery temperature change into account. The commonly used lithium-ion battery model is divided into the electrical (grey box) -thermal coupling model and electrochemical (white box) -thermal coupling model. In the electrical-thermal coupling model, the thermal power of the battery is calculated by the terminal voltage and current, so as to calculate the heat generation of the battery, and input it into the thermal model, and finally obtain the temperature change and temperature distribution of the battery during the working process. Subsequently, due to the change of battery temperature, the electric characteristic parameters of the battery change, and the electrical characteristic parameters are fed back to the electrical model to correct the instantaneous heating power, forming a coupling solution process. In recent years, Pan D. et al.[30] established the electric-thermal coupling model by measuring the battery open-circuit voltage, internal resistance, entropy heat coefficient and other model parameters. They completed the verification of the electric-thermal coupling model by comparing the results of the simulation and experiment. After that, the CC-CV method, the voltage drop between open circuit voltage and terminal voltage method and the HPPC test method are used to measure the internal resistance of the battery, and input into the electrical-thermal coupling model respectively. The simulation comparison and analysis show that the HPPC test method is the most ideal test method for internal resistance. Chen M.B. et al.[31] designed an electric-thermal coupling model for the soft-pack battery, considering that the electrical and thermodynamic characteristics of the battery would affect the battery performance. In this thesis, the battery is divided into multiple units, and the electric-thermal coupling model is established in a hierarchical form based on the equivalent circuit model. The finite difference method is used to solve the electric-thermal coupling model, and the nonuniformity of temperature and current distribution under different discharge rates is simulated. Finally, the model's accuracy is verified by experiments.

1.3 Thesis organization

In this thesis, we use a common 18650 cylindrical lithium-ion battery as the research object to model its electrical and thermal characteristics. It simulates the trends in battery terminal voltage and temperature changes under specific current loads and ultimately establishes an electrical-thermal coupling model. After that, a simplified electric vehicle dynamic model is built to explore common electric vehicle battery packs' terminal voltage and temperature changes under different driving conditions.
The main contents include the following:
Chapter One introduces the research content of this thesis and the background knowledge of related studies. It describes the significance and process of the development of electric vehicles. Regarding the establishment of the electrical-thermal model for lithium batteries, it reviews the research conducted by relevant scholars, particularly highlighting the research achievements in the field of model simulation related to the dynamic characteristics of lithium batteries.
Chapter Two mainly introduces the basic knowledge of the 18650 cylindrical lithium battery and briefly describes the chemical reaction principle and structural characteristics of lithium-ion batteries. After that, the principle of HPPC experiment is introduced, and the parameters in the battery electrical characteristic model (equivalent RC circuit model) are identified according to the experimental data obtained previously. Based on the identified parameter results, an electrical characteristic model is built on the Matlab Simulink platform.
Chapter Three mainly analyses the establishment process of the battery electrothermal coupling model, introduces the structure of the model on the simulink platform and the derivation of the relevant theoretical formulas.
Chapter Four describes the process of establishing the dynamic driving model of an electric vehicle, focusing on defining the vehicle's basic parameters, the electric motor's parameters of the powertrain system and the related Matlab model.
Chapter Five, according to the battery electrothermal coupling model and vehicle dynamic driving model introduced in the previous chapters, the variation trend of related parameters (voltage, current, temperature, etc) of lithium battery is studied under specific road profiles (NEDC, WLTC, etc). Additionally, the electrical and thermal characteristics of lithium batteries were analysed, which will become the basic part of BMS.
Chapter Six summarises the results obtained above, introduces some highlights of this study.

2 Research on equivalent circuit model of Li-ion battery

This chapter first introduce the working principle and basic structure of lithium-ion batteries. After studying the structural characteristics of the battery, the second-order RC equivalent circuit model is selected as the basis of the electric characteristic model of the lithium battery. Some studies have pointed out that the parallel number of inductors and capacitors in the equivalent RC circuit model is not the more the better. Compared with the second-order and the third-order RC, the simulation accuracy is not significantly increased, but the calculation workload is clearly higher. Therefore, the second-order RC model is more suitable for accuracy and computation aspects. Then the parameter identification process in RC circuit is described, and the HPPC experiment is briefly introduced. Because the experimental data of HPPC plays an important role in identifying parameters. Finally, the parameter identification results are listed, and the simulation error is analysed.

2.1 Working principle of lithium battery

It has been more than 30 years since a Japanese company announced the output of lithium-ion battery production in 1991. Lithium-ion batteries have become an indispensable energy source in our lives and have been applied to various fields, from smartwatches and mobile phones to unmanned aircraft and electric vehicles. However, the development process of lithium-ion battery as an important energy storage element is not easy. In 1972, Whittingham found that Li+ could be embedded in TiS2, so TiS2 was used as the positive electrode and Li material was used as the negative electrode to form a lithium-ion battery. However, the capacity of the battery with this material decreases significantly with the increase of charging and discharging cycles, and the lithium dendrites on the negative electrode surface will cause the battery short circuit. In 1980, Goodenough used LiCoO2 as the cathode material of lithium battery, and provided Li+ to the battery structure through the oxidation reaction of LiCoO2, which proved that Li material in cathode was not needed to provide Li+ to the electrolyte. In 1985, Japanese scientist Akira Yoshino used polyacetylene as a battery cathode, lithium cobalt oxide battery cathode, this is the original prototype of lithium battery at past. Although the technology of lithium-ion battery has matured after decades of rapid development, it still faces many challenges, such as whether the energy density of the

battery can be further improved, the reliability of the battery can not be better guaranteed, and whether more efficient battery materials can be found to improve the cycle life of the battery.

In recent years, many automakers have used lithium battery packs as a power source for their vehicles. Because compared with the NIMH battery, lithium ion battery has higher energy density, long cycle life, more safety, no memory effect, less pollution and some other advantages. A generic lithium battery consists of a positive electrode, a negative electrode, many diaphragm, and a kind of electrolyte. The positive and negative electrodes are usually two different compounds that can embed and release lithium ions. Usually, cathode materials are lithium iron phosphate, lithium manganate, lithium cobaltate, etc., and cathode materials are generally graphite, carbon and other low-potential materials that are easy to obtain electrons, which are mainly responsible for storing lithium ions oxidised from cathode materials. The diaphragm is a porous material between the positive and negative electrodes of the battery that allows lithium ions to pass through but blocks electrons, thereby preventing short circuits within the battery. Currently, to increase the amount of charge available in batteries, diaphragms are usually stacked like a sandwich or rolled into a cylinder. Usually the diaphragm is mainly made of polyethylene material. The composition of the electrolyte is mainly a mixed material made of lithium salt and organic solvent. Its function is to conduct lithium ions, lithium ions through the electrolyte to achieve shuttle between the positive and negative poles. Because the electrolyte and the positive and negative electrodes of the battery and the film material are in direct contact with each other, they all need to have good compatibility. Figure 2.1.1 shows the basic principle of lithium battery.

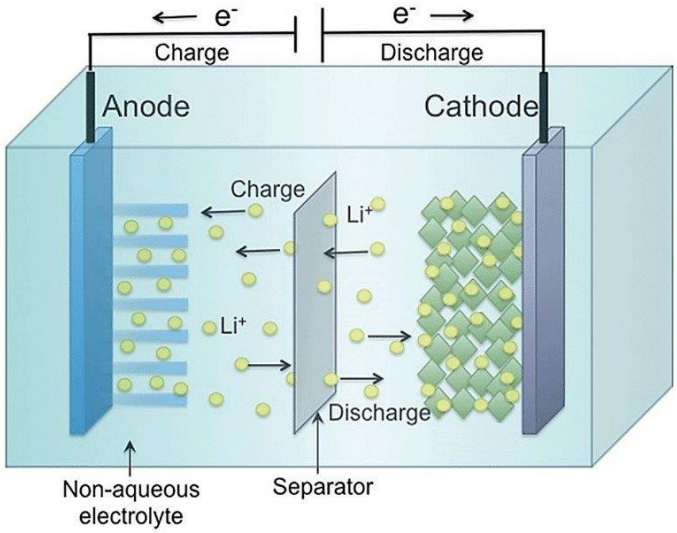

Figure 2.1.1 The principle of the lithium-ion battery[32]

From the point of view of the chemical reaction principle, the REDOX reaction

occurring inside the lithium-ion battery converts the chemical energy into the electric potential energy between the positive and negative electrodes, so as to achieve the purpose of providing power for electrical equipment. Taking the commonly used ternary lithium battery as an example, the positive electrode material is LiNiCoAlO2, and the negative electrode is LiC6. In the process of charging and discharging, the battery reacts as follows:

Charging：

Cathode $LiNiCoMnO_2 \rightarrow NiCoMnO_2 + Li^+ + e^-$

Anode $Li^+ + 6C + e^- \rightarrow LiC_6$

Discharging：

Cathode $NiCoMnO_2 + Li^+ + e^- \rightarrow LiNiCoMnO_2$

Anode $LiC_6 \rightarrow 6C + Li^+ + e^-$

Combained equation：

$$LiC_6 + LiNiCoMnO_2 \rightleftharpoons 6C + NiCoMnO_2 + 2Li^+$$

Through the general chemical reaction equation of lithium battery, it is obvious to say that the movement of Li+ between the positive and negative electrodes realises the charging and discharging function of the battery. When the battery is connected to an external current (charging), the lithium compound in the positive electrode precipitates Li+ and electrons, and the reduction reaction occurs, causing the valence to rise. The selective penetration of the thin film in the cell structure leads to the passage of Li+ and the inability of electrons. So electrons can only pass through the outer conductor to complete the circuit. At the same time, Li+ migrates through the electrolyte to the negative side of the cell and diffuses into the material lattice at the negative side. When the battery is used as an energy source (discharge), the negative electrode material loses electrons and produces Li+, and the reduction reaction occurs. Li+ passes through the diaphragm to the positive electrode to participate in the reaction. The electrons pass through the cable to the positive electrode. Specifically, the amount of Li+ reflects the charging and discharging capacity of the battery. It can also be said that the larger the capacity of the battery, the larger the total amount of Li+ inside. Figure 2.1.2 shows several commonly used lithium batteries with different electrode materials.

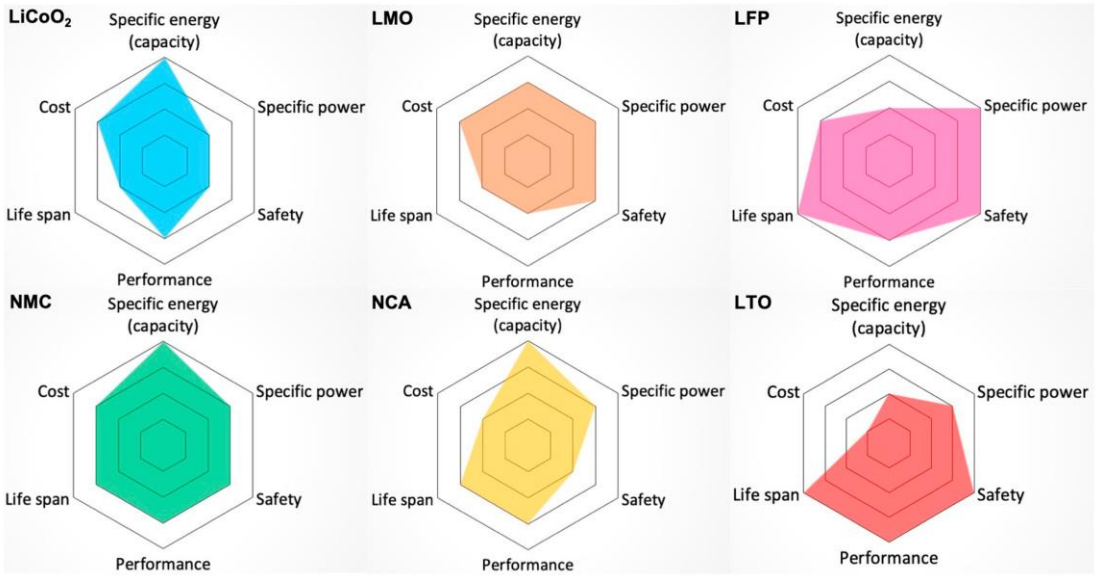

Figure 2.1.2 Several different types material of lithium-ion batteries in the market[41]

The above figure shows the types of cathode materials for lithium batteries that can be found on the market at present, and measures these batteries by several factors such as cost, safety, specific energy and life span. The most expensive battery is the LTO battery, which is also excellent in safety and performance, but its low energy density makes it suitable for stationary energy storage devices. LFP and NMC and NCA batteries are more likely to be used in vehicle battery packs at the present stage. NCA and NMC batteries are commonly referred to as ternary lithium batteries, and their cathode materials use lithium nickel-cobalt manganate or lithium nickel-cobalt aluminate. The remarkable feature of ternary lithium battery is that the specific energy is very high, which can reach 220Wh/Kg, and that is significantly higher than the LFP battery whose value is about 140 Wh/Kg. LFP battery is the use of lithium iron phosphate as a cathode material, in the safety aspect it is better than ternary lithium battery. Because lithium iron phosphate crystal in the P-O bond is very stable, difficult to decompose. It will not easily explode even in the overcharge state, lithium iron phosphate decomposition temperature at about 600℃, so this is the reason why it has good safety index. Ternary lithium materials decompose at around 200 degrees Celsius. The chemical reactions become more intense, releasing oxygen molecules, which cause the electrolyte to rapidly combust at high temperatures, potentially leading to a chain reaction. But from the life span point of view, LFP battery life is higher than ternary (NMC/NCA) battery, so in these years many low price electric vehicles use LFP battery, and some high-end vehicle use ternary lithium battery. From the point of view of the barrel effect, NMC battery is more balanced from the above aspects, so it is also favored by vehicle

manufacturers. Meanwhile, LFP batteries are also widely used because of their high stability and relative low cost.

2.2 Electrical characteristic model

Equivalent circuit model is a kind of grey model, which does not consider the electrochemical mechanism inside the battery, but reflects the terminal voltage and current change rule of the battery through the combination of capacitors and resistors in different places in the circuit, and intuitively reflects the relationship between battery voltage and current. So, the equivalent circuit model can be used to evaluate the current state of the battery and can also be used to estimate the future condition of the battery. Because the resistance and capacitance in the circuit model have clear physical meaning, in recent years, some scholars have used them in the state assessment module of batteries, and also applied in the BMS for some vehicles. In the following pages, some equivalent models will study,

The Rint model is an equivalent circuit model that was initially proposed. Its structure is simple, only a resistor is directly connected in series with an ideal voltage source, and the structure is shown in Figure 2.2.1.

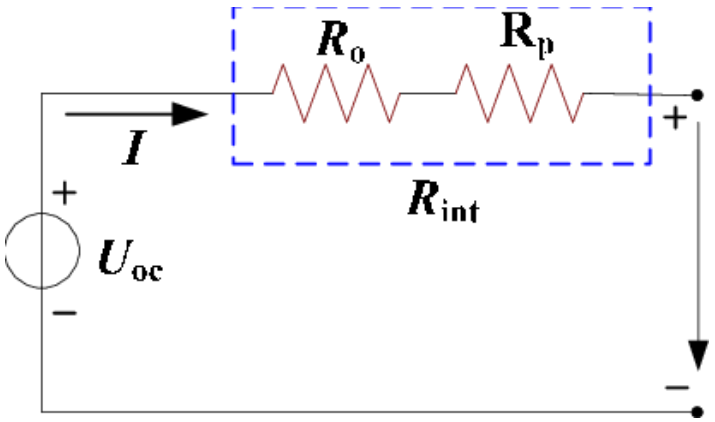

Figure 2.2.1 The Rint battery model[33]

From picture 2.2.1 to say, it is easy to find that this model structure is extremely simple so the Li+ diffusion and polarization effects of lithium batteries cannot be reflected at all but only reflect the ideal linear relationship between terminal voltage and current. The formula representing its circuit is given by 2.1.

$$E = U_{ocv} - IR_0 \tag{2.1}$$

In this formula, E is the terminal voltage in unit as V; U_{ocv} is open circuit voltage in unit as V; I is the current, the unit is A; R_0 is the internal resistance of the battery in Ω. Because it does not take into account the polarization effect of the battery, can not reflect the charging and discharging characteristics of the battery, so it is not suitable for the simulation of lithium battery electrical characteristics under complex working conditions.

Based on the Rint model, some researchers added an RC circuit behind the resistor, which is the Thevenin model. The structure is shown in Figure 2.2.2.

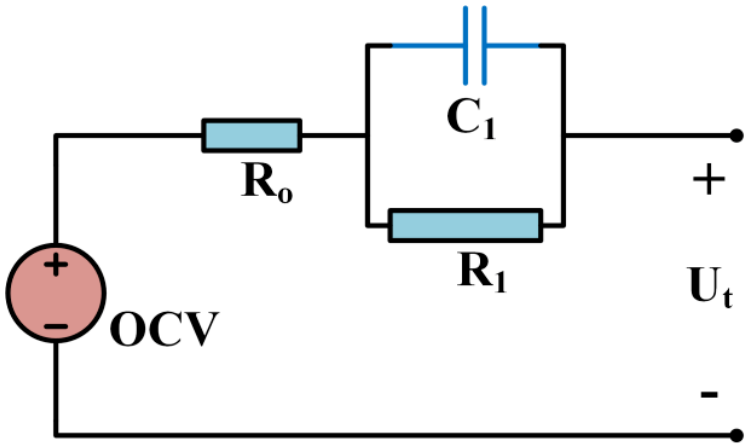

Figure 2.2.2 Thevenin equivalent model of battery[34]

The RC circuit in this model can well reflect the nonlinear behaviour of the voltage variation trend, and the polarization phenomenon of the battery is taken into account, which can better reflect the internal activities of the lithium battery under the working state. According to Kirchhoff's law, the equation of the model is shown in 2.2.

$$\begin{cases} I = \frac{U_1}{R_1} + C_1 \frac{dU_1}{dt} \\ E = U_{ocv} - U_1 - IR_0 \end{cases} \quad (2.2)$$

In this formula, U_{ocv} is the open circuit voltage of the battery, unit in V; E is the terminal voltage of the battery, unit in V; U_1 is the voltage V at C_1; R_0 is the ohmic internal resistance of the battery, unit in Ω; R_1 is the polarization internal resistance, unit as Ω; C_1 is the polarization capacitance with unit F. The capacitance C_1 reflects the equivalent capacitance of the transient response of the battery cell when it is excited by an external current.

Meanwhile PNGV model adds a capacitor in series with the ideal voltage source based on Thevenin model, and its structure is shown in Figure 2.2.3.

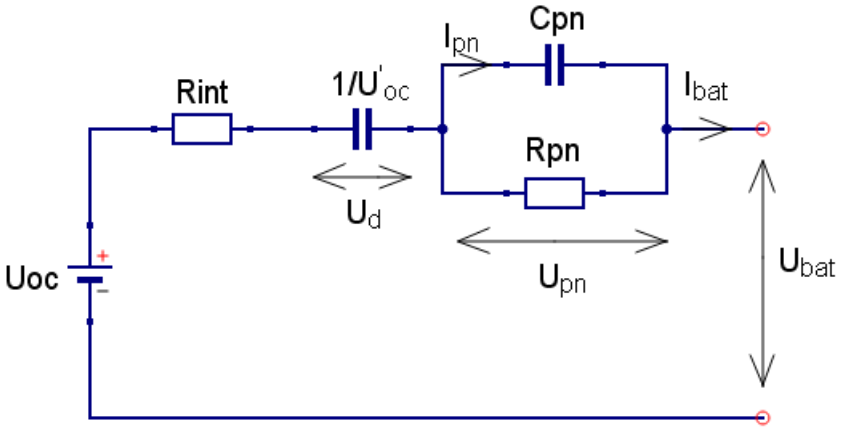

Figure 2.2.3 PNGV model of battery[35]

The newly added capacitance in the PNGV model can simulate the open-circuit voltage variation caused by the directional movement of Li+ inside the cell. The computational complexity of this model is larger than the two models mentioned before, but it has higher accuracy and is more suitable for offline battery model applications. The equation represented by its structure is shown in formula 2.3.

$$\begin{cases} I = C_d \frac{dU_d}{dt} \\ I = \frac{U_{pn}}{R_{pn}} + C_{pn} \frac{dU_{pn}}{dt} \\ E = U_{ocv} - U_d - U_{pn} - IR_{int} \end{cases} \tag{2.3}$$

In this formula, U_{ocv} is the open circuit voltage of the battery, unit in V; E is the terminal voltage of the battery, unit in V; U_d is the voltage of C_d, unit in V; U_{pn} is the voltage of C_{pn}, unit in V; R_{int} is the ohmic internal resistance of the battery, unit in Ω; R_{pn} is polarization internal resistance, unit in Ω; C_{pn} is the polarization capacitance, unit in F.

In the electrochemical research field, the polarization effect inside the battery is divided into concentration polarization effect and diffusion polarization effect. Therefore, two RC loops are used to represent the influence of these two polarization effects respectively, which is the second-order RC equivalent circuit model used in this thesis. The structure is shown in Figure 2.2.4. In this model, an RC loop is connected in series with the Thevenin model, which can more accurately simulate the influence of the polarization effect on the voltage of the battery in the working state.

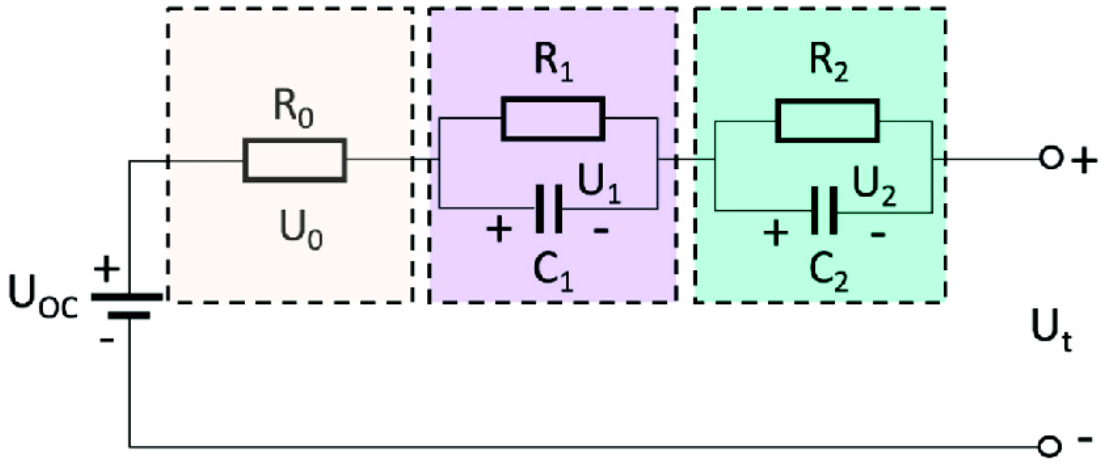

Figure 2.2.4 2RC circuit battery model[36]

According to Kirchhoff's law, the equation can be obtained as

$$\begin{cases} I = \frac{U_1}{R_1} + C_1 \frac{dU_1}{dt} \\ I = \frac{U_2}{R_2} + C_2 \frac{dU_2}{dt} \\ U_t = U_{oc} - U_0 - U_1 - U_2 \end{cases} \quad (2.4)$$

In formula 2.4, U_{oc} is the open circuit voltage of the battery, unit in V; E is the terminal voltage of the battery, unit in V; U_1 is the voltage of C_1, unit in V; U_2 is the voltage of C_2, unit in V; R_0 is the ohmic internal resistance of the battery, unit in Ω; R_1 is the internal resistance standby diffusion polarization effect, unit in Ω; R_2 is the internal resistance standby concentration polarization effect, unit in Ω; C_1 is capacitance standby the diffusion polarization effect, unit in F; C2 is the capacitance standby concentration polarization effect, unit in F. Obviously, according to the above structure diagram, it can be seen that the second-order RC equivalent circuit model has more parameters than the other three models, but it can also better reflect the internal features and external voltage characteristics of the battery. Therefore, the second-order RC model is selected as the basis for the battery electrical characteristics model in this thesis.

2.3 Identification for model parameters

2.3.1 Battery choose and HPPC test

The electrochemical reaction mechanism of lithium-ion battery is very complex, which

also leads to its external parameters are difficult to obtain by direct measurement method, such as the internal resistance of the battery, available capacity and so on. Even if the existing mathematical model is applied, the parameters of the model still need to be calculated through the experimental data of the battery. The lithium ion battery selected in this study is the 18650 type ternary lithium battery produced by LG with a rated capacity of 3Ah. The experimental data of the battery used for model parameter identification came from a professional laboratory[37]. The basic data of lithium batteries used in the experiment are shown in Table 2.3.1.1.

Due to the existence of the polarization effect inside the battery, the terminal voltage cannot immediately return to the stable state after the battery is charged and discharged, and the voltage rises or falls slowly for a short period of time after the current has disappeared. We refer to this phenomenon as hysteresis. Therefore, the components R1, R2, C1 and C2 in the model are used to describe this polarization phenomenon. In order to estimate these parameters accurately, Hybrid Pulse Power Characterization (HPPC) test is needed. In the HPPC test, the terminal voltage of the battery responds to a pulsed charge or discharge current. This abrupt voltage curve reflects exactly the influence of the ohmic and polarized internal resistance of the battery on the terminal voltage under the action of current. According to this principle, we can quantify the parameters of the battery model.

Table 2.3.1.1 Ternary lithium-ion battery parameters

Battery parameters	Property
Type	Li[NiMnCo]O2
Nominal Voltage	3.6V
Nominal Capacity	3 Ah
Charge cutoff voltage	4.2V
Discharge cutoff voltage	2.6V

Figure 2.3.1.1 shows the process of the HPPC test. The experimental data set[37] used in this study contains the experimental data of the battery at 25 degrees and 40 degrees. The experimental procedures are as follows:

1. Put the battery in the thermostat.
2. Charge with 1A current until it is fully charged battery according to the constant current-constant voltage principle.
3. Change the temperature to the experimental temperature and leave it for a long time。
4. Discharge at 1C/2C/4C/6C for 10s and set aside for 40s. Charge at 0.5C/1C/1.5C/2C for 10s and set aside for 40s.
5. Discharge to soc 0.9 with 1A current, and put battery stable for 1 hour.

6. Repeat steps 4 and 5 to decrease the soc by 10% in each round until the soc is equal to 0.1。
7. Record the data.

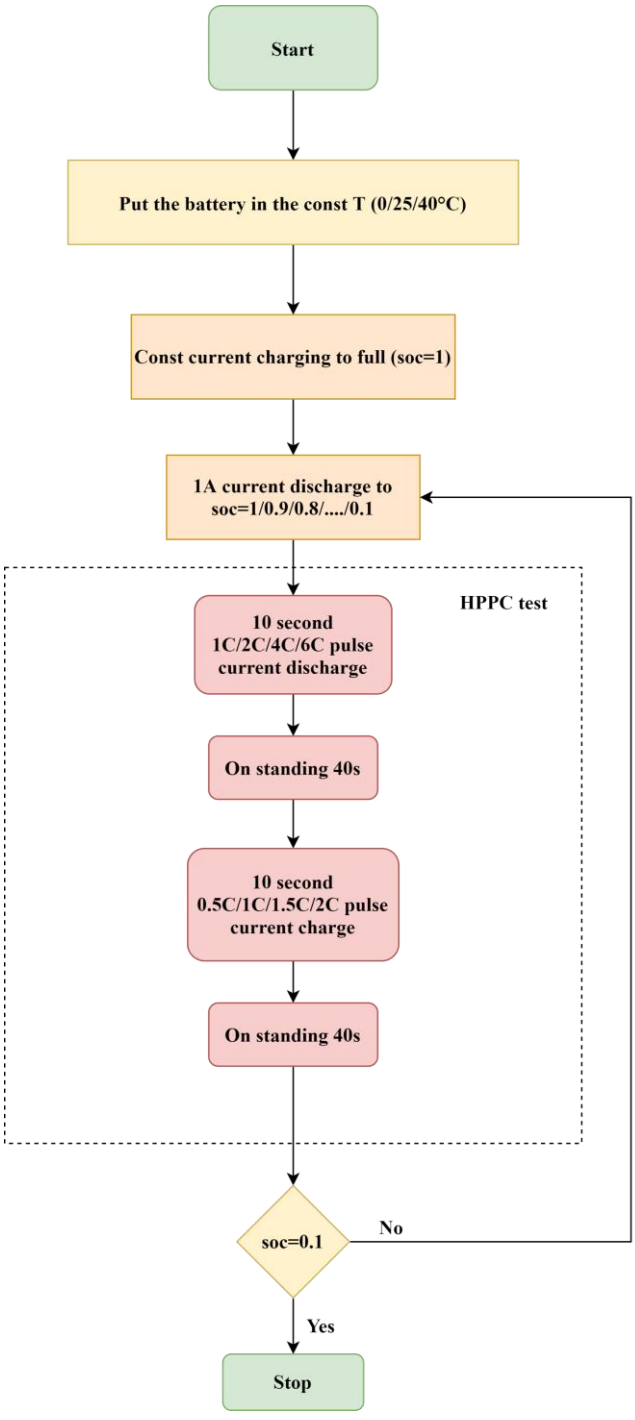

Figure 2.3.1.1 HPPC test profile

2.3.2 Open circuit voltage calibration

In the process of battery SOC estimation, there is a linear relationship between the open circuit voltage and the SOC of the battery, and this relationship can be used to estimate the remaining capacity of the battery roughly. When the battery has been standing for a long time, its internal state tends to be stable At this point, the potential difference between the positive and negative electrodes is referred to as the open-circuit voltage. In the HPPC experiment presented earlier, the results obtained at soc of 1,0.9, 0.8,...,0.1, pulse excitation starts after the battery stands for 1 hour. According to this, we can say that the battery interior is stable before the pulse excitation, and this voltage can be used as the open circuit voltage under the current soc. These voltage data were collected and plotted in Figure 2.3.2.1.

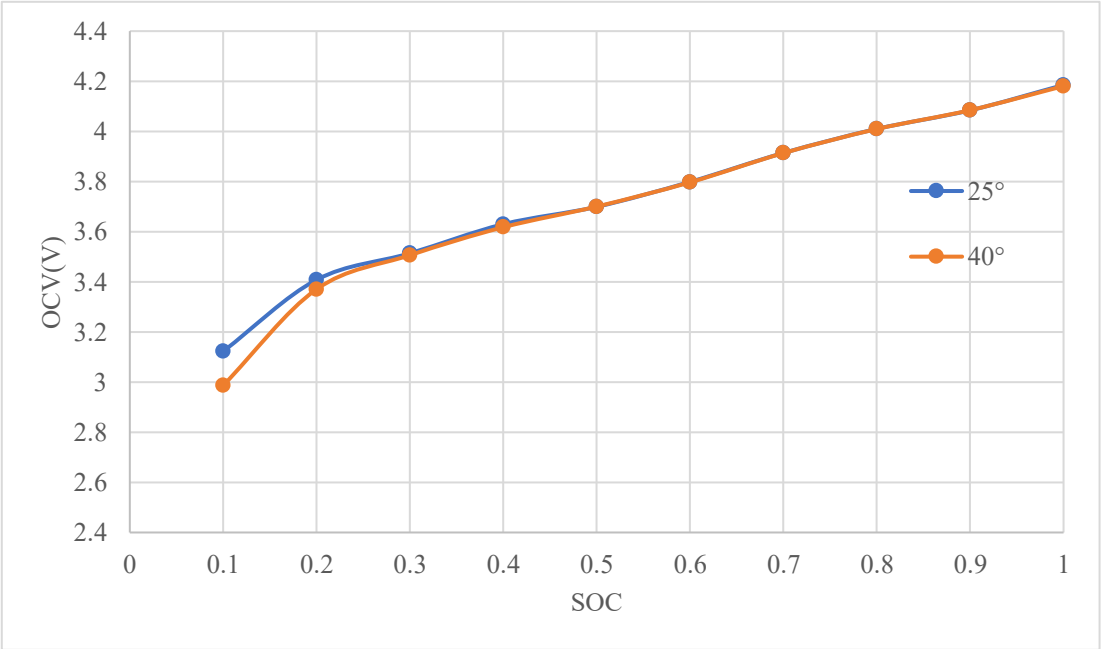

Figure 2.3.2.1 OCV-SOC based on different temperature

As can be seen from the figure, when soc is between 0.3 and 1.0, the OCV-SOC under the temperature of 25 degrees and 40 degrees tends to be consistent. Only in the low soc case, the higher the temperature, the lower the OCV. Also between soc 0.1 and 0.3, the OCV rise rate is larger compared to the case of soc greater than 0.3. Therefore, temperature has little effect on OCV, but SOC has a more obvious effect on OCV. The data of the battery in the state of 25° (room temperature) were taken, and the functional relationship of SOC-OCV was obtained by using the least square method. As can be seen from Figure 2.3.2.2, there is approximately linearity between OCV and SOC, we

choose the quintic polynomial used for fitting, and got the R^2 is 0.9993. So, it can be concluded that most of the data points are located on or near the fitting curve. The fitted polynomial is given in Eq. 2.5.

$$OCV = 14.479soc^5 - 45.058soc^4 + 53.102soc^3 - 29.35soc^2 + 8.4931soc + 2.5193 \quad (2.5)$$

In Table 2.3.2.1 the values of battery open circuit voltage at different temperatures are presented based on every 10%soc

Table 2.3.2.1 OCV-SOC based on T 25/40°C every 10% soc

SOC	0.1	0.2	0.3	0.4	0.5	0.6	0.7	0.8	0.9
OCV25°	3.123	3.408	3.514	3.630	3.699	3.799	3.914	4.010	4.084
OCV40°	2.987	3.370	3.506	3.618	3.700	3.797	3.914	4.009	4.085

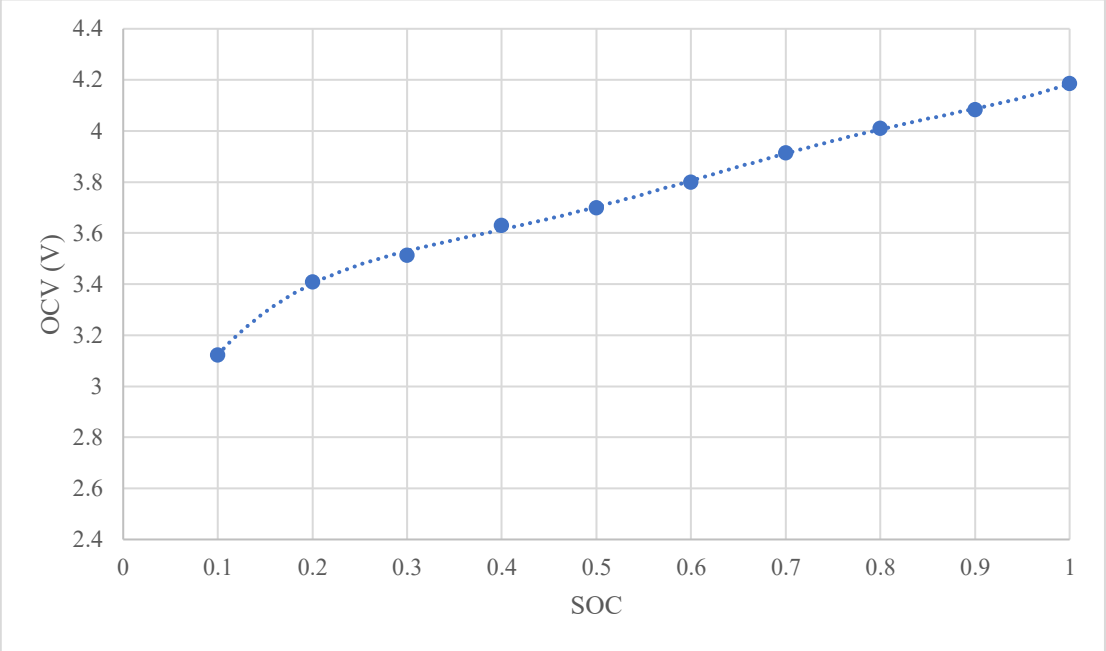

Figure 2.3.2.2 OCV-SOC data with matched curve of 25°C

2.3.3 Least square method

At present, there are many different mathematical methods to identify the parameters of various linear or nonlinear systems. The parameters of the RC equivalent circuit model in this thesis need to use effective mathematical methods to estimate the parameters. Over the past decade, a popular and effective mathematical method is called least squares method. This classical system identification method is used to estimate

the parameters of many models. Its geometric meaning is to calculate the error between the true value and the estimated value according to the input and output of the system. Finally, the sum of squared error is minimized by correcting the estimated value continuously. In the following pages, the least squares method is introduced.
Assume the following linear system: Let $U(k)$ be the system input and $Y(k)$ be the system output, and have:

$$A(z^{-1})Y(k) = B(z^{-1})U(k) \tag{2.6}$$

$$\begin{cases} A(z^{-1}) = 1 + a_1 z^{-1} + a_2 z^{-2} + \cdots + a_n z^{-n} \\ B(z^{-1}) = b_1 z^{-1} + b_2 z^{-2} + \cdots + b_r z^{-n} \end{cases} \tag{2.7}$$

Where a, b are the parameters to be identified in the system. In this case, the discrete transfer function of the system is

$$G(z^{-1}) = \frac{B(z^{-1})}{A(z^{-1})} = \frac{b_1 z^{-1} + b_2 z^{-2} + \cdots\ldots\ldots + b_1 z^{-n}}{1 + a_1 z^{-1} + a_2 z^{-2} + \cdots\ldots\ldots + a_r z^{-n}} \tag{2.8}$$

The corresponding difference equation is given as follows.

$$\begin{aligned} y(k) &= -a_1 y(k-1) - a_2 y(k-2) - \cdots - a_y(k-n) + b_u u(k-1) + b_2 u(k-2) + \cdots + b_u u(k-n) + e(k) \\ &= -\sum_{i=1}^{n} a_i y(k-i) + \sum_{i=1}^{n} b_i u(k-i) + e(k) \end{aligned} \tag{2.9}$$

Therefore, the least squares method form for the system with parameter identification is:

$$y(k) = \varphi(k)\theta^{\{T\}} + e(k) \tag{2.10}$$

Where θ is the set of system parameters to be estimated.

2.3.4 Parameter calculation

In the 2RC equivalent circuit model, there are parameters R0, R1 and R2 representing the ohmic and polarization internal resistance, respectively. And C1 and C2 represent the equivalent polarization capacitance. The current I in this model is a known quantity

and can be measured. Although the open circuit voltage U_{ocv} cannot be measured directly, it can be calculated from the OCV-SOC relationship curve fitted by the open circuit voltage calibration in the previous section. According to the response curve of the lithium battery voltage under the excitation of pulse current obtained in the HPPC experiment and the calibrated open circuit voltage, we can estimate the ohmic internal resistance and polarization internal resistance and other parameters according to the existing experimental data. Figure 2.3.4.1 shows the voltage variation relationship of a lithium battery under a 10s current pulse, which is a from part of HPPC test data.

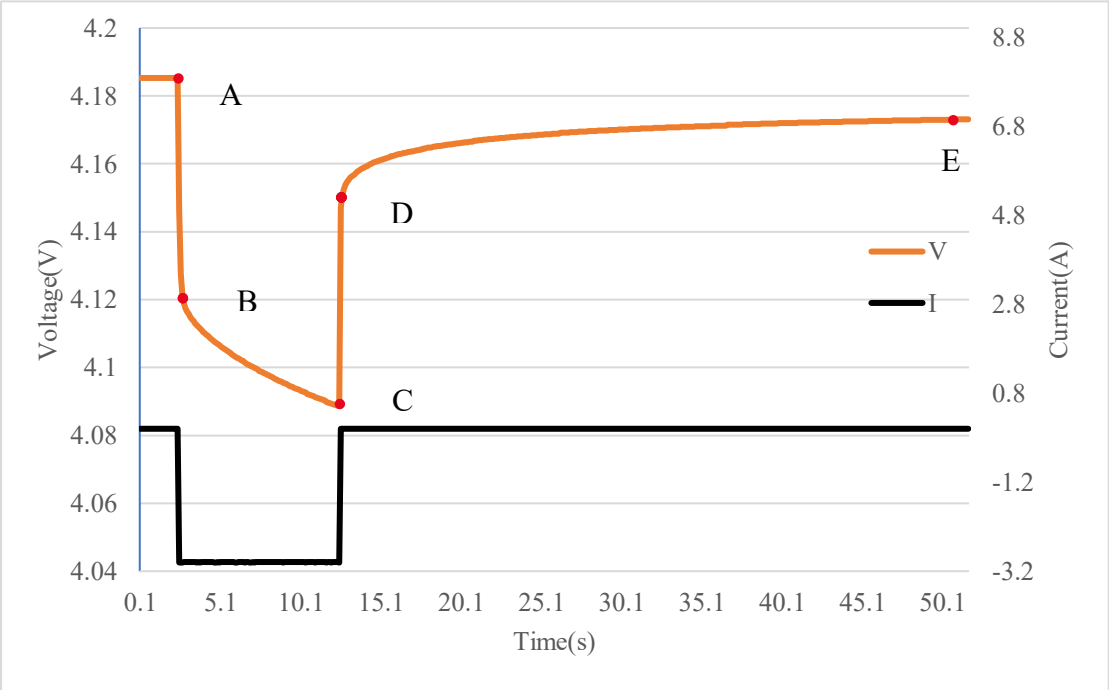

Figure 2.3.4.1 One pulse of HPPC test voltage and current

From the figure 2.3.4.1, point A starts the pulse discharge until point C ends. Similarly, it can be intuitively found from the figure that the voltage of the battery will drop and rise instantaneously at the beginning and end of the discharge current stage, and the mutation voltage is marked as point A-B and point C-D respectively. The main reason for this phenomenon is the existence of the ohmic internal resistance R_0 related to the battery material. At this time, in the case of knowing the discharge current value, and then measuring the difference of the variable voltage, the current ohmic internal resistance R_0 can be calculated according to equation 2.11.

$$R_0 = \frac{(U_A - U_B) + (U_D - U_C)}{2I} \tag{2.11}$$

Through this equation above, the ohmic internal resistance values under different SOCs can be calculated.

There are two more special points in Figure 2.3.4.1, namely the B-C and D-E phases. The main reason for these two special stages is the existence of polarization internal resistance inside the battery cell. Due to the existence of polarization resistance, the voltage appears "hysteresis effect". In the equivalent RC circuit model, two RC loops are used to simulate the polarization and diffusion effect of the battery, so the model parameters in the RC loop can be identified through the voltage variation of the two stages of B-C and D-E. In the D-E phase, the battery voltage slowly rises when the external load current turn to 0, which corresponds to the zero input response phase in the frequency domain.

$$E = U_{oc} - U_1 \exp\left(-\frac{t}{\tau_1}\right) - U_2 \exp\left(-\frac{t}{\tau_2}\right) \tag{2.12}$$

The voltage variation in the zero-input response phase of the battery can be expressed by equation 2.12, so we can calculate the parameters U_1, U_2, τ_1 , τ_2 in the formula by using the least square method. Here $\tau_1 = R_1C_1$, $\tau_2 = R_2C_2$ are the time constants of the two RC loops. The cftool tool in Matlab for curve fitting, and this tool is applied to fitting curve D-E, so it is easy to get the values of U_1, U_2, τ_1 , τ_2. Thus $R_1 = \frac{U_1}{I}$, $R_2 = \frac{U_2}{I}$, $C_1 = \frac{\tau_1}{R_1}$, and $C_2 = \frac{\tau_2}{R_2}$ are computed. According to this, the unknown parameters in the RC equivalent model can be calculated by this method, which provides a basis for subsequent modeling. Figure 2.3.4.2 shows the interface of the Matlab cftool toolbox.

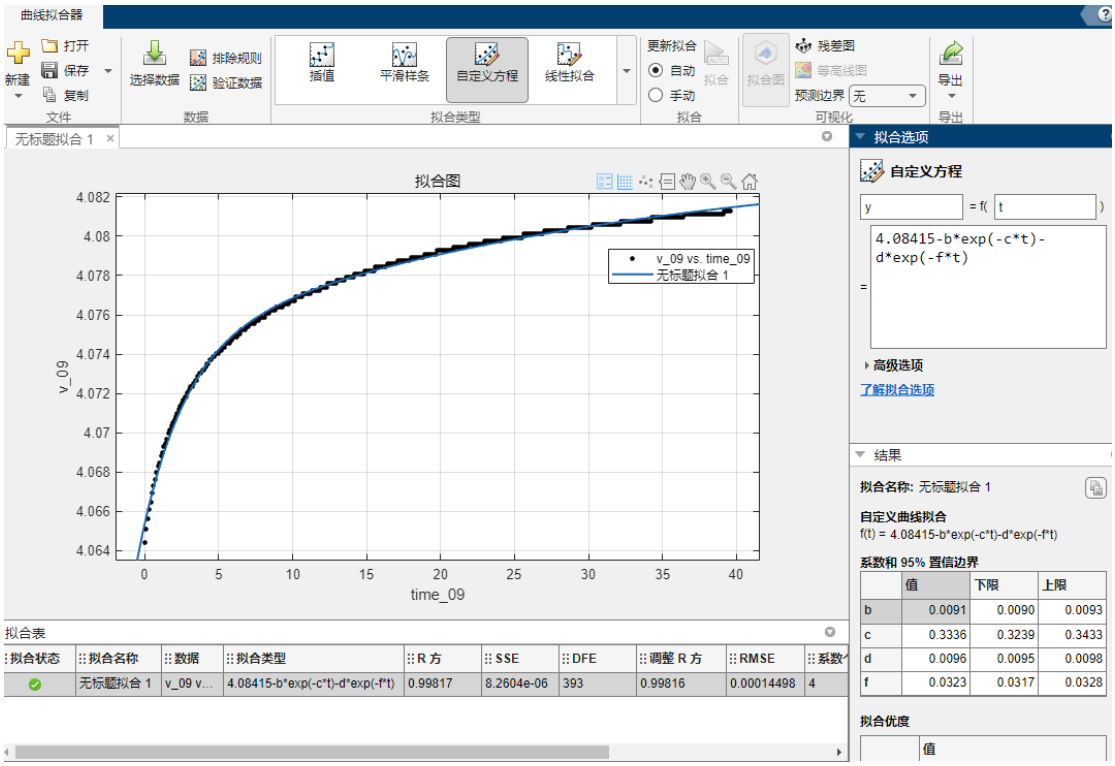

Figure 2.3.4.2 Matlab cftool operation interface

Stages B-C in Figure 2.3.4.1 correspond to the zero-state response of the RC loop of the lithium battery, where the battery is discharged at a constant current of 3A and the voltage tends to slow down. Equation 2.13 can be obtained from the physical meaning of the equivalent resistance and capacitance in the RC loop.

$$E = U_{\mathrm{oc}} - IR_0 - IR_1\left(1 - \exp\left(-\frac{t}{\tau_1}\right)\right) - IR_2\left(1 - \exp\left(-\frac{t}{\tau_2}\right)\right) \quad (2.13)$$

According to the above parameter identification method, using the logic that every 10% SOC serves as a reference point, the ohmic internal resistance R_0, polarization internal resistances R_1 and R_2, and equivalent capacitances C_1 and C_2 of the lithium battery are estimated. The results are shown in Table 2.3.4.1.

Table 2.3.4.1 Estimation result of lithium-ion battery parameters in 25 degrees

SOC	R0(Ω)	R1(Ω)	R2(Ω)	C1(F)	C2(F)
0.1	0.02916	0.00627	0.01910	566.07	9349.29
0.2	0.02105	0.00387	0.00930	1161.30	12359.41
0.3	0.01954	0.0024	0.00483	1627.61	16163.79
0.4	0.01923	0.00247	0.00510	1489.37	13711.78
0.5	0.01928	0.00267	0.00497	1462.56	13159.63
0.6	0.01929	0.0027	0.00477	1417.41	15313.15
0.7	0.01937	0.0033	0.00683	1136.80	9502.69
0.8	0.01949	0.0036	0.00677	1072.09	7902.85
0.9	0.02002	0.0044	0.00473	651.40	7883.12
1.0	0.02233	0.0039	0.00413	551.78	6048.39

Table 2.3.4.1 statistics the estimated parameters of the battery equivalent circuit model at 25°C. Parameter estimates at other temperatures will be calculated in the same way. Through the data in the table, it can be seen that the ohmic internal resistance value of the battery is relatively small, about 20mΩ, which is in line with the present common lithium battery internal resistance range. In the lithium battery products many years ago, the internal resistance value is about 50-100mΩ. With the progress of battery materials and electrolytes and winding methods, the capacity of single batteries has been greatly improved. The internal resistance of the battery also dropped significantly. Acturally the internal resistance value directly affects the heat generation of the battery core, so the correct of its value has a significant impact on the accuracy of the battery temperature estimation. Figure 2.3.4.3 shows the trend of ohmic internal resistance R0 changing with soc at 25 degrees (room temperature).

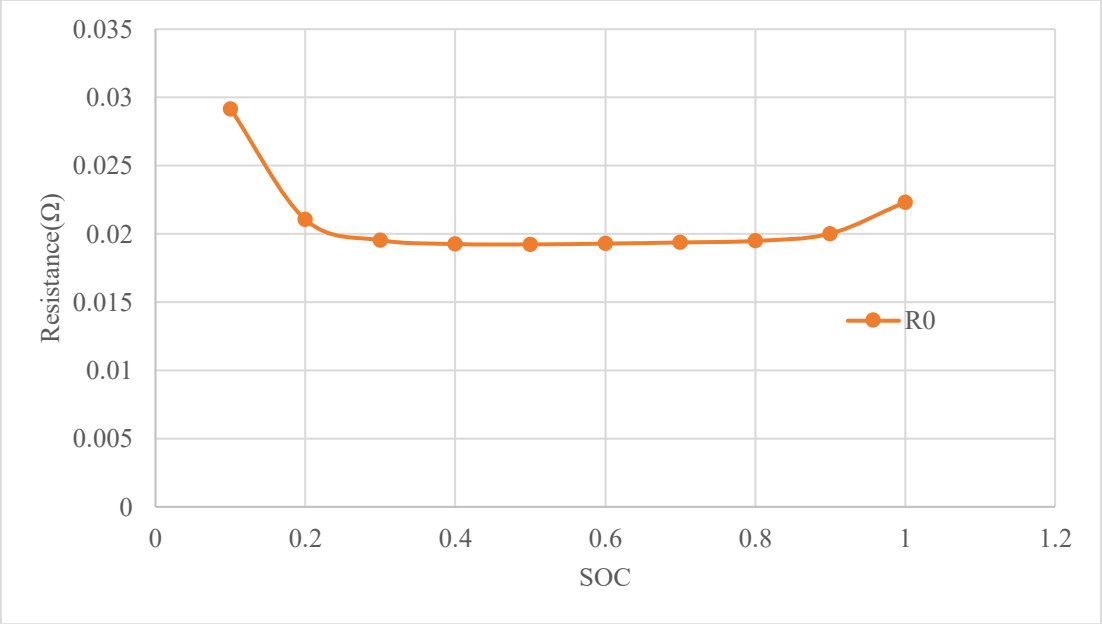

Figure 2.3.4.3 The trend of the ohmic resistance R0 as a function of soc at 25 degrees

According to the line chat above, it can be clearly seen that the value of the battery ohmic internal resistance has increased significantly at low soc, which is also in line with the physical law under normal conditions. When the available power of the battery is low, the internal reversible chemical reactions approach their upper limit, and the chemical reactions tend to proceed in the reverse (charging) direction. At this time, the movement resistance of Li+ in the electrolyte is significantly increased. When the values of soc between 0.2 and 0.9, the ohmic internal resistance R0 tends to be constant. Figure 2.3.4.4 illustrates the variation of polarization resistances R_1 and R_2 with SoC at a room temperature of 25 degrees.

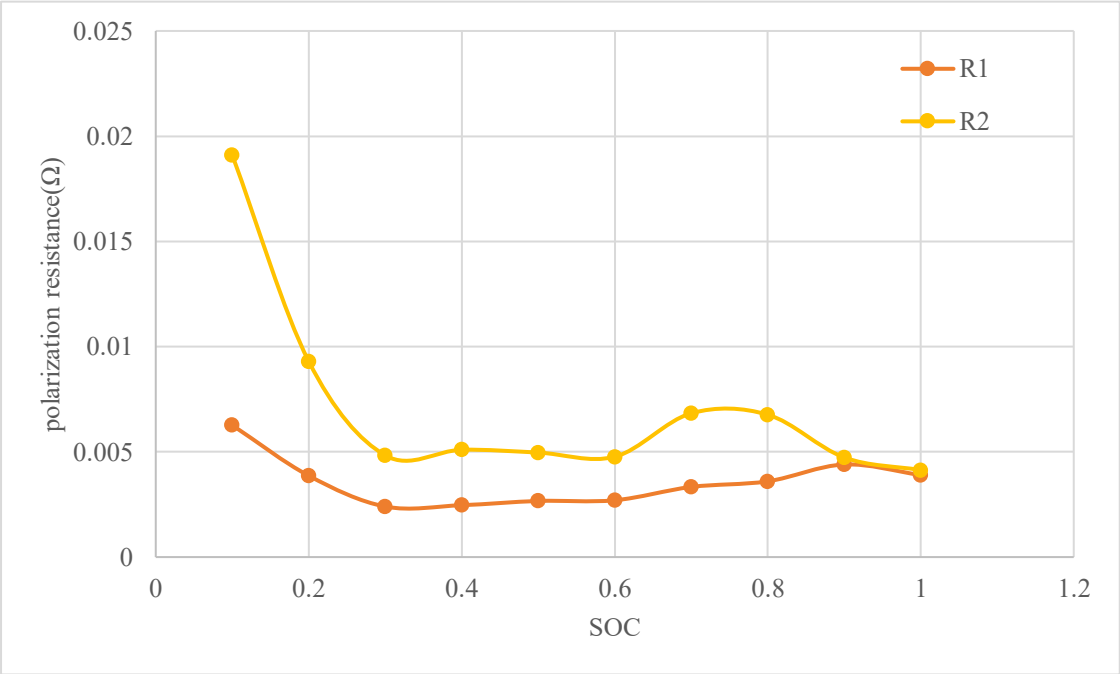

Figure 2.3.4.4 Variation of polarization resistance R1R2 with soc at 25 degrees

It can be clearly seen from the figure that the polarization internal resistance value is significantly smaller than the ohmic internal resistance, which is in line with the realistic physical law. The polarization resistance reflects the polarization and diffusion effect of the battery. Meanwhile the polarization and diffusion effects are hot research topics in the field of lithium battery electrochemistry in recent years. From a microscopic point of view, the magnitude of its resistance value reflects the resistance of Li+ in the process of diffusion from the surface to the interior of the electrode material. It also reflects the resistance caused by the uneven distribution of Li+ in the electrolyte. At the same time, the voltage fluctuations caused by the mismatch between the rate of chemical reactions occurring on the electrode surface and the current intensity outside the cell are reflected by the polarization resistance. When the battery level is low (soc=0.1), both R_1 and R_2 significantly increase, reflecting the phenomenon that the electrochemical reaction occurring on the electrode surface is more difficult to proceed toward one side (positive or negative). At the same time, it also reflects that the discharge performance of the battery will be weakened in the low soc value.

2.4 Matlab model development and error analysis

After identifying the parameters in the RC equivalent circuit model by using the data

obtained from the battery HPPC test, it needs to be verified by Matlab modelling. Matlab platform is integrated with visual mathematical model programming interactive window simulink program. Through visual modular programming operations, users can save a lot of programming time and realize the goal to construction of complex mathematical models. Therefore, we use simulink for the construction of the second-order RC model and the verification of the results. The overall architecture of the second-order RC equivalent circuit model on the simulink platform is shown in Figure 2.4.1.

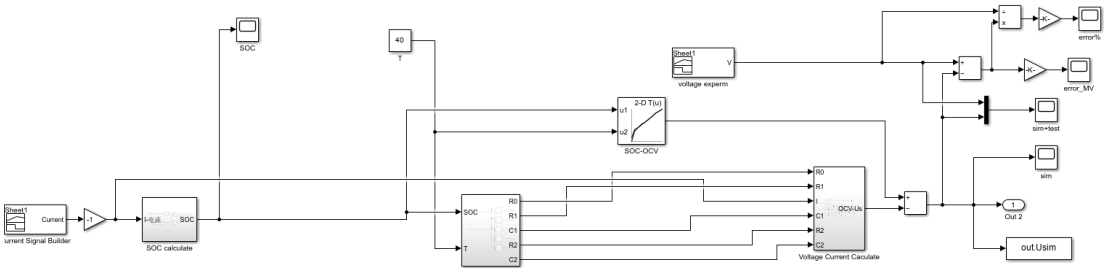

Figure 2.4.1 The structure of second order RC model of Matlab simulink

The calculation method used in the SOC calculation module is the ampere-hour integration method. At present, there is no unified standard for the definition of battery SOC. In the international standard, SOC is mainly defined by battery power. The SOC used in this thesis is defined as the ratio of the remaining capacity to the rated capacity. The expression is as follows:

$$SOC = \frac{1-Q_C}{Q_r} \times 100\% \tag{2.14}$$

In Equation 2.14, Q_C is the power consumption of the battery at the current time, and Q_C is the rated power of the battery. SOC value ranges from 0 to 100%. When SOC=100%, the battery is fully charged, and when SOC= 0, the all battery power is released. Where the calculation of Q_C is defined by:

$$Q_c = \int_{t0}^{t1} I \, dt \tag{2.15}$$

Where I is the discharge current, t0 and t1 are the discharge start and stop times, respectively. The computation module architecture of the SOC is shown in Figure 2.4.2.

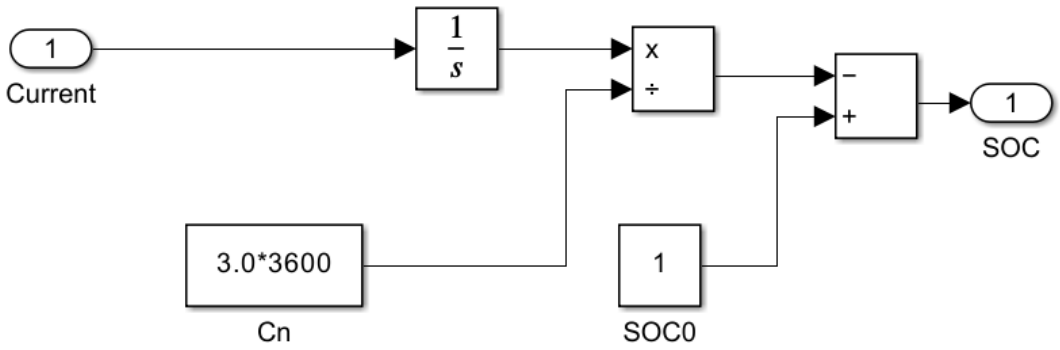

Figure 2.4.2 Structure of SOC calculation model

What is defined in Cn is the rated capacity of the battery, unit in Ah. Soc0 is the initial state. The whole module finally outputs the value of the present soc of the battery. The calculation module of the battery equivalent circuit is shown in Figure 2.4.3 below.

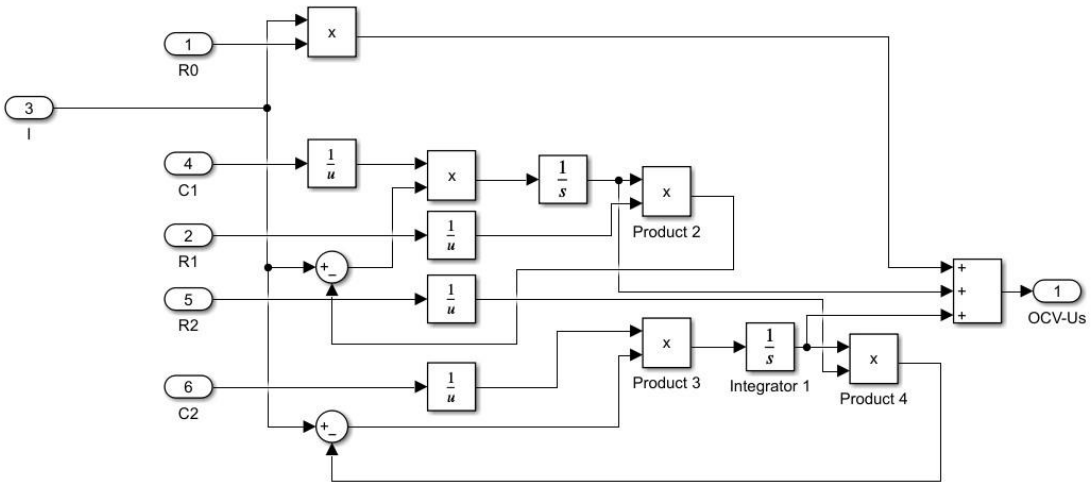

Figure 2.4.3 Structure of RC circuit model of Matlab simulink

The theoretical basis of the second-order RC model comes from Kirchhoff's law of voltage and current. Therefore, according to the knowledge of circuit science, the voltage and current relationship in the equivalent circuit model can be expressed by the following formula.

$$dU_1/dt = \frac{I}{C_1} - \frac{U_1}{R_1 C_1} \tag{2.16}$$

$$dU_2/dt = \frac{I}{C_2} - \frac{U_2}{R_2 C_2} \tag{2.17}$$

$$U_t = U_{ocv} - U_1 - U_2 - IR_0 \tag{2.18}$$

U_{ocv} represents the open circuit voltage of the battery, R_0 represents the ohmic internal resistance of the battery, R_1C_1 represents the polarization resistance and polarization capacitance of the battery, R_2C_2 represents the equivalent resistance and capacitance of Li+ diffusion effect in the battery. U_t and I denote the terminal voltage and current when the battery is working. Figure 2.4.4 shows a comparison of the simulated and experimental data.

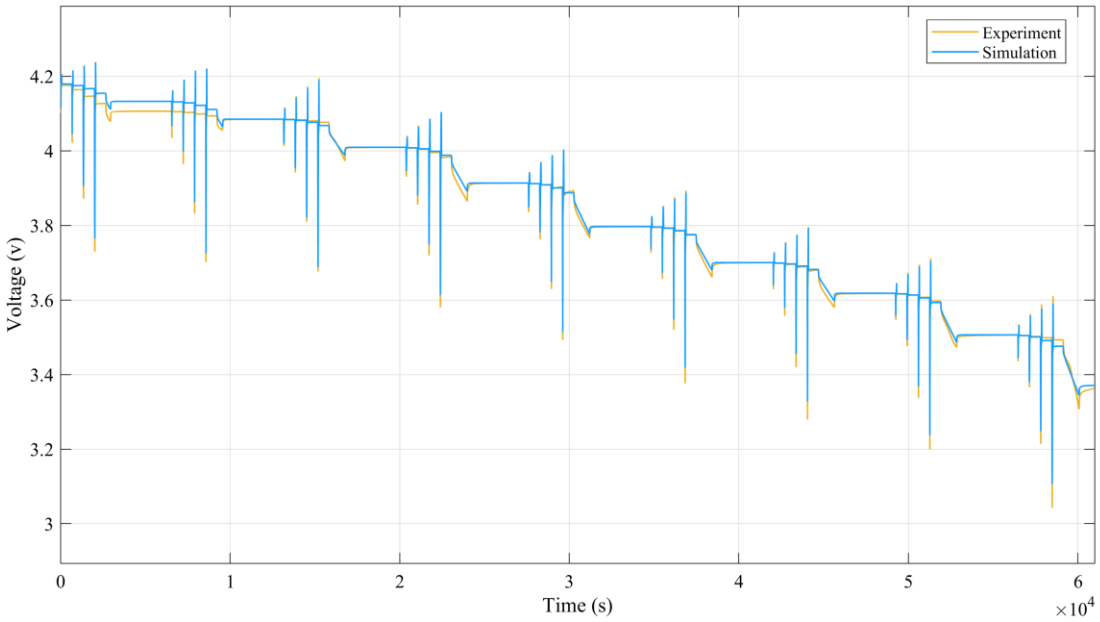

Figure 2.4.4 Comparison of experimental and simulation data of HPPC test

The blue curve in Figure 2.4.4 represents the simulation data, and the yellow curve represents the experimental data. From the overall trend of the two curves, the two curves basically coincide. Only at low soc, the simulation has some error. Also in the state of high current (6C/18A) load, the simulation data and the experimental data show certain errors, which can be observed at the lower edge of the pulse curve in the figure. Figure 2.4.5 shows the error of experimental data and simulation data, and the error value unit is mV.

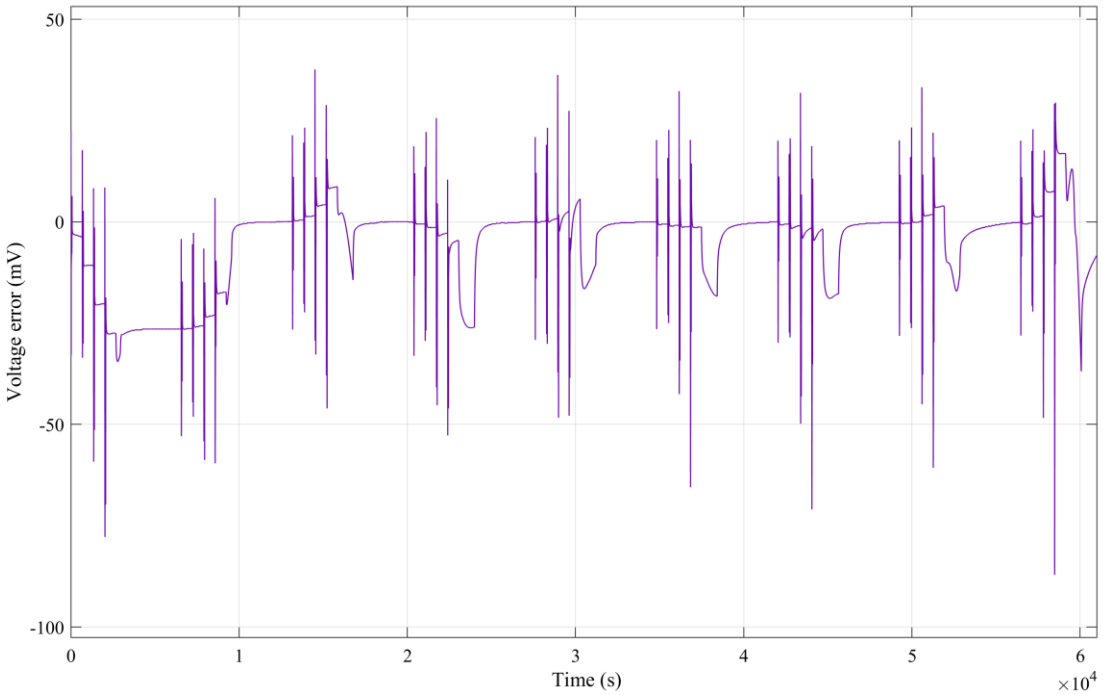

Figure 2.4.5 The error of simulation and experiment data in mV

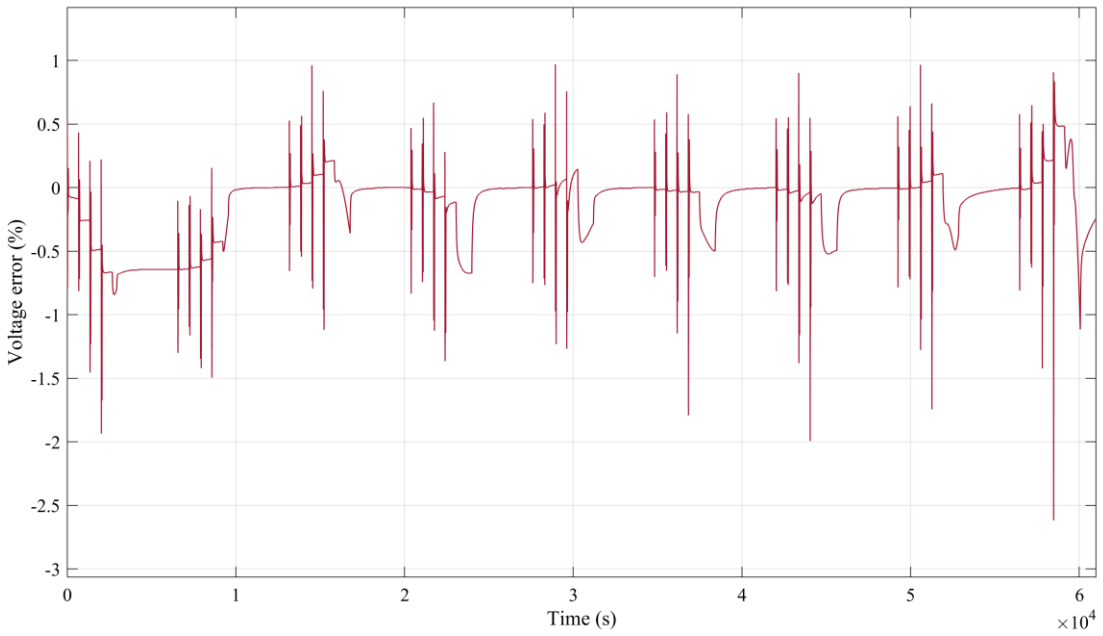

Figure 2.4.6 The error of simulation and experiment data in percentage

From the overall trend of the curve in the figure above, under the state of general intensity current (less than 2C/6A), the calculation error of the model is mostly within 40mV and around 1.0%. Only in the high current state, the calculation error is greater than 50mV and raise to around 1.5%, but for the application scenario of lithium battery, the high current state is not usually the case, so the error in the case of high current

charging and discharging phase can be tolerated. The total RMS error is 0.0115. From the overall error value, the calculation error of the model is acceptable, which proves the validity of the equivalent circuit model and the accuracy of the parameter identification.

3 Research on electrothermal coupling model of lithium-ion battery

3.1 Study on heat generation mechanism

In most cases, lithium-ion batteries are placed in the vehicle's battery pack regularly, one by one, causing limited space between the cells, so heat can accumulate in the battery pack, causing the overall battery pack temperature to rise. This is the reason why people focus on the temperature issue of battery. Normally, chemical reactions inside the battery convert chemical energy into electricity. Still, the technology level of humans limits any energy conversion efficiency to less than 100%, so the conversion of energy types comes with energy loss. The battery has the phenomenon of energy loss in the process of charging and discharging. Much of the energy lost is in the form of heat. As the battery's chemical reactions proceed, heat is generated and absorbed. At present, in the field of electrochemical research, many scholars have proposed that the heat generation of batteries is divided into: Joule heat, chemical reaction heat, polarization reaction heat and a very small amount of battery self-discharge heat generation. The formula for the total heat generation of the battery is given in 3.1.

$$Q = Q_r + Q_{ir} + Q_s \tag{3.1}$$

The heat generated in the chemical reaction inside the lithium battery is expressed by Q_r.While Q_{ir} is irreversible heat and Q_s is the heat caused by battery self-discharging. In fact, the chemical reaction inside the battery is carried out in the positive direction or the reverse direction during the charging and discharging of the battery. This process is accompanied by the generation or absorption of heat. And we call this heat as the reversible heat of reaction. In particular, the charging process is an endothermic reaction marked with a negative value, and the discharging process is an exothermic reaction marked with a positive value. The expression for the heat of reversible reaction is given in 3.2.

$$Q_r = \frac{nmQI}{MF} \tag{3.2}$$

Where, n is the number of single cells; m is the mass of the battery, unit in kg; Q is the

algebraic sum of the heat generated by the electrochemical reaction, unit in J; I is the current, unit in A; M is molar mass, unit in kg/mol; F is Faraday's constant.
The heat of reversible reaction is different from that of irreversible reaction Q_{ir}, which includes Joule heat Q_j and polarization heat Q_p. Usually in the process of discharging and charging lithium battery, Li+ moves between the positive electrode and the negative electrode, and the heat generated in the process of overcoming the resistance is called Joule heat. In the total heat generated by lithium batteries, Joule heat is the majority source. Because the magnitude of its value is related to the battery materials, it is similar to the heat generated by the resistance of a cable. The amount of Joule heat is related to the current magnitude of the battery. The ohmic internal resistance R_0 identified in Chapter 2 is related to Joule heating. So the calculation formula is given in 3.3.

$$Q_j = I^2 R_0 \tag{3.3}$$

I is the current, unit in A; R_0 is the ohmic internal resistance, unit in Ω.
In the process of battery charging and discharging phase, its internal polarization effect, which external behaviour is battery terminal voltage will have a small drift phenomenon. Thus, the concept of polarization internal resistance is derived from this. In Chapter 2, the values of R1 and R2 in the equivalent circuit model are coming from the polarization phenomena of the battery cell. Of course, polarization internal resistance will also generate heat under the action of current load, which is called polarization reaction heat Q_p. The formula is shown in 3.4. It contains the heat related to ohmic polarization, electrochemical polarization and concentration gradient polarization.

$$Q_p = I^2(R_1 + R_2) \tag{3.4}$$

Therefore, the heat of irreversible reaction is the sum of the of polarization reaction heat and Joule heat, as shown in Equation 3.5

$$Q_{ir} = Q_p + Q_j = I^2(R_1 + R_2 + R_0) \tag{3.5}$$

In fact, a small part of the heat production of the battery is generated by the side reaction. For example, the battery capacity will drop after a long period, which is due to the chemical reaction of the battery electrode material. This reaction does not generate external current, but internal decomposition. So finally resulting drop in battery power. This heat produce situation belongs to a kind of side reaction. Another side reaction is the decomposition of the battery electrolyte at higher temperatures, which is

accompanied by the release of heat. However, the magnitude of the side reaction heat production of the battery at room temperature is very small, and the specific calculation formulas are very complex, so this part of the calculation can be ignored.

To sum up, when lithium-ion batteries are charged and discharged, there many internal reactions happen, and the real process of heat generation is very complex, and cumbersome formulas are needed to express all the processes through mathematical modelling. Besides, many electrochemistry parameters are also not easy to obtain by testing. Therefore, the calculation formula of lithium battery heat generation needs to be simplified reasonably.

At present, there are two main methods to build the heat generation rate model of lithium-ion batteries. One is mainly dependent on experimental data and summarizes the empirical formula, and the other is based on theory, such as the battery heat generation formula described above. These two methods have advantages and disadvantages, the establishment of empirical formula needs to rely on a large number of experimental data, but according to the existing theory to establish the formula is quite complex process. Therefore, at a very early stage, D.Bernardi[38] et al. proposed a simplified calculation model of battery heat generation rate by combining the electrochemical and thermodynamic theories, which ignored the heat generation of side reactions of batteries and focused on the heat generation of reversible and irreversible reactions of batteries. This formula is shown in 3.6.

$$Q_{all} = I(U_{ocv} - E) - IT\frac{dU_{ocv}}{dT} \tag{3.6}$$

In the formula 3.6, Q_{all} represents the total heat generation power, I represents the battery charge and discharge current, and U_{ocv} and E represent the battery open circuit voltage and terminal voltage, respectively. Therefore, the first term on the right side of the formula represents the irreversible reaction heat generation of the battery, which is mainly related to the ohmic and polarization internal resistance of the battery. The second term is the reversible reaction heat generation, where T represents the average temperature of the cell and $\frac{dU_{ocv}}{dT}$ represents the level (derivative) of the open-circuit voltage change with temperature. In summary, through the simplified formula, it is relatively easy to calculate the heat generation power of the battery. Combined with the heat dissipation formula that needs to be studied later, the change of the battery temperature can be obtained.

3.2 Study on heat dissipation mechanism

According to the study in the previous subsection, the lithium battery will be accompanied by the generation of heat when it is charged and discharged, so the heat power will not be concentrated in one point forever, and the generated heat will affect the heat source surroundings through heat conduction, heat convection and radiation. Of course, some of the heat generated by the battery is absorbed by itself, causing the battery temperature to rise, and some of the heat is dissipated to the environment.

For the heat absorbed by the battery itself, the specific heat capacity of the battery material and electrolyte has a significant impact on how much heat it absorbs, and Equation 3.7 shows the capacity of the battery to absorb heat.

$$Q_b = C_p m \Delta T \tag{3.7}$$

In the formula 3.7, C_p is the specific heat capacity of the battery in J/ (Kg*K), m is the battery mass in kg, and ΔT is the temperature change value of the battery during the measurement period.

There is a battery temperature detection module in the BMS of the car, which has the ability to control the cooling system. Usually, the cooling method of battery pack is mainly air cooling, which is mainly based on the theoretical basis of convective heat dissipation. Heat convection refers to the process of heat exchange between a fluid and a solid. In the lithium-ion battery pack, the heat exchange between the battery surface and the internal air fluid causes the temperature of the battery cell to change. Under normal conditions, we consider the natural convection of air, rather than turbulence and other non-general conditions. Therefore, the process of convective heat transfer can be shown by Equation. 3.8.

$$q_e = hA(T_b - T_a) \tag{3.8}$$

Where, h is the convective heat transfer coefficient, unit in W/m2·K; A is the area of convective heat transfer, unit in m3; T_a is the ambient air temperature, unit in K; T_b is the battery surface temperature, unit in K.

In addition, after the heat source of the battery core generates heat, the heat is transferred to the battery surface by means of heat conduction, so that the data of temperature change of the sensor fixed on the battery surface is obtained. It follows from Fourier's law that the heat flux is got in equation 3.9.

$$q_x = -\lambda \nabla T = -\lambda \frac{\partial T}{\partial x} \tag{3.9}$$

Where, q_x is the heat transfer rate along the x direction, unit in Wm^{-2}; λ is the thermal conductivity, unit in W/ (mK); $\frac{\partial T}{\partial x}$ is the temperature gradient along the x direction; T is the temperature; The negative sign indicates the transfer of thermal energy in the direction of decreasing temperature. Fourier's law assumes that the direction of heat flow transfer of objects is isotropic, while the actual heat transfer process of lithium-ion batteries is anisotropic, and the heat flow transfer in all directions is not the same. It is necessary to establish the mathematical model of 18650 lithium-ion batteries according to the actual situation, so the cylindrical coordinates are selected to establish the mathematical model of cylindrical batteries. Consider the heat inflow of a microelement from cylindrical coordinates in three directions:

$$\phi_r = -\lambda A \frac{\partial T}{\partial r} = -\lambda r d\phi dz \frac{\partial T}{\partial r} \tag{3.10}$$

Equation 3.10 shows the heat inflow in the radial direction; of course, the heat inflow in the z-axis direction and the heat inflow in the Angle φ should also be considered. Therefore, we finally obtain the differential equation of heat conduction in cylindrical coordinate system as shown in Equation 3.11

$$\rho C_p \frac{\partial T}{\partial \tau} = \frac{1}{r}\lambda \frac{\partial T}{\partial r} + \lambda \frac{\partial^2 T}{\partial r^2} + \lambda \frac{\partial^2 T}{\partial z^2} + q \tag{3.11}$$

Where $\frac{\partial T}{\partial \tau}$ is the change rate of temperature, C_p is the specific heat capacity of the battery, unit in J/ (Kg*K), ρ is the density of the battery, unit in kg/m^3, q is the heat generation rate of the battery, unit in w/m^3

In addition to the heat conduction mode described above, there is a form of heat transfer type, which is heat radiation. The sun shines light on the earth, and things on the earth warm up. This is the typical heat radiation familiar by us. Its formula is given in 3.12

$$q_{radio} = \varepsilon A \sigma (T^4 - T_a^4) \tag{3.12}$$

Here, ε is the emissivity of the object, σ is the Stefan Boltzmann constant, A is the surface area of the object, T is the battery temperature, and $T_a$is the temperature of the external environment.

Generally, part of the thermal motion of molecules and atoms in the internal structure

of an object is converted into the energy of an electromagnetic wave, which is absorbed by another object and causes a change in temperature. This process is called heat radiation. As long as the temperature of the object is higher than absolute zero, electromagnetic waves will be emitted outward, so the lithium battery has the effect of heat radiation in the battery pack, but this effect can be ignored in statistical significance. Therefore, in this study, the thermal radiation factor of the battery itself is ignored.

3.3 Development of Matlab electrothermal coupling model

Lithium-ion batteries will generate heat in the process of discharging and charging. The heat mainly comes from the ohmic internal resistance related to the battery material and internal reversible chemical reactions, in which the heat power generated by the ohmic internal resistance accounts for a large part. Under the joint action of the battery's own heat absorption and external heat dissipation conditions, the internal and surface temperature of the battery is also changed. When the temperature increases and decreases, it is known from physical knowledge that the resistance and chemical reaction rate of the battery will change. In other words, the ohmic internal and polarization internal resistance of the battery are related to the temperature. Even if the battery is idle, as long as the temperature changes, the internal resistance parameters of the current battery will change. When the internal resistance changes, the heat production rate associated with it changes. In the previous section, the internal resistance of the battery is also related to soc, that is to say, the internal resistance parameter of the battery is affected by both temperature and soc. As the battery continues to be charged or discharged, the SOC will change, which will cause the heat generation rate to change again (the heat dissipation rate is related to the external environment) and affect the total heat output of the battery. To sum up, the working process of lithium-ion batteries is a process of interaction between electricity and heat. Therefore, when modeling the battery through mathematical methods, it is necessary to consider the linkage between the electrical characteristic model and the thermal model, so as to ensure that the parameters in the electrical model can be updated according to the temperature various, and finally realize the research goal of electro-thermal coupling model. Figure 3.3.1 illustrates the logical structure of the electrothermal coupling model.

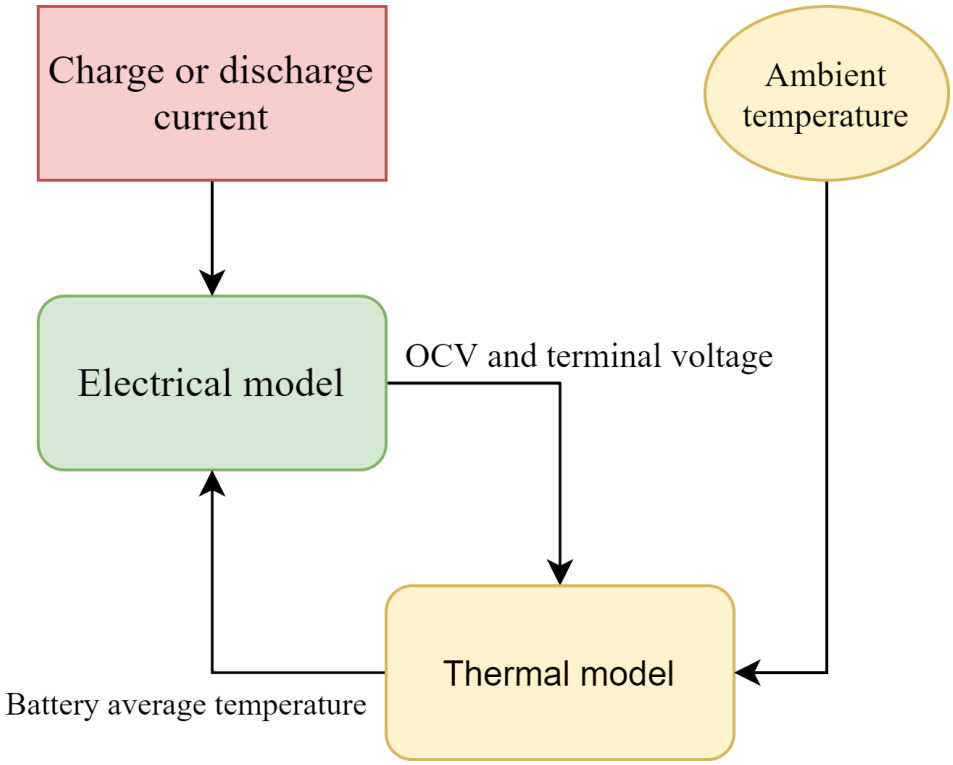

Figure 3.3.1 Logical structure of the electrothermal coupling model

It can be seen from the structure diagram 3.3.1 that when the lithium battery is discharged or charged, the electric model takes the current as the input, and the open circuit voltage and terminal voltage as the output values into the thermal model. After calculation, the thermal model takes the average temperature of the battery as the output and passes it to the electrical model as the updating value for the next step to update the battery terminal and open circuit voltage.

The previous sections of this chapter introduced the heat generation and heat dissipation mechanism of lithium batteries, which will serve as the theoretical basis for subsequent matlab modeling. In terms of the heat generation model construction, it is mainly according to the heat generation rate model of lithium batteries which proposed by D. ernardi et al many years ago, the formula is shown in Eq 3.6 in the first section of this chapter. The simplified model uses the open circuit voltage and terminal voltage of the battery calculated from the electrical model to get the heat generation power of the lithium battery. However, the value of $\frac{dU_{ocv}}{dT}$ (which represents the degree of open-circuit voltage variation with temperature) in this formula needs to be realized by well designed battery CC-CV experiments with different ambient temperatures, so the data of this variable comes from the experiment of Y.Kuai[39] who used the same type battery of the electrical model in chapter two. So based on the above research, a

simplified heat generation rate model of lithium battery is built on the Matlab Simulink platform, as shown in Figure 3.3.2.

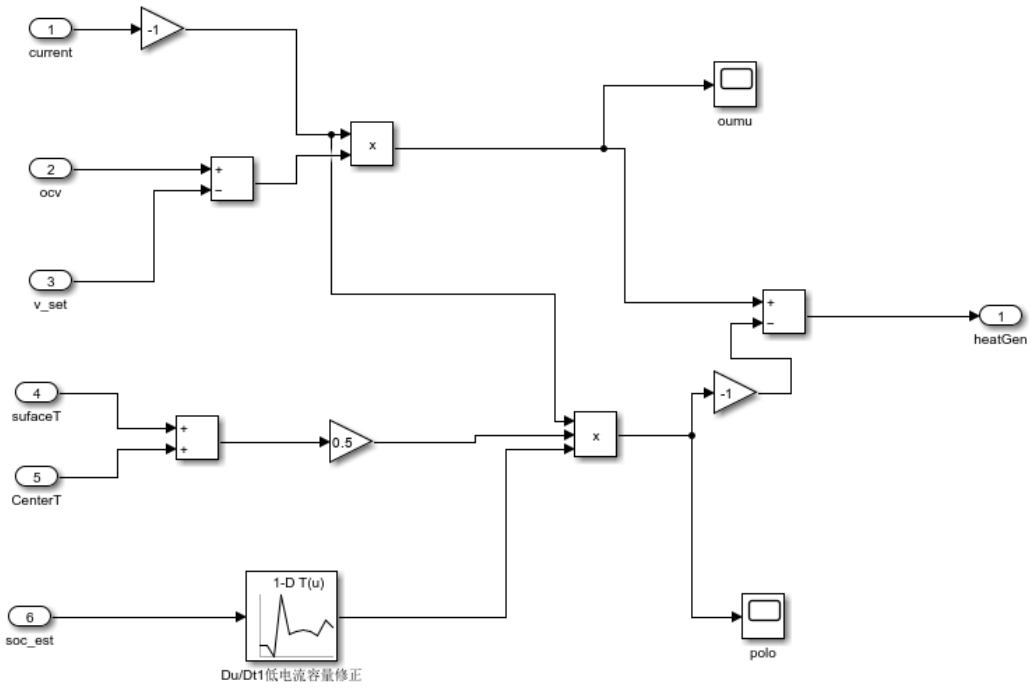

Figure 3.3.2 Heat generation rate Matlab model of lithium battery

Similarly, according to the heat dissipation mechanism of lithium batteries described in the previous subsection, we also need to make some assumptions to simplify the mathematical formula of heat conduction, so that the temperature change of the battery can be obtained with less calculation workload. Therefore, we need to reduce the complexity of the practical case, which is to make some assumptions about the conditions under which the model will be applied.

a. The internal heat of the lithium-ion battery is generated by the core, and the heat is uniformly transferred in the battery.

b. The thermal properties of the inner materials of lithium ion batteries are little affected by temperature, and their main properties do not change with temperature

c. The temperature distribution in the Z axis of the lithium-ion battery is uniform, and the heat is only generated by the center and transmitted along the radial direction.

d. Ignore the side reaction heat generation of lithium batteries, and only consider the heat generated under the action of ohmic and polarization internal resistance (assumption of heat generation model proposed by D.Ernardi).

f. Only the influence of internal heat transfer and surface convective heat transfer of the battery is considered, and the thermal radiation effect is ignored (the main reasons are analyzed in 3.2).

According to the above assumptions, the lumped parameter model is finally used as the basis for the thermal model. The overall architecture of the thermal model is shown in Figure 3.3.3.

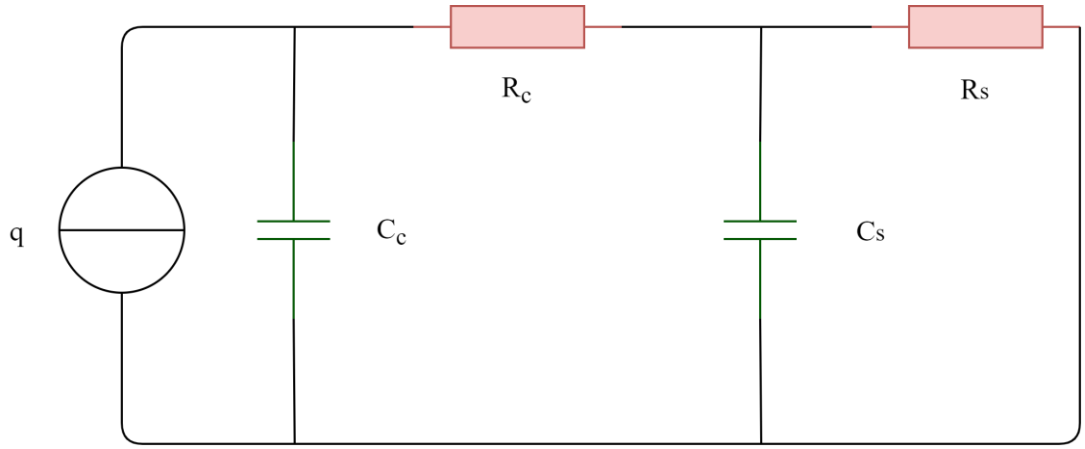

Figure 3.3.3 The overall architecture of the thermal model (thermal dissipation part).

The structure of the thermal model in the figure implements the function of internal and external temperature estimation of the lithium battery. The lumped parameter model applies the thermoelectric analogy principle, using the equivalent substitution method to represent the battery's temperature field as an equivalent electric field. The ideal current source in the figure can be considered as a battery heat source. The resistance R_c expresses the thermal resistance from the center to the edge of the battery, the capacitance C_c expresses the thermal capacity of the material inside the battery, the resistance R_s represents the thermal resistance of the convection heat transfer between the battery shell and the ambient air, and the capacitance C_s represents the thermal capacity of the battery shell. Therefore, the circuit nodes voltage can be regarded as the core temperature and surface temperature of the battery. Finally, combined with the knowledge of electrotechnics, we can derive the expression of the lumped parameter thermal model, as shown in 3.13 and 3.14.

$$C_c \frac{d(T_c - T_0)}{dt} = q - \frac{T_c - T_s}{R_c} \tag{3.13}$$

$$C_s \frac{d(T_s - T_0)}{dt} = \frac{T_c - T_s}{R_c} - \frac{T_s - T_0}{R_s} \tag{3.14}$$

However, the numerical calculation of the heat capacity and thermal resistance in the lumped parameter thermal model depends on the data of the battery heating experiment,

especially the estimation of the equivalent resistance R_c which represents the heat capacity between the core and the edge of the battery depends on the core temperature data of the battery heating experiment. In general, the battery core temperature data has been difficult to obtain, because it is difficult to place temperature sensors in the battery core. Kuai.Y[39] et al., an experimental team from a university in China, put a temperature sensor into the center of a ternary 18650 lithium battery (the same type as the battery used in the electrical characteristic model in this thesis) to obtain the core temperature data of this type of battery in the process of discharging and charging. The Partical Swarm Optimization method is used by them research team to estimate the equivalent resistance and capacitance values of the lumped parameter thermal model, and the parameters of the thermal model are successfully determined under the general condition. The specific parameters are shown in Table 3.3.1

Table 3.3.1 Results of parameter identification of the lumped thermal model[39]

R_c (K/W)	2.82
R_s (K/W)	9.73
C_c (J/K)	41.73
C_s (J/K)	12.85

Finally, according to the structure of the lumped parameter thermal model and related physics knowledge, the mathematical model was built on Matlab Simulink, and the structure is shown in Figure 3.3.4.

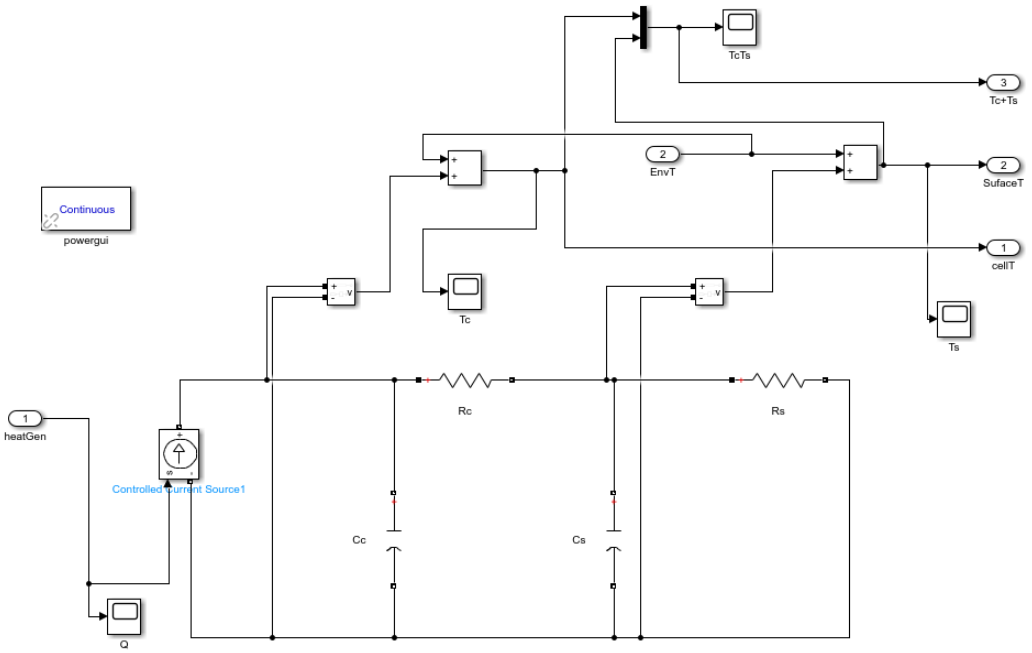

Figure 3.3.4 Structure of lumped parameter thermal model in Matlab

Matlab provides integrated components in physics for users to build mathematical models and reduce the complexity of model construction. The ideal current source in the figure simulates the heat source of the battery. According to the similar characteristics of thermoelectricity, the voltage at both ends of the capacitor C_c can be compared to the core temperature of the battery, and the voltage at both ends of the capacitor C_s can be compared to the surface temperature of the battery. Therefore, the temperature change of the battery can be estimated by this lumped parameter thermal model. Of course, we regard the temperature distribution in the Z-axis of the battery as a uniform distribution, and only consider the temperature change in the radial direction of the battery, so as to reduce the complexity and calculation workload of the model. Finally, the electro-thermal coupling model of lithium battery is obtained by combining this model with the electric characteristic model of battery. The overall structure is shown in Figure 3.3.5.

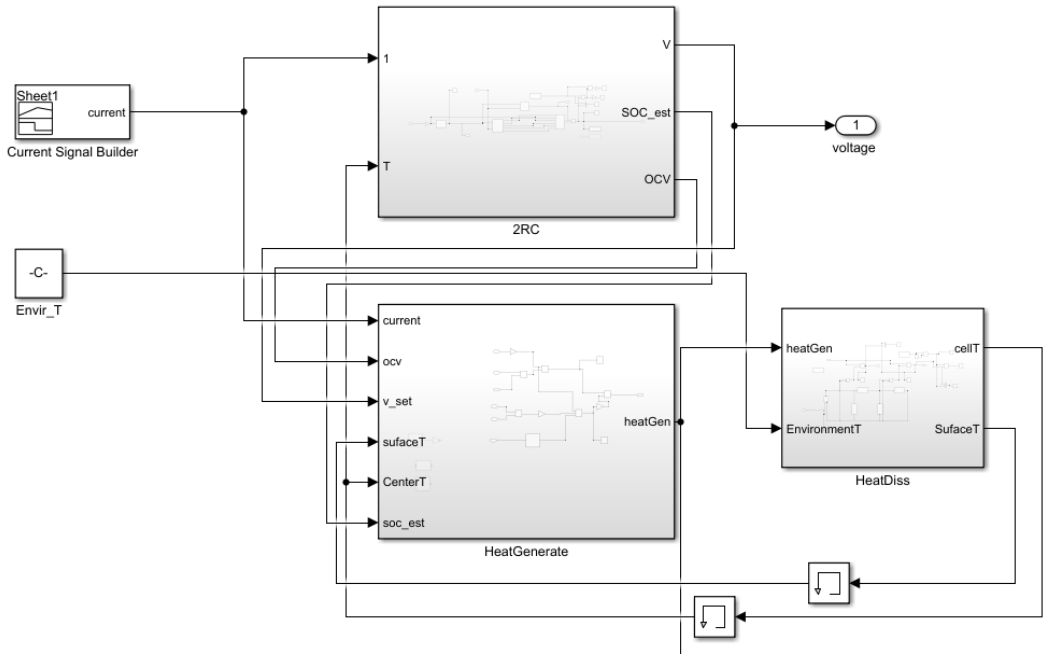

Figure 3.3.5 Architecture of electrothermal coupling model of battery on Matlab.

In the electro-thermal coupling model shown above, we set the temperature value input to the electrical model as the average of the surface temperature and the core temperature of the battery. This approach aims to balance the impact of temperature differences across the radial direction of the battery. The temperature variation data output from the electro-thermal coupling model, reflecting the battery characteristics, will be discussed and analyzed in Chapter 5.

4 Development of Matlab EV motion system model

In the previous section, we established the electrothermal coupling model of lithium battery, which can simulate the temperature and terminal voltage changes of lithium battery in the process of discharging or charging. This model can be used as a basis for an automotive BMS. However, in order to study the electrothermal characteristics of lithium batteries in the actual use process of vehicles, it is necessary to obtain the power demand data of automobile motors. Therefore, in this chapter, the electric vehicle is selected as the research object and the power device of the vehicle is modeled. The established model is a simplified model, which considers the longitudinal motion and ignores the pitch or roll motion of the vehicle. Thus the modeling focuses on the powertrain force aspect of the vehicle.

4.1 Vehicle structure and parameters

Compared with traditional internal combustion engine vehicles, electric vehicles are relatively more flexible in the arrangement of power transmission systems and related components. Typically, electric vehicles have a simpler powertrain architecture than vehicles with internal combustion engines, because electric vehicles have few transmissions. The reason for this is that the efficient working area of the electric motor is significantly larger than that of the internal combustion engine, which makes the transmission play a small role in the electric car, and also designing complex transmission increases the complexity and production cost of the powertrain system, and eventually many electric car manufacturers simply eliminate the transmission configuration. At present, the transmission of electric vehicles is divided into two types, one is driven by a single motor, and the other is driven by multiple in-wheel motors. In this thesis, we mainly consider the case of single motor drive, while ignoring the role of inverter. In the real world, the inverter converts the DC from the battery pack into AC to drive the motor, but this also depends on the specific type of motor. In this study, automotive powertrain modeling is mainly concerned with obtaining the power demand curve of the motor and applying it to the current demand calculation of the battery pack, which is finally used to simulate the multi-parameter response of the battery pack in response to standard road testing cycles. In Figure 4.1.1 a powertrain system architecture for an electric vehicle is shown.

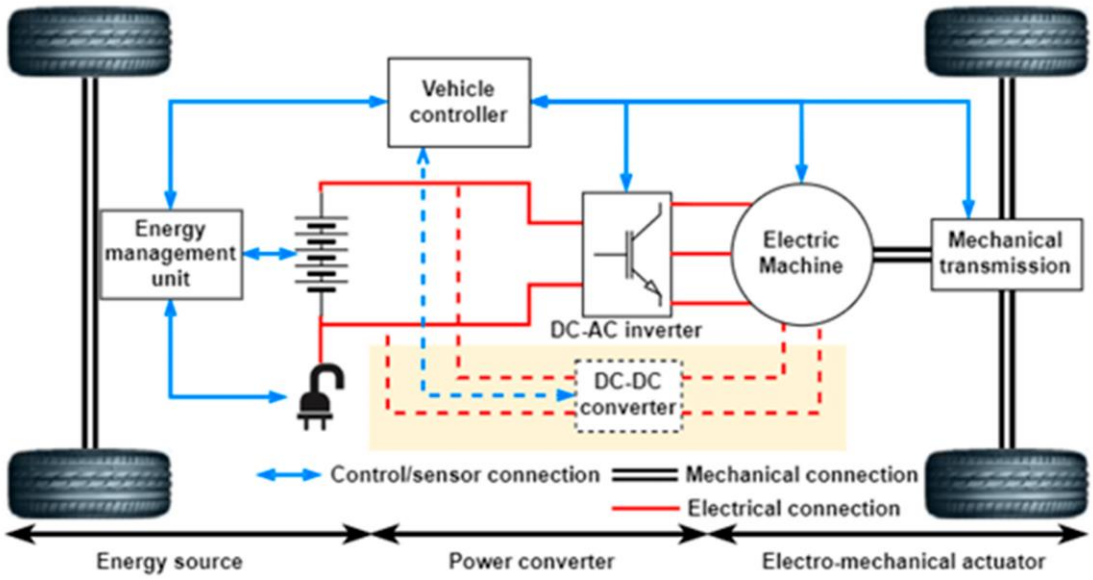

Figure 4.1.1 A kind of EV powertrain architecture[40]

From the picture above, it can be seen that the powertrain architecture of electric vehicles is relatively simple, and the design is more inclined to the collaborative work of electromechanical systems. During the construction of the mathematical model of the vehicle in this chapter, we consider the electric motor connected to a differential with a fixed transmission ratio. The basic parameters of the EV are presented in Table 4.1.1.

Table 4.1.1 Basic parameters of electric vehicle

Main parameters	Value
Mass (empty load)	1170 Kg
Radius of tire	0.284
Front area	2.6 m^2
Drag coefficient	0.3
Mass (battery pack)	245 Kg
Reduction gear	9.3
Transmission efficiency	0.9
Total mass (empty load with battery and passenger)	1515 Kg

The data in Table 4.1.1 are only the most important data needed for the longitudinal dynamic simulation of electric vehicles. From the researchers side, the dynamic parameters of the vehicle are difficult to obtain through the public database. So for these kind of parameters that are difficult to measure, so general values are used in the

modeling process of the simulation. For example, front area, drag coefficient and so on, because such values need to be obtained through wind tunnel experimental data. In summary, the longitudinal motion simulation of electric vehicle focuses on the acquisition of the power demand, which will serve as the basis for the subsequent simulation of the electric-thermal characteristics of the battery.

4.2 Matlab model of transmission system

The automobile transmission system mainly transfers the torque of the electric motor to the wheel, so that the wheel can turn against the resistance. For the internal combustion engine, the output power is low at low speed and the efficiency value is relatively low. Therefore, in order to improve the working efficiency of the engine, the automobile transmission system adjusts the gear ratio of the transmission box to realize the engine speed in the best working range. In this way, the traction characteristics of the vehicle are close to the ideal condition. However, for the motor, its working characteristics are close to the ideal engine, that is, it still has a good torque output ability at low speed, and a constant power output at high speed. So for electric vehicles, the transmission system can be simplified, using two gears or no gearbox directly, using only the reducer. If we know the output torque of the engine, the driving force F_t of the car can be calculated by Eq. 4.1.

$$F_t = \frac{T_e i_0 \eta_t}{r_w} \tag{4.1}$$

In Equation 4.1, F_t is the driving force of the vehicle, and the unit is N;

T_e is the output torque of the engine in N m;

i_0 is the ratio of the reducer;

η_t is the transmission efficiency;

r_w is the radius of the wheel, here the effective radius approximately equal to the radius of wheel, the unit is m.

From Equation 4.1, it can be seen that the role of the reducer helps the car to ensure a sufficiently large traction force at low speed, because a larger reduction ratio will increase the traction force when the torque is constant. Of course, the acceleration of a vehicle is determined by both traction and resistance.

In the process of driving, the resistance of the car includes rolling resistance and air resistance. If there is a slope on the road surface, the car gravity component parallel to the slope will become the driving resistance of the car. If the speed of the vehicle is

increasing, its acceleration will also produce what is called acceleration resistance. Here, the rolling resistance F_r is defined as Eq. 4.2.

$$F_r = mg(f_0 + Kv^2) \tag{4.2}$$

Where f_0 is the rolling coefficient and K is a very small value to correct the influence of the rolling resistance coefficient on the speed. In the simulation of this thesis, the value of f_0 is 0.0136, which is used to simulate the driving state of the vehicle on the general road. The value of K is 0.4e-7, which is the empirical value of the correction coefficient of the radial tire under the condition that the speed is not higher than 150km/h. Figure 4.2.1 shows the structure of the rolling resistance calculation module of the Matlab.

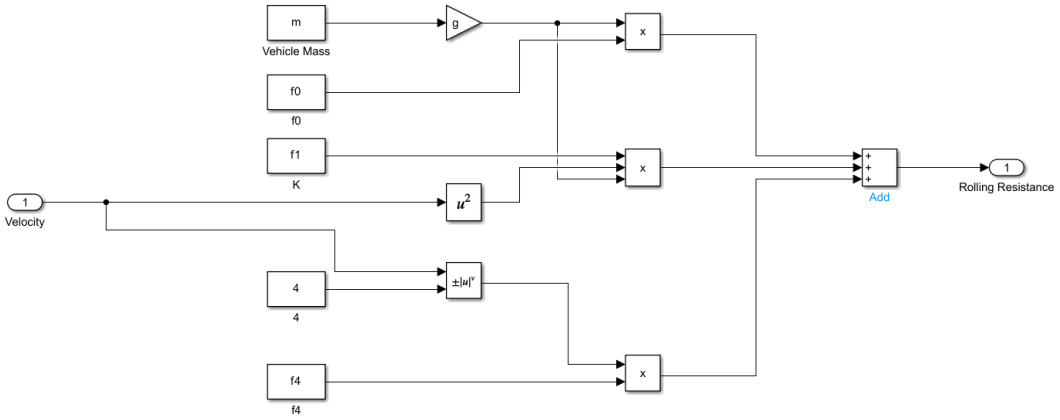

Figure 4.2.1 Matlab model of rolling resistance

In Figure 4.2.1, parameter f_1 represents the K rolling resistance correction coefficient in Formula 4.2, and f_4 represents the modification value of the resistance change caused by the lift force received by the vehicle, which is set to 0 in this simulation, because the lift impact on the car is small in the state of non-high speed, so this effect is ignored.

In the process of driving, the vehicle is also subjected to the friction between the air and the body surface, called friction resistance. At the same time, there are induced resistance and interference resistance and so on. Induced resistance is the drag caused by the presence of turbulence at the rear of the car due to the difference in air pressure between the upper and lower parts of the vehicle. Similarly, the exterior surface of the vehicle is not perfectly streamlined. For example, components such as rear-view mirrors and door handles protrude from the surface, which will destroy the streamline shape of the car body. When the air flow passes through these components, small eddies will be generated, and these small eddies will affect each other to produce resistance

called interference resistance. Therefore, it is defined in aerodynamics that the air resistance suffered by the car can be calculated by Eq. 4.3.

$$F_a = \frac{1}{2} C_d A \rho v^2 \tag{4.3}$$

In Equation 4.3, C_d is the coefficient of air resistance. Generally, this value is related to the shape of the vehicle. The closer the shape of the vehicle is to the streamline, the lower the value is;

A is the longitudinal projection area of the car, the unit is m^2;

ρ is air density in kg/m^3;

v is the current speed of the car in m/s.

However, if the unit of speed is changed to km/h, and the air density is taken as $1.23 g/m^3$ at 15 degrees, Equation 4.3 will be simplified as follows.

$$F_a = \frac{1}{21.15} C_d A v^2 \tag{4.4}$$

It can be seen that the air resistance of the car is greatly affected by the speed, which is proportional to the square of the driving speed. So the higher the speed of the car, the greater the air resistance. In the design phase, the value of area A is generally difficult to make a lot of optimization, but the value of C_d can be greatly optimized. Therefore, the design iteration of modern cars is to reduce the drag coefficient to reduce the fuel consumption per unit trip. The Matlab air resistance calculation module is designed according to Equation 4.4, as shown in Figure 4.2.2.

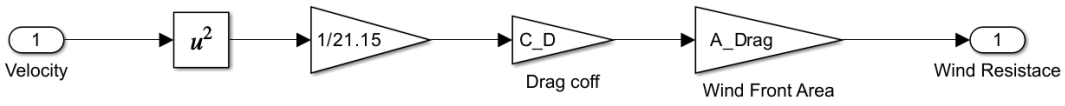

Figure 4.2.2 Matlab model of air drag calculation

From the perspective of evaluating air resistance, the body should be designed with the overall streamline in mind. The streamlined object ensures that the airflow in the wake area behind the object is relatively stable. Usually, when the car is running at a high speed, turbulence will occur in the area at the rear of the body, which will relatively increase the drag coefficient. Therefore, the installation of a deflector plate can try to smooth the air flow in the rear area of the car to reduce the drag.

In addition to air resistance, the slope of the road surface also increases the driving resistance of the car. Of course, the slope refers to the uphill, in the uphill, the car by the gravity along the road parallel direction of the component force will be seen as resistance to increase the power load of the motor. Ramp resistance is calculated in the same way as Eq. 4.5.

$$F_i = mgsin(a) \tag{4.5}$$

Where a is the slope of the road surface, generally when the vehicle is running at a high speed, its climbing ability is relatively limited, usually highest 3% slope is allowed. While the vehicle has a good climbing ability at low speed, generally at the speed of 20 Km/h, the maximum allowable slope is 9%. In the modeling of this section, we assume that the car travels on a level road surface, so the slope resistance is approximately 0, which also reduces the complexity of the model.

There is also a kind of resistance called acceleration resistance F_{acc}. As the vehicle accelerates, the engine needs to provide extra energy to overcome the drag caused by inertia. Its calculation formula is given in 4.6.

$$F_{acc} = \frac{m_e dv}{dt} \tag{4.6}$$

Where m_e is the equivalent mass of the vehicle, which consists of the weight of the car body and the mass transformed by the inertia torque caused by the flywheel rotation. The internal combustion engine is equipped with a flywheel to eliminate the vibration and speed fluctuations caused by piston movement at different angles. The inertia torque generated by the flywheel rotation needs to be calculated as a mass and added to the mass of the car. In the model establishment of this chapter, the equivalent mass is approximated as the mass of the car itself, so as to reduce the complexity of calculation. Equation 4.7 represents the relationship between traction and resistance.

$$F_t - F_r - F_a - F_i = \frac{m_e dv}{dt} \tag{4.7}$$

According to the content above, the calculation model of resistance and traction force of the car is finally established as shown in Figure 4.2.3.

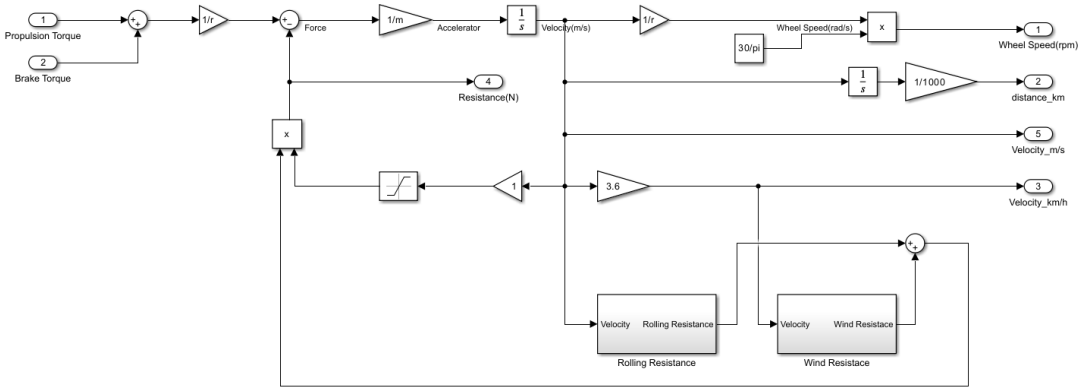

Figure 4.2.3 The resistance and traction force calculation model of Matlab

From the above description, we know that when the traction force is equal to the sum of the rolling resistance and the air resistance (assuming the road surface is level), the car will keep moving at a constant speed, because Eq. 4.7 shows that this makes the acceleration 0. Therefore, only when the traction force produce by the engine is greater than the resistance, the car can accelerate, which is in line with the universal laws of physics. At the same time, we can use the model structure shown in Figure 4.2.3 to obtain the mathematical relationship between traction force and vehicle speed.

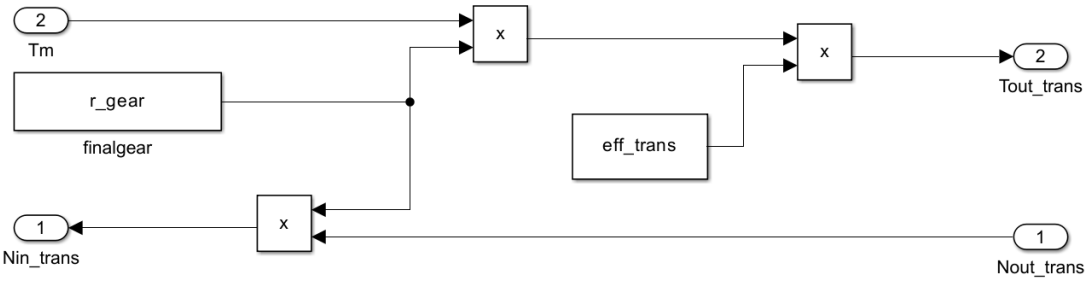

Figure 4.2.4 The Matlab model for reduction gear part

Finally, regarding the establishment of the reducer module, in fact, the transmission structure of electric vehicles is more flexible than that of fuel vehicles. In the modeling of this chapter, only the fixed ratio reducer is considered. Therefore, the transmission module mainly converts the torque of the engine into the torque of the wheel shaft. Usually, the reducer will increase the torque from the engine and convert the wheel speed less than the engine shaft speed. According to this relationship, the reducer module shown in Figure 4.2.4 is established. To sum up, the model structure of the transmission system is composed of the module discussed above.

4.3 Matlab model of motor system

The biggest difference between electric vehicles and gasoline vehicles is that the energy source of the engine is different and the characteristics of the engine are completely different. Usually, the working characteristic curve of the electric motor is divided into constant torque region and constant power region. When the rotor speed is low, the output torque of the motor is constant, and the output power has a linear relationship with the speed range, so the higher the speed, the greater the output power. However, when the speed reaches the base speed of the motor, the motor enters the constant power region. With the increase of the speed, the output power of the engine is unchanged, but the output torque is decreased, which is hyperbolic with the speed. Figure 4.3.1 illustrates the output power curve of the motor. Table 4.3.1 shows the main properties of the motor.

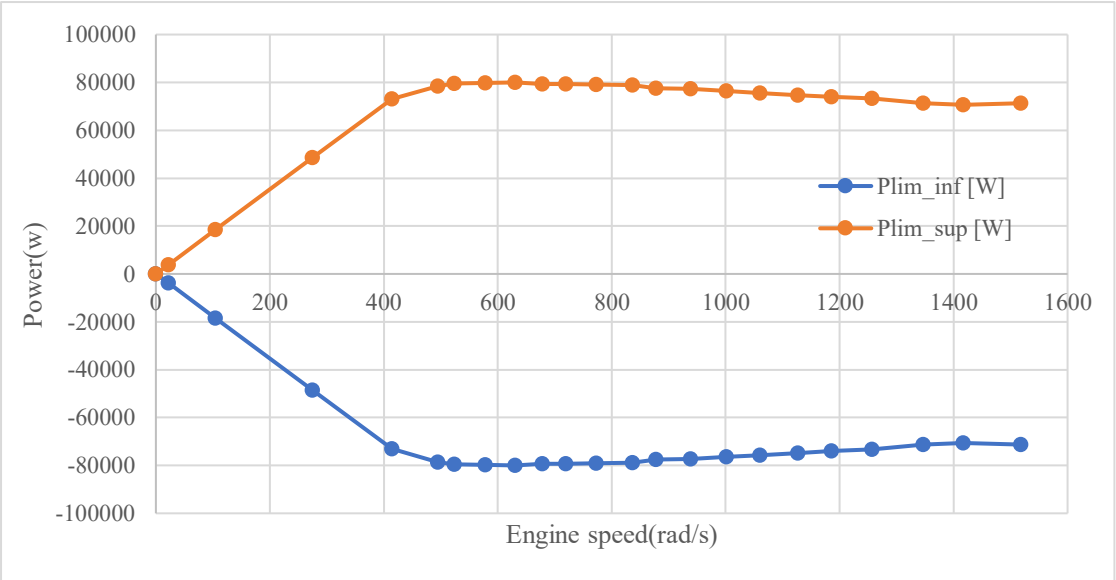

Figure 4.3.1 Engine power output curve

Table 4.3.1 The main properties of the motor

Type	Maximum power	Maximum torque	Maximum speed	Rated voltage
permanent magnet synchronous motor	80 kw	176 Nm	14500 rpm	380 V

It can be seen from the figure that the rotor speed starts to enter the constant power region at about 500rad/s, which is about 80kw output power. In the constant power region, the speed of the rotor increases while the output power of the motor remains

constant (although the power decreases slightly at high speeds), so that the torque produced by the engine is inversely proportional to the speed. The torque of the engine is constant until the speed is 500rad/s, but the output power increases linearly with the speed. This is the main difference between the electric motor and the internal combustion engine, and it is this characteristic that the electric motor has a better torque output performance than the internal combustion engine at low speed. Equation 4.8 reflects the relationship between torque and speed and power.

$$P_e = \frac{Tn}{9550} \tag{4.8}$$

The unit of power P_e is kw; T is the torque in Nm; n is the rotational speed in rpm and 9550 is the coefficient resulting from the unit conversion.

Although the energy conversion efficiency of the electric motor is much higher than that of the traditional internal combustion engine, which can reach 90% in most working ranges, but still, this energy loss must be considered in the calculation of the electric motor power. Therefore, engine map needs to be integrated into the Matlab motor model. Figure 4.3.2 shows the engine map of the engines selected in this chapter.

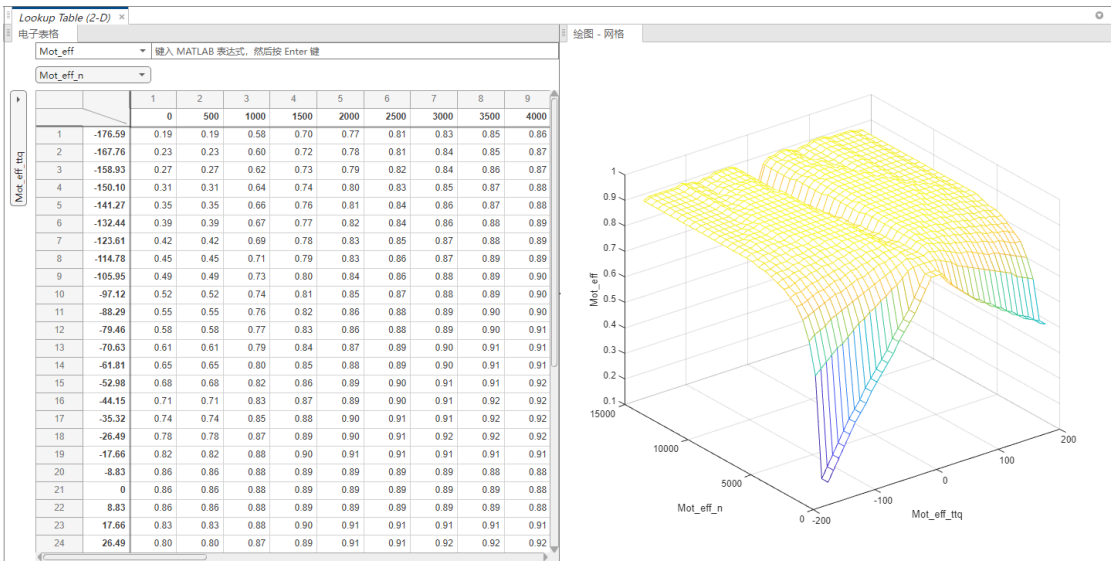

		1	2	3	4	5	6	7	8	9
		0	500	1000	1500	2000	2500	3000	3500	4000
1	-176.59	0.19	0.19	0.58	0.70	0.77	0.81	0.83	0.85	0.86
2	-167.76	0.23	0.23	0.60	0.72	0.78	0.81	0.84	0.85	0.87
3	-158.93	0.27	0.27	0.62	0.73	0.79	0.82	0.84	0.86	0.87
4	-150.10	0.31	0.31	0.64	0.74	0.80	0.83	0.85	0.87	0.88
5	-141.27	0.35	0.35	0.66	0.76	0.81	0.84	0.86	0.87	0.88
6	-132.44	0.39	0.39	0.67	0.77	0.82	0.84	0.86	0.88	0.89
7	-123.61	0.42	0.42	0.69	0.78	0.83	0.85	0.87	0.88	0.89
8	-114.78	0.45	0.45	0.71	0.79	0.83	0.86	0.87	0.89	0.89
9	-105.95	0.49	0.49	0.73	0.80	0.84	0.86	0.88	0.89	0.90
10	-97.12	0.52	0.52	0.74	0.81	0.85	0.87	0.88	0.89	0.90
11	-88.29	0.55	0.55	0.76	0.82	0.86	0.88	0.89	0.90	0.90
12	-79.46	0.58	0.58	0.77	0.83	0.86	0.88	0.89	0.90	0.91
13	-70.63	0.61	0.61	0.79	0.84	0.87	0.89	0.90	0.91	0.91
14	-61.81	0.65	0.65	0.80	0.85	0.88	0.89	0.90	0.91	0.91
15	-52.98	0.68	0.68	0.82	0.86	0.89	0.90	0.91	0.91	0.92
16	-44.15	0.71	0.71	0.83	0.87	0.89	0.90	0.91	0.92	0.92
17	-35.32	0.74	0.74	0.85	0.88	0.90	0.91	0.91	0.92	0.92
18	-26.49	0.78	0.78	0.87	0.89	0.90	0.91	0.92	0.92	0.92
19	-17.66	0.82	0.82	0.88	0.90	0.91	0.91	0.91	0.91	0.91
20	-8.83	0.86	0.86	0.88	0.89	0.89	0.89	0.89	0.88	0.88
21	0	0.86	0.86	0.88	0.89	0.89	0.89	0.89	0.89	0.88
22	8.83	0.86	0.86	0.88	0.89	0.89	0.89	0.89	0.89	0.88
23	17.66	0.83	0.83	0.88	0.90	0.91	0.91	0.91	0.91	0.91
24	26.49	0.80	0.80	0.87	0.89	0.91	0.91	0.92	0.92	0.92

Figure 4.3.2 The engine map of E-motor

We tabulated the working efficiency of the engine as a function of torque and speed and put it into the Matlab 2D lookup table using interpolation, as shown in the figure above. In this way, accurate engine power demand data can be calculated. Finally, the engine model is built according to Formula 4.8, as shown in Figure 4.3.3 below.

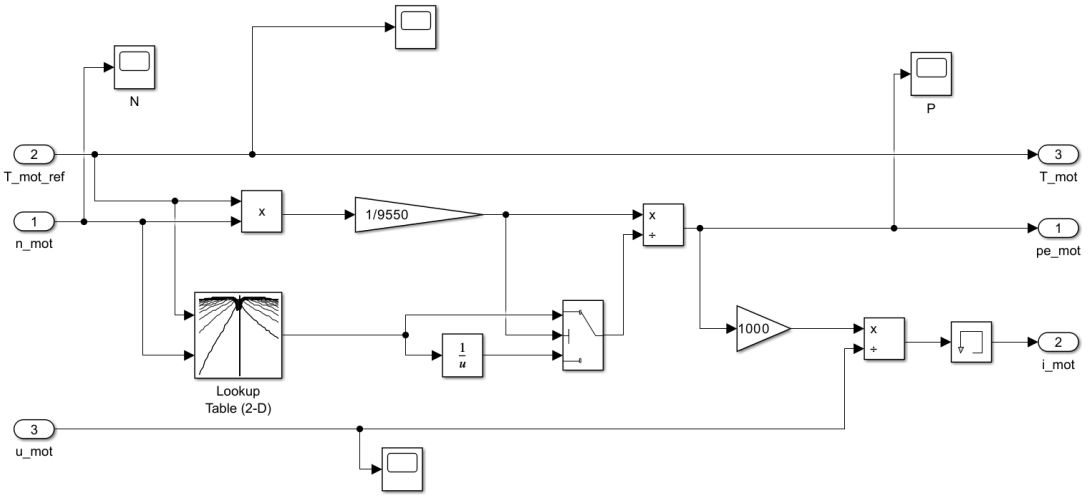

Figure 4.3.3 The Matlab E-motor model structure

The lookup table in the figure is to store the working efficiency data of the selected motor, and the condition selector on the right is used to judge the state of the motor. The motor is divided into two states: power output and power recovery, which correspond to its output mechanical energy or electric energy. Finally, the calculation of the voltage and current required by the motor is realized through such a module, which will be used as the input data of the voltage and current of the battery module.

4.4 Matlab model of driver

In the process of model construction in this section, the problem of the car speed input command should be considered. Generally, a simple method is to directly input the speed information of the engine to simulate the car driving according to the required speed. But this method is easy to cause wrong estimation of the car acceleration, so that there are some problems in the calculation of acceleration resistance. Therefore, another method is to design a PID controller to simulate the driver's operation of the pedal, so that the set vehicle speed curve data is used as the reference of the PID controller, and then the controller directly controls the position of the throttle to calculate the engine output torque under the current wheel speed. Finally, the current vehicle speed is input into the PID controller as feedback. The overall structure of the driver model is presented in Figure 4.4.1.

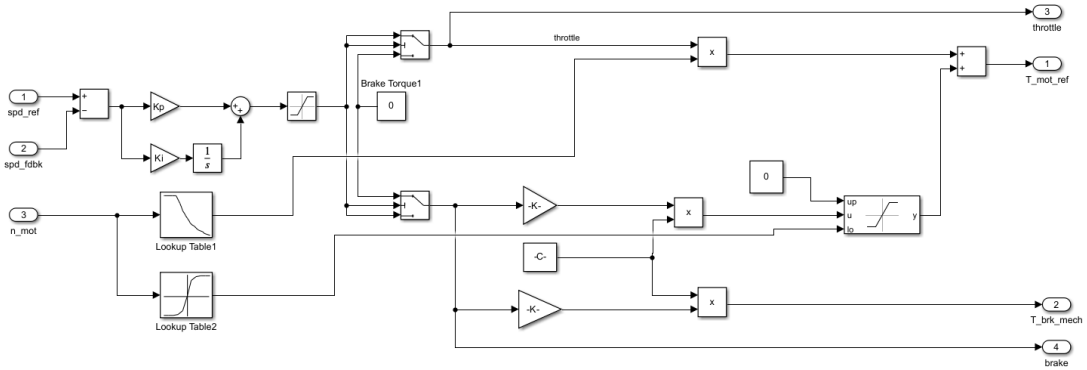

Figure 4.4.1 The Matlab model of driver

In general, the proportion and integral parts need to be combined in PID controller, because only the proportion part will lead to a large error and cause the error to oscillate in a certain interval, so the integral part is needed to reduce the amplitude and overshoot of the error oscillation, and finally make the error tend to 0. In order to reduce the parameter complexity of the controller, the differential part can be ignored for systems that do not require high control accuracy. Because the differential part can increase the damping of the error shock, it is the judgment of the future state of the system. Therefore, in the model in the figure, we only choose the PI controller to simulate the driver's operation of the accelerator pedal. For the parameter estimation of the controller, we combine the parameters according to the empirical method, as long as the error can converge in a short time, and at the same time the acceleration of the car remains within a reasonable range.

5 Simulation on electrothermal characteristics under specific procedures

In real life, vehicles will go through a variety of conditions during driving (such as the change of road conditions, the increase and decrease of car speed according to the driver's demand). So the discharge rate and output power of the battery are changing rapidly as different drivers drive the car. Even on the same road, different drivers will lead to different battery discharge rate curves. According to the previous study, the battery is charged or discharged with its own temperature change. Based on this, this chapter uses the vehicle longitudinal motion model introduced in the previous chapter to simulate and analyze the electric thermal characteristics of the battery under the actual driving condition of the vehicle. We compared the sensitivity of parameters in the RC equivalent circuit model and studied the changes in battery thermal and electrical characteristics under different test cycles such as NEDC and WLTC.

5.1 Parameters sensitivity analysis

In the simulation of some physical variables in the system, the most effective way to verify the accuracy of the simulation results is to compare the experimental data with the simulation data, and use some mathematical algorithms to calculate the error. However, if there is not enough detailed experimental data, we can also change some parameters in the simulation process to explore the influence of parameter numerical changes on the simulation results, so as to judge the robustness of the simulation results. Therefore, in this subsection, we try to conduct parameter sensitivity analysis to explore the reliability of the electro-thermal coupling model established in the previous chapters. In the RC equivalent circuit model established in Chapter 2, we use the data in the battery HPPC test to estimate the RC parameters in the model by the least square method. We then used this set of parameters to explore whether the model could simulate the voltage and current changes of other batteries of the same type (same electrode material, same capacity, different production batches). The experimental data of the battery in the parameter identification link introduced in the second chapter come from an LG 18650 lithium battery with a rated capacity of 3Ah. In this subsection, we use the CC-CV experimental data of another LG 18650 lithium battery with a rated

capacity of 3Ah to explore the difference between the voltage simulated by the electrical model (without changing the RC parameter) and the experimental data. It is first necessary to estimate the open-circuit voltage for the new group battery. Because the discharge current of the battery in the experiment is 0.14A, the current is small enough that the voltage change caused by the internal resistance can be neglected, so the terminal voltage can be approximated as the open-circuit voltage. Therefore, the open circuit voltage of this battery at 25 degrees is shown in Figure 5.1.1

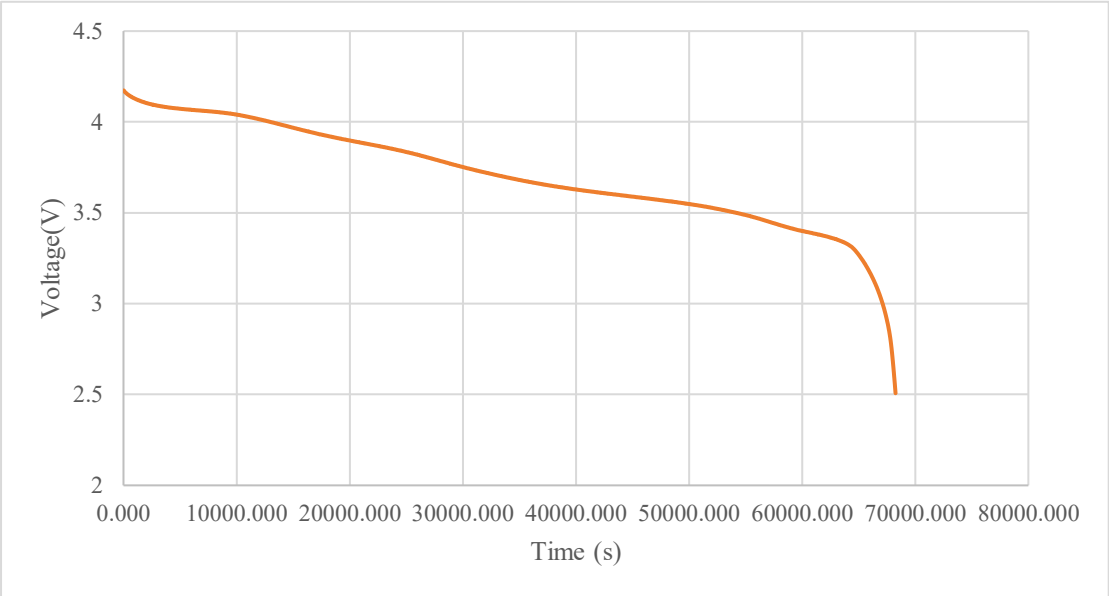

Figure 5.1.1 The open circuit voltage of the new battery

After that, the current curve in the experimental data is used as the current input command of the equivalent circuit model, and the temperature is set to 25 degrees, which is the same as the temperature value in the experimental data. Finally, observe the difference between the simulated and experimental data. This is used to determine the sensitivity of RC parameters to different batteries. Figure 5.1.2 shows the CC-CV experimental data and the simulated output voltage data of the model for another group battery.

The orange line in Figure 5.1.2 is the experimental data of constant current discharge, and the blue line is the simulated data of the equivalent circuit model. It is obvious that the two curves basically coincide, which indicates that the identified RC parameters can be used for terminal voltage simulation of other batteries of the same type. At the same time, the data shown in the figure is the battery soc ranging from 1 to 0.1. When the battery power is too low, the terminal voltage of the battery will drop sharply. Therefore, the data simulated by the model corresponds to the situation that the battery soc is greater than 0.1. Figure 5.1.3 illustrates the error values in mV between the

experimental and simulated data.

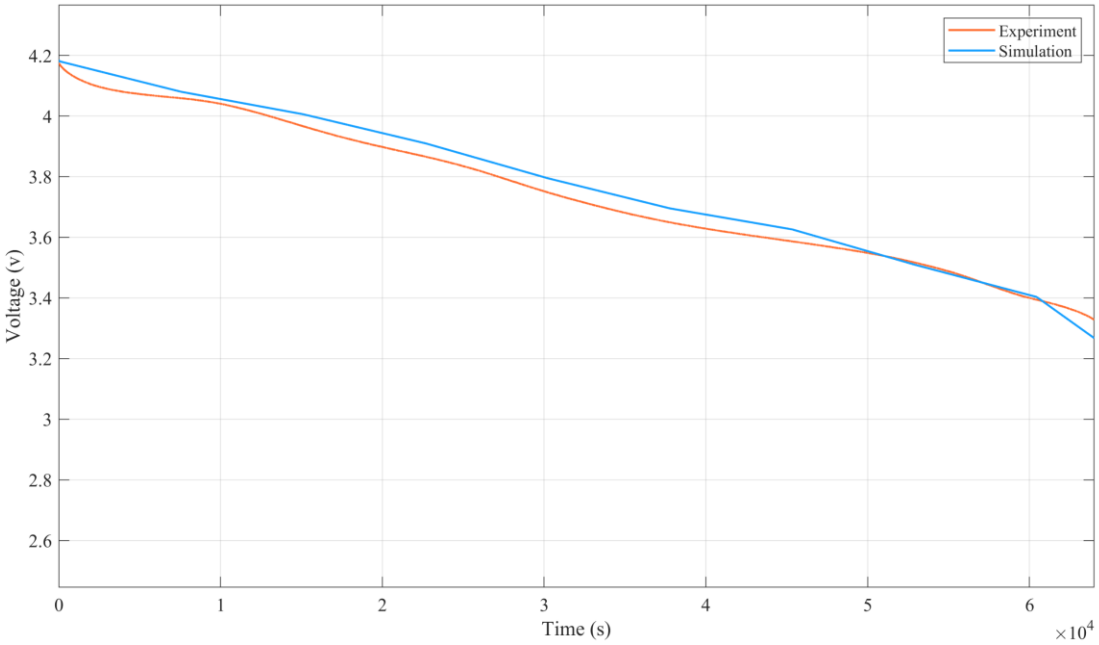

Figure 5.1.2 Model simulation output voltage data of another battery

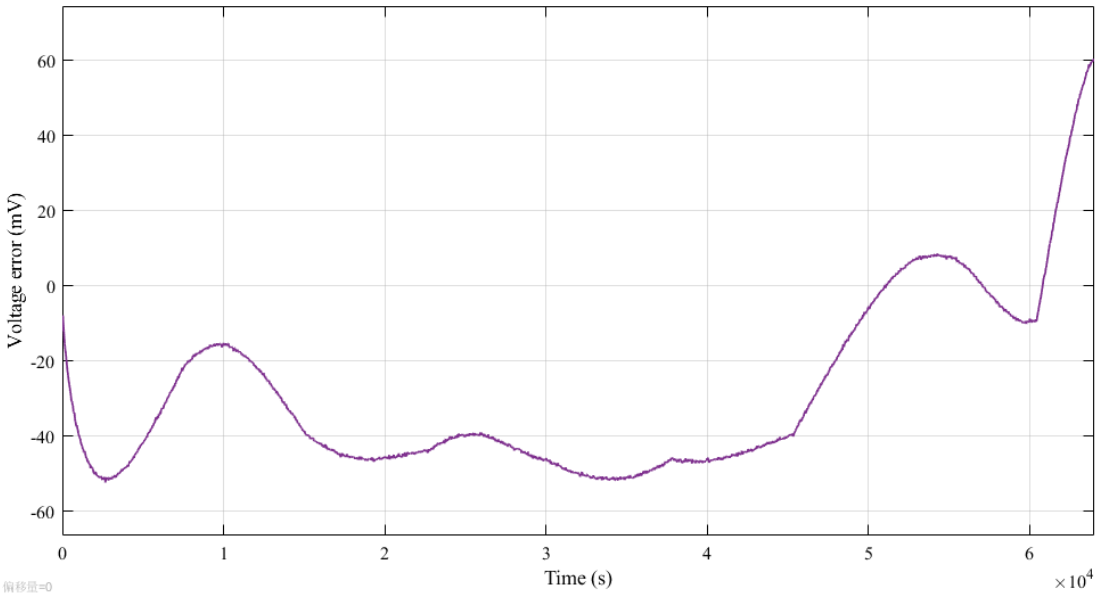

Figure 5.1.3 The error between experiment and simulation data of the new group battery

As can be seen from Figure 5.1.3, after comparing the simulation data of the model with the experimental data of another battery, it is found that the error value fluctuates at 40 mV (around 1.2% error) most of the time, and only reaches 60 mV (around 1.7% error) in the final time period of the simulation. The total RMS error is 0.0369 for this

simulation. As we all know when the soc below 0.1, the terminal voltage will drop sharply and cause much error in this region. So normally we main focus on the region of soc from 1 to 0.1. Therefore, it can be clearly said that equivalent circuit model RC parameters have better adaptability to the similar type of battery.

For the parameter sensitivity analysis of the electrothermal coupling model, we tried the scenario hypothesis of using constant current discharge with different intensities to explore the battery temperature calculated by the electrothermal coupling model. Figure 5.1.4 shows the battery surface temperature variation under 3A/6A/9A constant current discharge scenario.

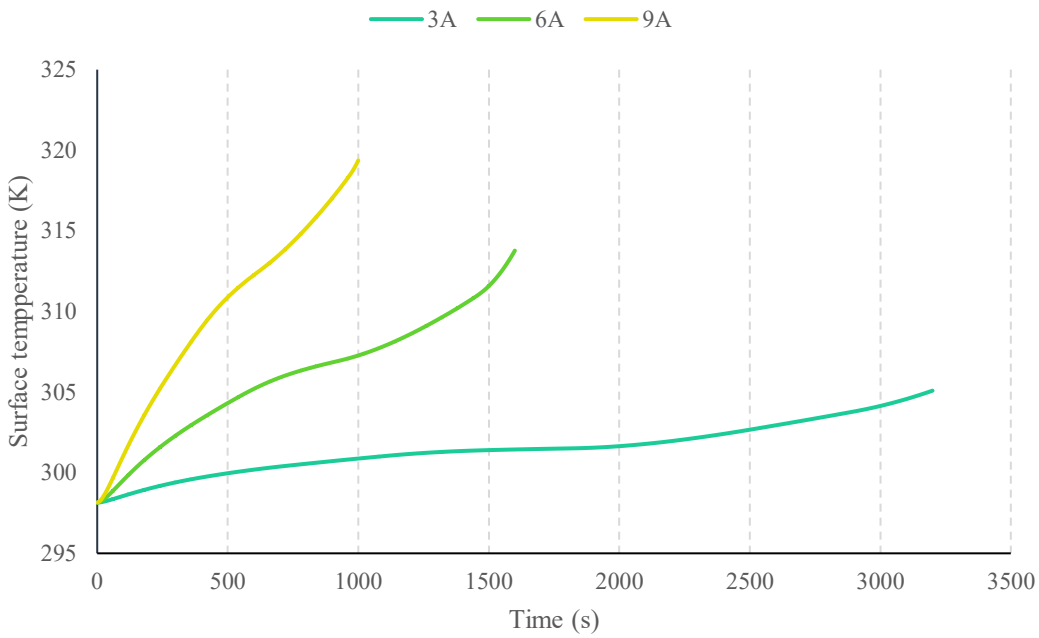

Figure 5.1.4 Battery surface temperature changes in 3A/6A/9A constant current discharge scenarios

It can be seen from the information in the figure that under the discharge situation of 3A current, the overall temperature of the battery rises from 298K (25 degrees) to 303K after about one hour of discharge. However, when the current intensity is doubled to 6A, the temperature rises to 315K (42 degrees) at 1600 seconds (about 25 minutes), and the overall curve is steeper than that in the 3A discharge scenario, indicating that the heat generation rate of the battery increases with the increase of the current intensity. When the battery is in the 9A high-current discharge situation, the temperature has risen rapidly from 298K to 320K (about 47 degrees) at 1000 seconds (about 15 minutes). It is obvious that the temperature of the battery does not increase in a fixed proportion with the current intensity. This also indicates the need to be vigilant about the temperature effect of high-current discharge on the battery, and also indicates that the

battery temperature change is sensitive to the current value. Of course, it is difficult to encounter constant current discharge in the actual application scenario of automobile battery, and the current value changes irregularly in most cases. Therefore, we will explore the electric thermal characteristics of the battery in some actual vehicle driving scenarios.

5.2 NEDC procedures

At present, in the field of electric vehicle production and manufacturing, many countries have established testing standards. After all, there are many individual differences in the way consumers drive cars in real life, but it is necessary to find a standard to simulate the road driving scenario of cars. Therefore, this section uses the road test profile's speed curve commonly used by some large automobile manufacturing enterprises as the speed information input of the model, so as to explore the electric thermal characteristics of lithium battery in the actual working state of the vehicle. For example, the New European Driving Cycle is a driving standard used by many automobile manufacturers to measure the endurance of a certain vehicle model. The standard originated as ECE15 in the 1970s, underwent several upgrades, and was officially named NEDC in 1997, and now it is still used today in Europe, China, and Australia.

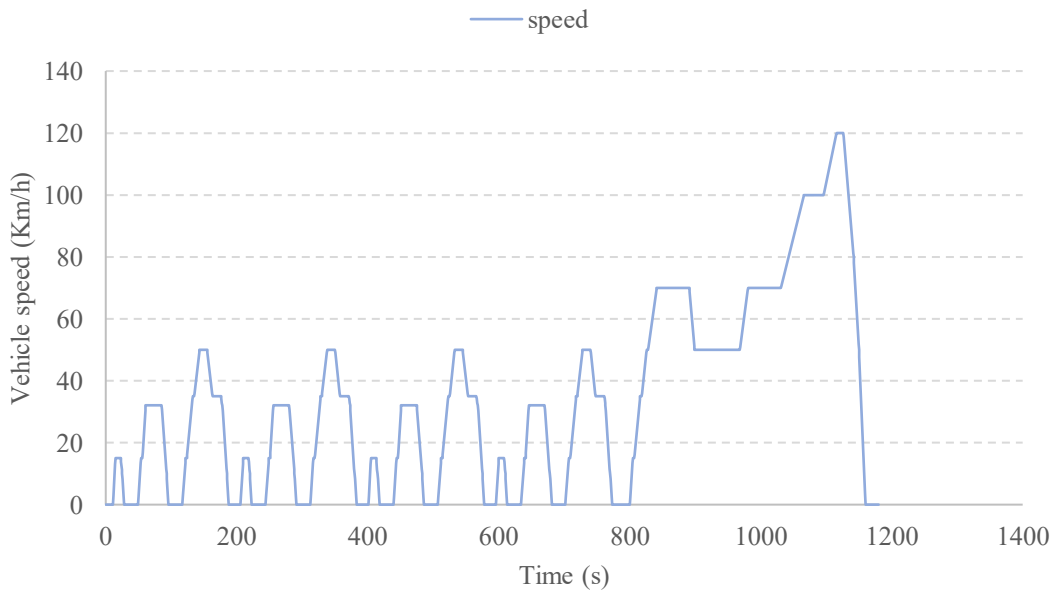

Figure 5.2.1 The speed curve of New European Driving Cycle road profile

The NEDC included five operating conditions: four urban cycles and one simulated suburban cycle. The speed and time curves in NEDC are presented in Figure 5.2.1. As can be seen from the figure, the test of NEDC is relatively simple, from 0 to 780 seconds is the simulation of the car driving in the city. The overall speed is not higher than 60km/h, and the average speed is 18.5km/h. That is more accurately reflects the actual situation of vehicle driving in the city. This process was repeated four times, from the beginning of the car accelerating to maintaining speed, then decelerating to past a pedestrian or intersection, and finally stopping. After 780 seconds, the car travels to the outskirts of the city with a maximum speed of 120km/h and an average speed of about 60km/h. From the overall speed curve, it can be seen that both the city cycle and the suburban cycle reflect the car driving process under ideal conditions. In fact, depending on the driver's driving style, the speed curve of the real car is different from the standard test. However, we still use this test file because it can basically reflect the driving conditions of the car in urban and suburban areas. By taking this speed curve as the speed signal input of the vehicle longitudinal motion model that have developed in chapter 4, we can obtain the variation trend of the voltage and current of the battery, as well as the variation trend of the battery temperature under the situation of this testing cycle.

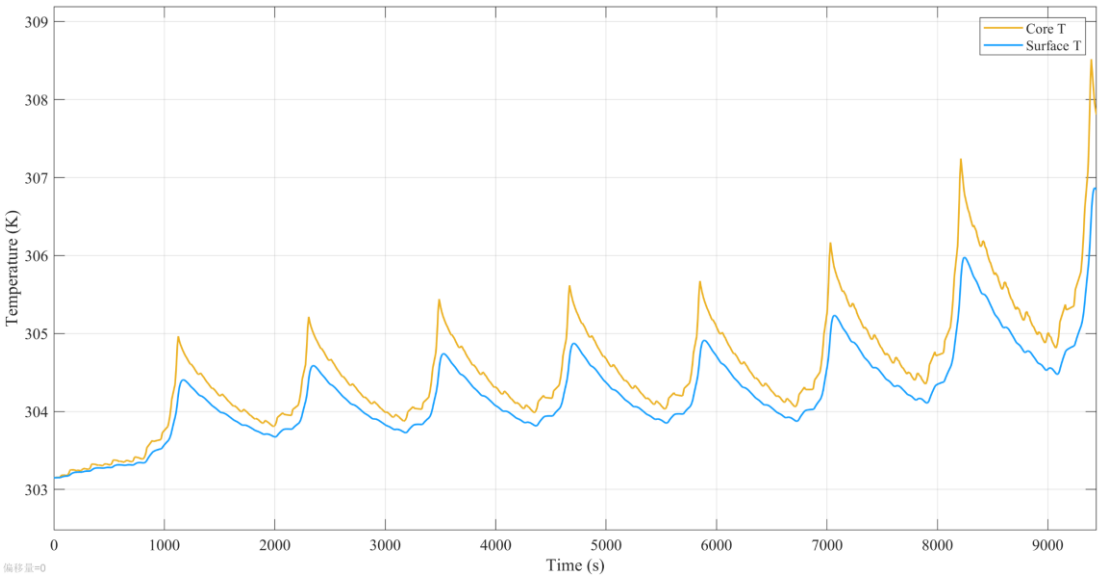

Figure 5.2.2 The simulation result of battery core and surface temperature over NEDC

For the simulation in this subsection, it is assumed that there are 103 lithium batteries connect in series in a unit, and the rated voltage of a single lithium battery is 3.7v, then the output rated voltage of the whole battery unit is about 380v, and there are a total of

16 battery units connect in parallel in a total battery pack, and cause of 48Ah rated power in all. After eight rounds of NEDC simulation, the surface and core temperature changes of the battery are shown in Figure 5.2.2.

It is assumed that the ambient temperature is 303K (30 degrees) at the beginning of the simulation and it does not change during the simulation. It can be seen from the figure that after eight rounds of testing cycles, both the surface and core temperatures of the battery show a fluctuating upward trend, with the core temperature reaching a maximum of 308.5K and the surface temperature reaching a maximum of 306.9K. Meanwhile the core temperature is always higher than the surface temperature, which also confirms the importance of estimating the core temperature. At the same time, it is also easy to find that when the battery is in the high-current discharge phase, its temperature rise rate is the largest, and is significantly greater than the case of small current. Therefore, more attention needs to be paid to the heat generation of the battery when the car is running at high speed. Figure 5.2.3 shows the current variation trend of single lithium battery.

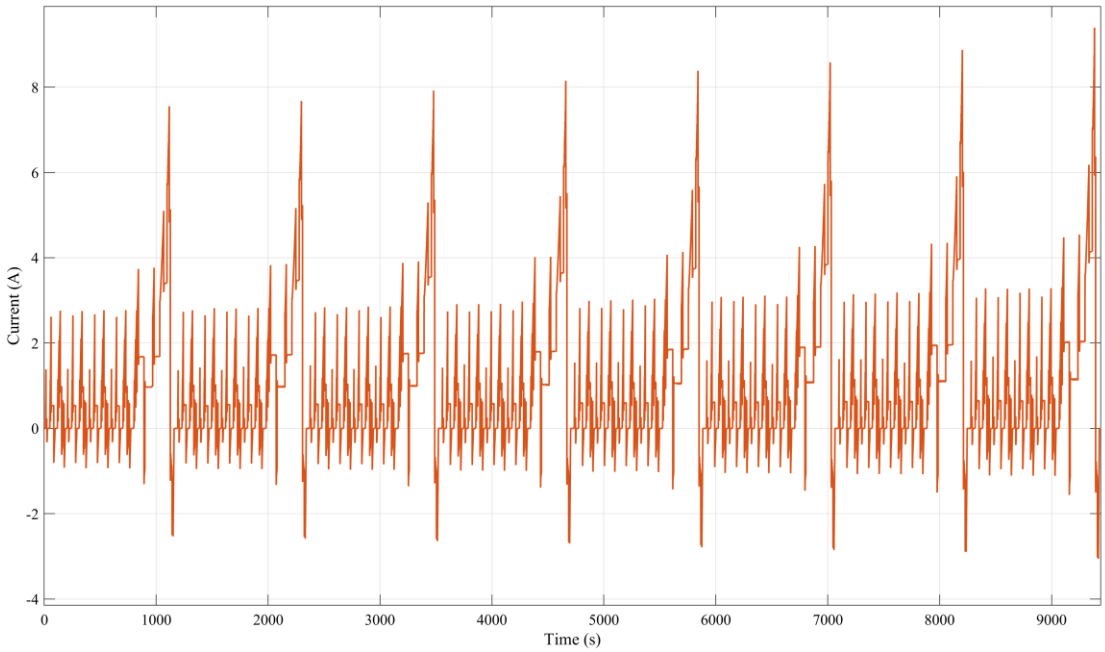

Figure 5.2.3 Current variation trend of single battery over NEDC

There are current values in the figure that are in negative values, which represents the charging current. Normally, when the driver brake the car, it will recovers some of its braking energy and uses it to drive the motor to generate electricity that recharge the battery. Therefore, in the simulation, we set the discharge current to a positive value and the charging current to a negative value. It is clear to see in the figure the charging current is much smaller than the discharging current, because only part of the braking energy is recovered, In the simulations in this section, we assume that the braking

energy recovery ratio is 0.3. while it can be seen from Figure 5.2.3 that when the car is running at a high speed on the suburban road, the battery discharge current reaches 4 to 8A, and the heat generation of the battery also increases significantly. Figure 5.2.4 shows the variation trend of the battery terminal voltage.

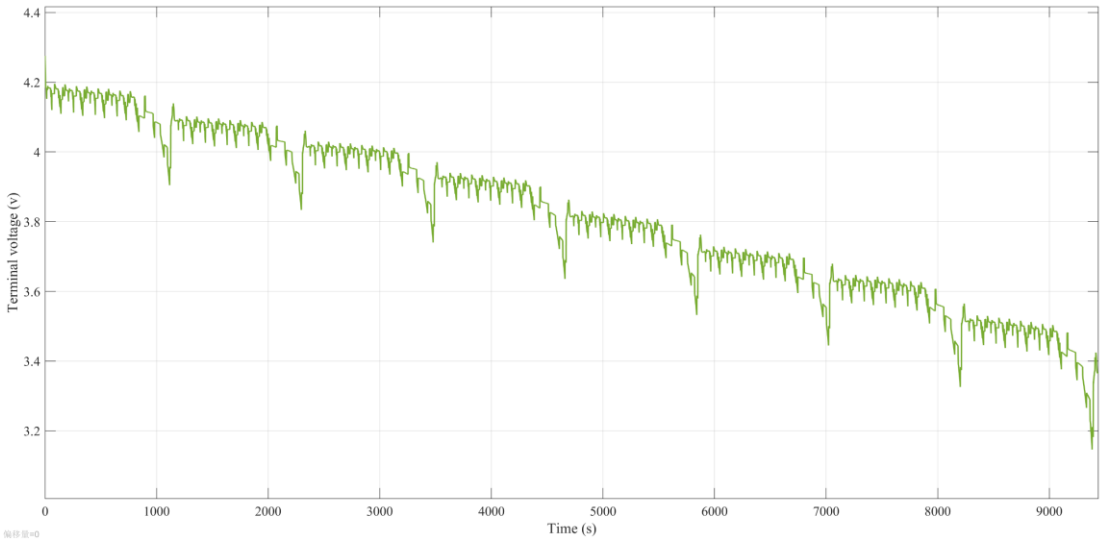

Figure 5.2.4 The terminal voltage of single battery over NEDC

As can be seen in Figure 5.2.4, the terminal voltage drops from 4.2v to 3.2v with the battery soc drops approximately from 1 to 0.2 when the car experiences eight rounds of NEDC. It is obvious that when the battery under low soc, its terminal voltage also drops significantly. In the image, the terminal voltage has a short period of rise callback, which is mainly because the car is in the deceleration phase, the motor recovers a part of the energy, and the battery is charged during this period. Therefore, it can be seen that there is a pulsation phenomenon in the terminal voltage. In addition, in the later stage of each cycle, the vehicle is in a high-speed driving stage, and the battery terminal voltage has a rapid downward trend, which is also related to the change of the internal electrochemical reaction state caused by the high-current discharge. At the same time, it is also easy to see that when soc is low, the high-current discharge causes the terminal voltage to drop more obviously, so the high-speed driving performance of the car is significantly weaker under this condition.

5.3 WLTC procedures

At present, the electric-only range of many cars is measured by NEDC, but the high-speed driving stage of NEDC is less, and more emphasis is put on simulating the

medium and low speed driving stage of the car. Therefore, the European Union, Japan and the United States jointly developed the World Light Vehicle Test Procedure, referred to as WLTP, in which the cycle test in this procedure was referred to as WLTC. In fact, there are three different cycles in WLTP, and its level 3 testing cycle is used in this section, because level 3 is most relevant to the passenger cars, and most of the passenger cars selling in the market belong to this class. The WLTC corresponding to level three defines four speed stages of the vehicle: low speed, medium speed, high speed and ultra-high speed. Each stage lasts 589s, 433s, 455s and 323s respectively, and the corresponding maximum speed is 56.5km/h, 76.6km/h, 97.4km/h and 131.3km/h respectively. A single cycle lasts 1800 seconds and covers a total distance of 23.3 km. Compared with NEDC mentioned in Section 5.2, WLTC has more high-speed driving phases. Figure 5.3.1 shows the speed curve of the whole test cycle.

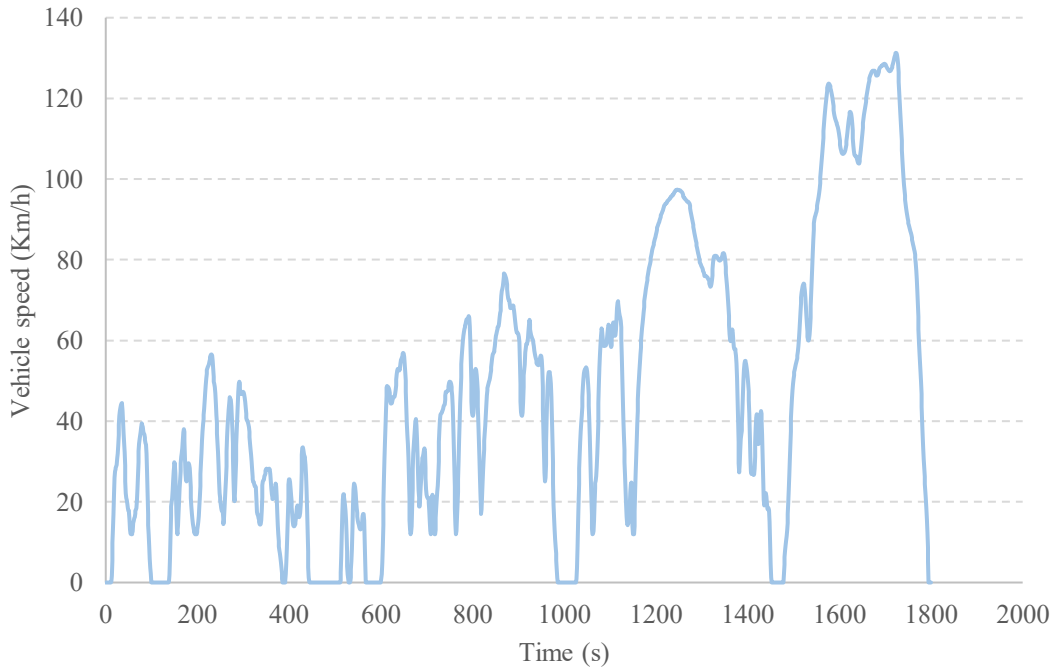

Figure 5.3.1 The Speed curve of World Light Vehicle Test Procedure level 3

It is also not difficult to see from the figure that the high-speed stage (speed greater than 80km/h) in the whole cycle is significantly more than NEDC, which is also seen from the vehicle electric-only range information marked by many automobile manufacturers, the mileage measured by WLTC as the standard is smaller than NEDC. Therefore, it is necessary to use the WLTC speed curve as the input of the model speed command in order to explore the electric heating characteristics of the lithium battery. Figure 5.3.2 shows the core and surface temperature changes of a single lithium battery after 4.5 cycles of WLTC. In the initial simulation stage, the vehicle battery pack is set up the

same as in Section 5.2, assuming that each battery unit consists of 103 batteries in series to a rated voltage of 380v, and a total of 16 units are connected in parallel to form a 48Ah battery module. The ambient temperature is set to a fixed value of 303K (30 degrees).

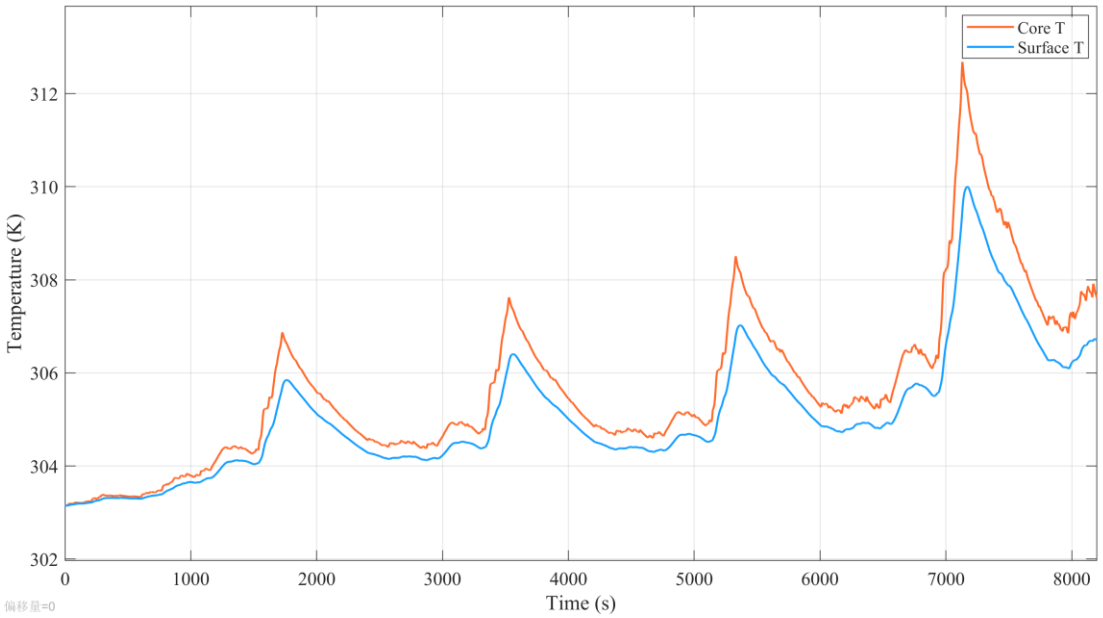

Figure 5.3.2 The simulation result of battery core and surface temperature over WLTC

Throughout the simulation process, the soc of the battery drops from the initial value of 1 to about 0.1. It can be seen from Figure 5.3.2 that the peak temperature occurs around 7200 seconds, around the ultra-high speed stage at the end of the fourth test cycle, when the core temperature of the battery reaches 312.5K (about 39 degrees) and the surface temperature is about 310K. This shows that the heat production of the battery increases significantly at the ultra-high speed stage (130km/h). At the same time, under the lower soc, the heat generation of the battery in the state of high current discharge is much more obvious. In addition, the core temperature of the battery is always 0.5 to 2K higher than the surface temperature, which is relative to the cylindrical battery. If it is a rectangular or soft-pack battery, the temperature difference between the core and the surface will be different than this. Figure 5.3.3 shows the current change of a single lithium battery during the simulation process, where positive values represent discharge state and negative values represent charge state.

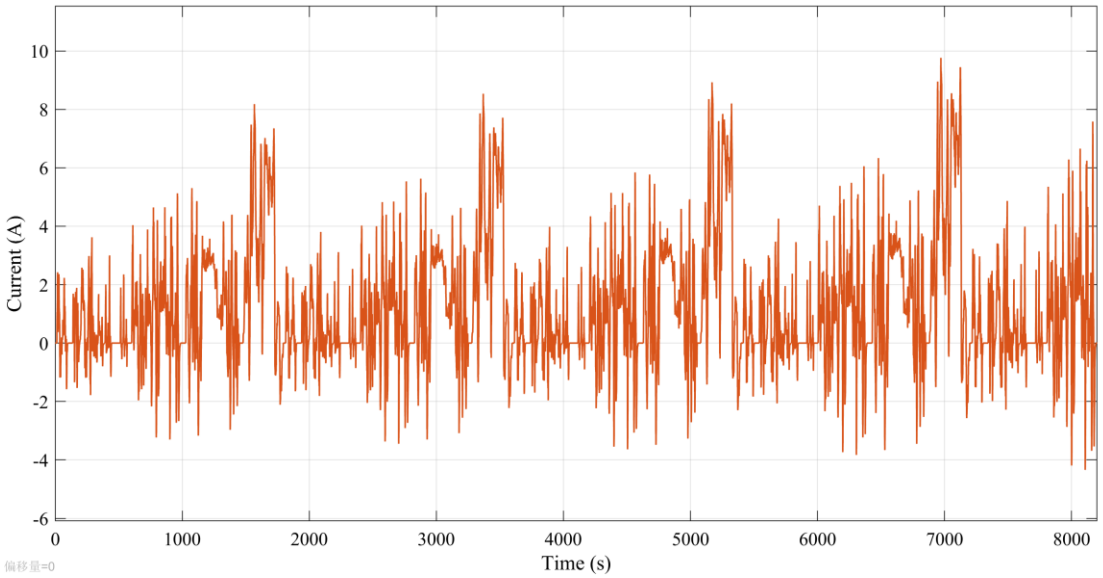

Figure 5.3.3 Current variation trend of single battery over WLTC

As can be seen from Figure 5.3.3, the discharge current of the battery is about 0 to 4A at the low and medium speed stages. In the high-speed and ultra-high-speed stage, the current reaches 6 to 8A, that is, in this stage, corresponding to the peak of the temperature curve in Figure 5.3.2, the temperature of the battery increases significantly under the state of high discharging current. In WLTC, the driving speed of the car is less regular, but it can more truly reflect the driving state on the actual road. The current curve of the battery fluctuates more than that of the NEDC, indicating that the battery faces a more challenging work load. The variation trend of battery terminal voltage is shown in Figure 5.3.4.

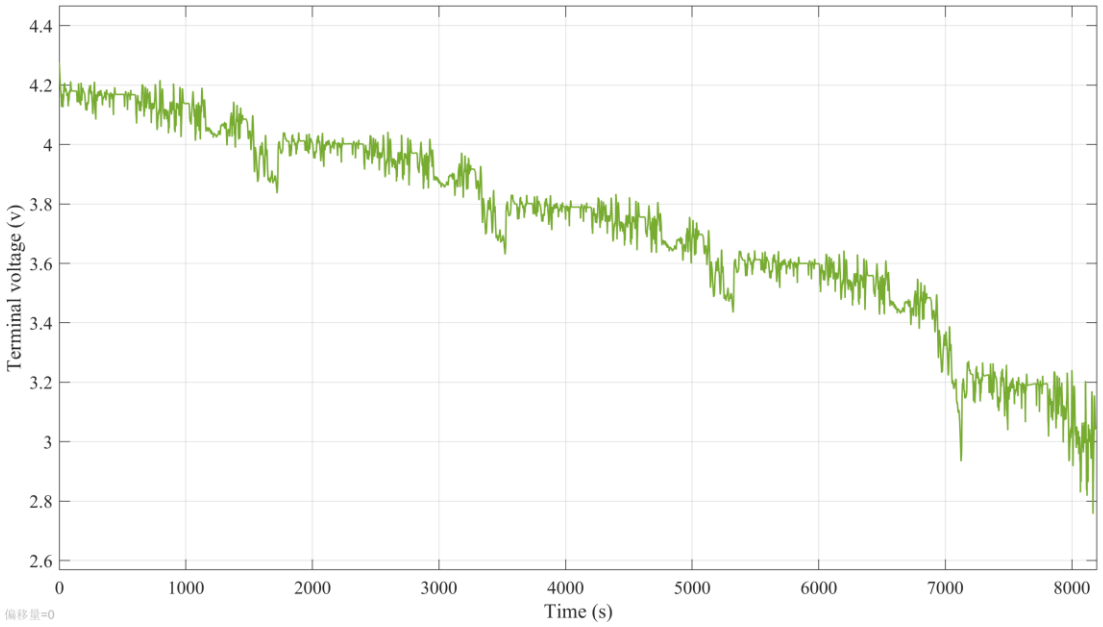

Figure 5.3.4 The terminal voltage of single battery over WLTC

It is also obvious from the voltage variation curve that the battery terminal voltage becomes more volatile under complex current excitation. Especially when the soc is low, the voltage drops significantly around 7000 seconds in the figure, once reaching 2.9v and then rising again. This shows that when the battery power is low, its high-power energy output capacity becomes fragile, and the terminal voltage drops significantly. This is also related to the electrochemical reaction inside the battery, in the case of low chemical reaction rate, the polarization effect leads to more obvious fluctuations in the terminal voltage. Therefore, from the point of view of the healthy use of the battery, it is necessary to avoid large current discharge behavior in the state of low battery as much as possible, which avoid to a faster decline in the battery terminal voltage and more heat generation.

5.4 DST procedures

The electric vehicle battery test manual of the United States has introduced a battery dynamic test profile, which is simplified based on the current requirements generated by the actual driving of electric vehicles in cities. In the electrothermal analysis of the battery, it is necessary to study the response of the battery to the scenario of large current shock and fast charge-discharge conversion. Based on the dynamic stress test (DST), the above two scenarios can be reflected. Figure 5.4.1 shows the current curve in DST.

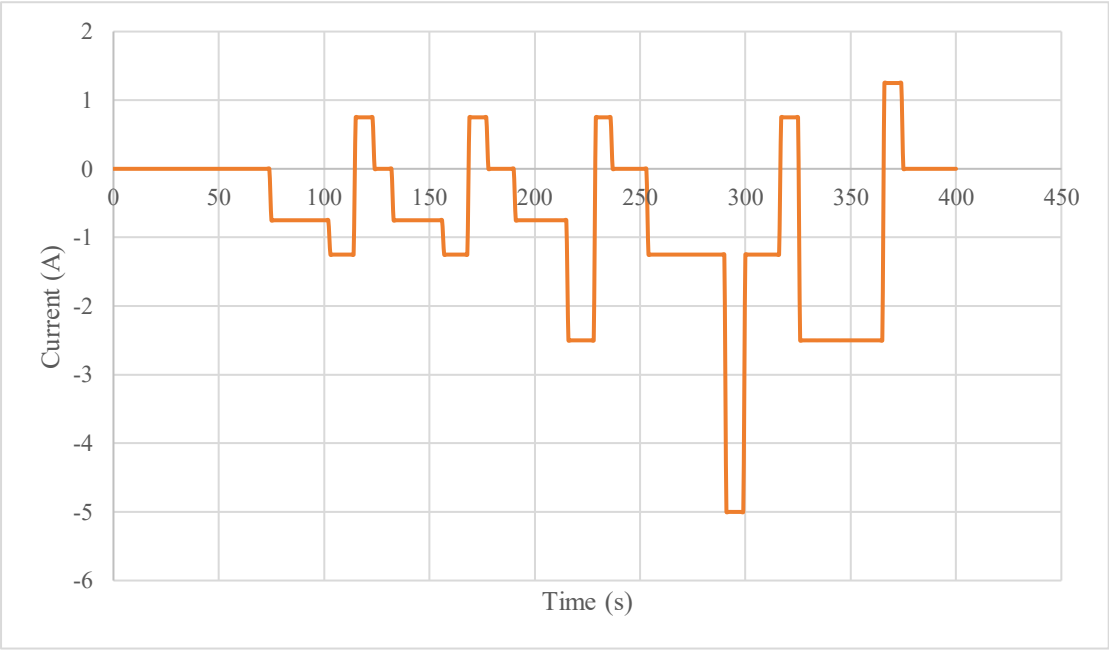

Figure 5.4.1 The current variation in the DST of single cycle

As can be seen from the figure 5.4.1, a DST cycle is only about 300 seconds, which includes the fast switching of charging-discharge current, 5A large current load and other scenarios. A negative current in the figure indicates discharge state, while a positive current indicates charge state. In this section, we use DST current as input data to explore the electrothermal characteristics of the battery. Because a DST cycle is only about 300 seconds, we combined several test cycles as the current command input for the model, as shown in Figure 5.4.2.

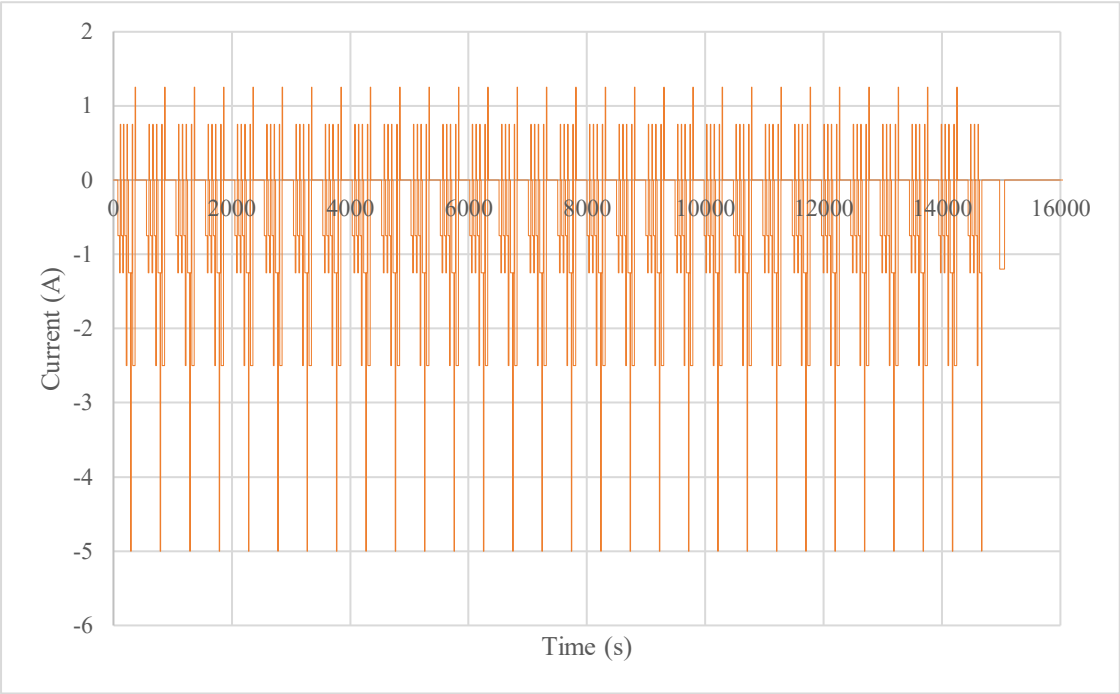

Figure 5.4.2 The total DST current curve in the simulation process

Throughout the simulation, the battery undergoes a 16,000-second DST cycle, and the soc stops from an initial 1 to 0.2. Figure 5.4.3 shows the battery terminal voltage variation throughout the simulation.

In this simulation, the terminal voltage of the battery shows a step-type downward trend, but there is also a pulsating phenomenon among simulation. Especially under the excitation of large current discharge, the terminal voltage value appears obvious dip, but soon recovers. While by looking on the side, the curve has a linear downward trend.

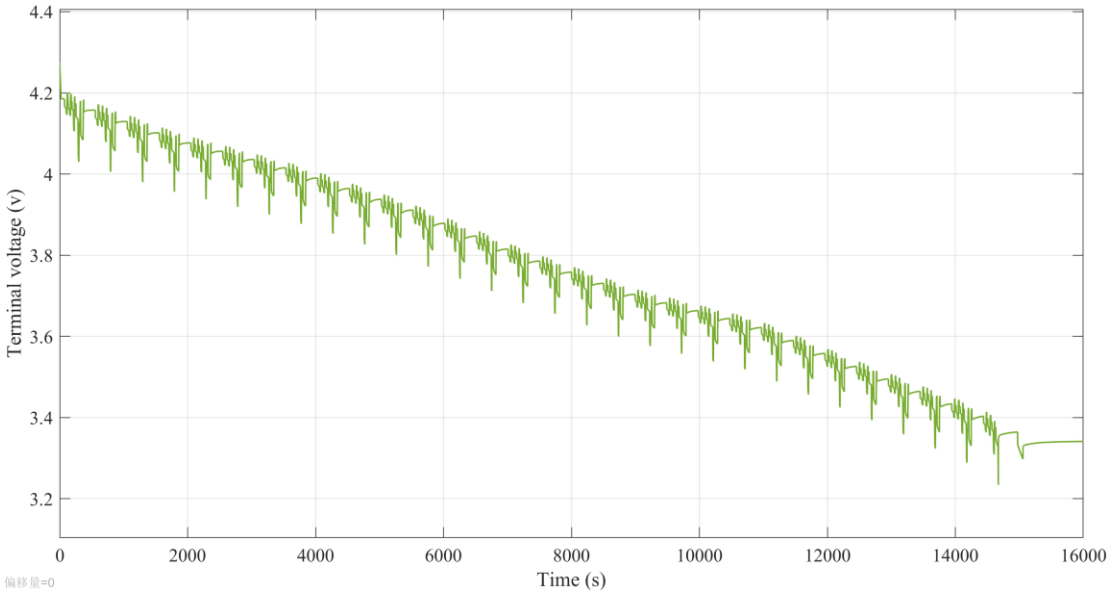

Figure 5.4.3 The terminal voltage variation trend of DST simulation

In the rapid change of charge and discharge current, the terminal voltage also shows a similar trend, the first rapid decline and then rapid recovery, but the overall recovery is less than the decline, which is also related to the discharge current is greater than the charging current. Figure 5.4.4 shows the temperature curve of the battery cell and surface. In the simulation, the ambient temperature is set to a fixed value of 303K.

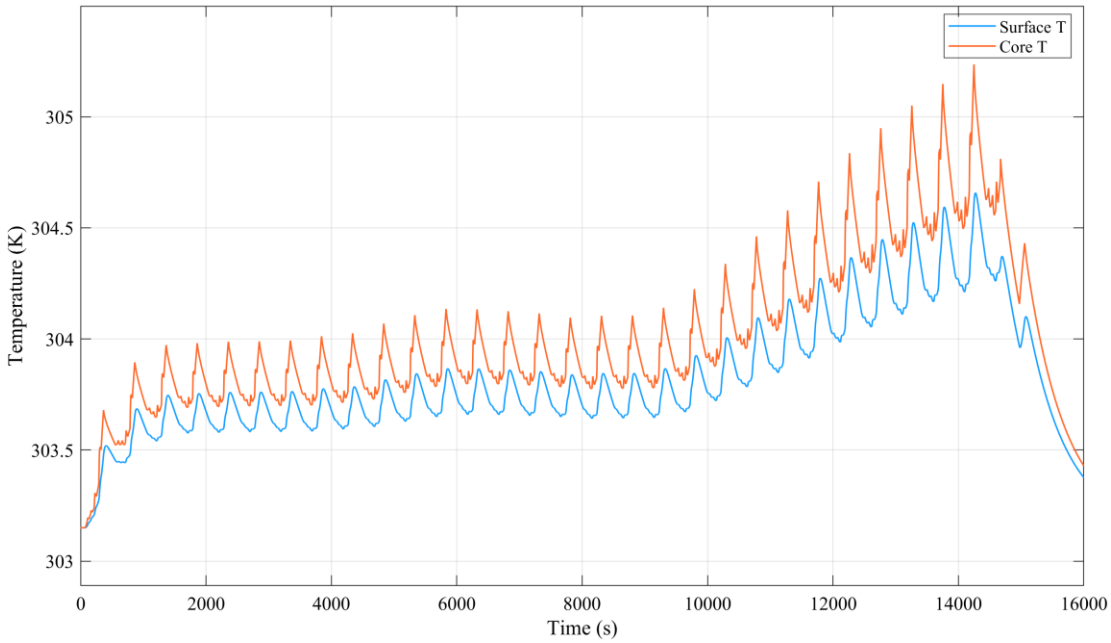

Figure 5.4.4 The surface and core temperature of battery over DST simulation

It can be seen from the figure that both core temperature and surface temperature

fluctuate and rise, especially in the latter half of the simulation, the internal resistance and reversible reaction heat of the battery show an increasing trend, resulting in increased heat production and intensified temperature rise of the battery at a lower soc. At the same time, there is a difference of 0.25K to 1K between the simulated core temperature and surface temperature. At low soc, the gap between the core and the surface temperature of the battery becomes larger, reaching about 1K. While look at ahead, the battery temperature experienced 16,000 seconds from the initial 303K to the final 305.2K. And the temperature change was very small, which was related to the small overall charge and discharge current value. It may be seen from Figure 5.4.2 that the current value was within 3A for most of the time in the simulation, so it is logical that the overall battery temperature changed little. To sum up, the change of battery temperature is mainly affected by high current charging and discharging state, and during the actual battery working process, people should focus on monitoring the change of temperature under the condition of high current.

5.5 Summary and comparison

In the previous sections, we selected commonly used automotive test cycles, including NEDC, WLTC, and DST. The ambient temperature was fixed at 303K (30 degrees). During the simulations, the battery soc varied from 1 to 0.1. In this section, we summarize the results and compare the maximum battery current and temperature variation amplitude across different test cycle simulations. The specific comparative information is presented in Table 5.5.1.

Table 5.5.1 The results comparison in different testing cycles

	NEDC	WLTC	DST
Speed range (km/h)	0-120	0-131.3	/
Maximum discharge current (A)	9.5	10	5
Maximum core T of battery (K)	308.3	312.8	305.3
Maximum surface T of battery (K)	306.9	310.0	304.6
Maximum ΔT between surface and core of battery (K)	1.4	2.8	0.7

Maximum ΔT between environment and core of battery (K)	5.3	9.8	2.3

From the table, it can be seen that the WLTC test cycle exhibits the largest range of vehicle speed variations, which results in the battery core temperature reaching 312.8K, the highest among the three different tests. The maximum difference between the core and surface temperatures is 2.8K, and the difference from the ambient temperature is 9.8K. In the NEDC simulation, the maximum core temperature of the battery is 308.3K, with a difference of 1.4K between the core and surface temperatures. The DST simulation shows the smallest current variation, with a maximum current of 5A. Consequently, the maximum core temperature of the battery in the DST test is lower than in the other two tests, at 305.3K, with a difference of 0.7K between the core and surface temperatures, and a difference of 2.3K from the ambient temperature. Therefore, the battery temperature variation is smallest during the DST cycle, whereas the WLTC cycle, which includes longer high-speed scenarios, leads to a more significant increase in battery temperature.

6 Conclusion

Battery management system plays an important role in electric vehicles. At the same time, the fast and efficient operation of BMS and the completion of its function purpose need to rely on accurate measurement and evaluation of the status of lithium batteries. Therefore, the more accurate the battery status evaluation is, the more the system function can ensure the reliability and safety of the vehicle, and the service life of the lithium battery can also be extended. At present, BMS takes the detection of battery status as the basic function of the system, but the prediction and evaluation of battery status require the help of a battery mathematical model. Therefore, this thesis studies the modelling and simulation of batteries' electrothermal characteristics. The main contents are as follows:

First, the research progress in the mathematical modelling and electrothermal characteristics estimation of lithium batteries was analyzed. It was found that accurate modelling and precise electrothermal characteristics estimation of batteries are of great significance. After reading many papers, the evaluation methods of the electrical and thermal characteristics of batteries were analyzed, and effective modelling methods were found to realize the estimation of the battery voltage, temperature and other parameters. This will become the basis for the following study.

Then the structure and chemical reaction principle of lithium batteries are introduced, the lithium battery model used in this article is explained, and the battery experimental data provided by professional laboratories are analyzed. The basic principles and processes of HPPC experiments are introduced to lay the foundation for subsequent modelling.

After consulting a lot of information, several popular electrical characteristic models were analyzed, including the white box model for direct modelling of chemical reactions, the black box model based on deep neural networks, and the grey box model for the physical relationship between voltage and current of battery cells. The analysis shows that the second-order RC equivalent circuit model has high accuracy and low computational complexity, and is more suitable for application in battery management systems. Finally, this thesis uses the second-order RC equivalent circuit model as the electrical characteristic model of the battery, and uses HPPC experimental data to identify the parameters in the model. At the same time, the model mentioned previously is established on the Matlab platform with updated identified parameters, and the simulation data is compared with the experimental data. It is found that the error value is basically maintained within 50mV. This shows that the accuracy of the electrical

characteristic model meets the requirements.

Then, the heat generation and heat dissipation mechanism of the battery was analyzed and studied. It was found that many factors need to be considered in real-world situations, and many parameters are difficult to obtain through the author's ability. Therefore, reasonable assumptions are made on the thermodynamic model of the battery, and finally the formula proposed by D.Bernardi et al. is used as the theoretical basis for the heat generation model. The heat dissipation model of the battery chooses to use a lumped parameter model. The lumped parameter model is based on the electrothermal similarity theory, which regards the heat generation source as an ideal current source, and the heat capacity and thermal resistance are analogous to capacitance and resistance respectively. In this way, the voltage value can be analogous to the temperature value. Due to the limited ability of the author, the parameters in the lumped parameter model are difficult to set through experience, so choose the parameters identified by other scientific research teams who use the same type of battery data.

Finally, a longitudinal motion model of the vehicle was established, and the previously established battery electrical and thermal characteristics models were integrated into the vehicle model, realizing the simulation of the battery terminal voltage, current, temperature and other data during the specific vehicle driving cycle (NEDC, WLTC, DST). Through simulation, it was found that there was a difference of 0 to 2K between the core temperature and the surface temperature of the battery, and the greater the discharge current, the greater the temperature difference. It was also found that at the end of the driving simulation, when the battery was at a lower soc, its heat generation rate increased, and the temperature reached a maximum value as the heat accumulated. Therefore, we need to pay special attention to the temperature change of the battery at high current and low soc condition. In summary, the entire electrothermal coupling model realizes the evaluation and prediction of data such as the terminal voltage and temperature of lithium-ion batteries, while ensuring accuracy and saving computing resources, providing a reference for the estimation and prediction of the battery status by the vehicle's BMS.

Reference

[1]. Shu H, He Y X. The Economic Analysis of Pure Electric Vehicle Replacement Scheme (In Chinese)[J]. Electric Power Science and Engineering, 2017,33(4):26-31.

[2]. Notter D A, Gauch M, Widmer R, et al. Contribution of li-ion batteries to the environmental impact of electric vehicles[J]. Environmental Science and Technology, 2010, 44(17): 6550-6556.

[3]. Xiong R. Core algorithm of power battery management system (In Chinese) [M].Beijing: China Machine Press, 2018.

[4]. Chen X D, Sun D. Research on Lithium-ion Battery Modeling and Model Parameter Identification Methods (In Chinese)[J]. Proceedings of the CSEE,2016,36(22):6254-6261.

[5]. https://zhuanlan.zhihu.com/p/401444472

[6]. Zou C, Hu X, Dey S, et al. Nonlinear Fractional-Order estimator with guaranteed robustness and stability for Lithium-Ion batteries[J]. IEEE Transactions on Industrial Electronics,2018,65(7):5951-5961.

[7]. Ren D S, Feng X N, Lu L G, et al. An Electrochemical-thermal Coupled Overcharge-to-thermal-runaway Model for Lithium-ion Battery[J]. Journal of Power Sources. 2017, 364: 328-340.

[8]. Jiang F C, Zhang F S, Xu C S, et al, Experimental Study on the Mechanism of Thermal Runaway Propagation in Lithium-ion Battery Pack for Electric Vehicles (In Chinese)[J]. Journal of Mechanical Engineering, 2021, 57(14): 23-31.

[9]. Yao M L, Gan Y H, Liang J L, et al. Performance Simulation of a Heat Pipe and Refrigerant-based Lithium-ion Battery Thermal Management System Coupled with Electric Vehicle Air-conditioning[J]. Applied Thermal Engineering, 2021, 191: 116878.

[10]. Dubarry M, Liaw BY. Development of a universal modeling tool for rechargeable lithium batteries[J]. Journal of Power Sources, 2007, 174 (2): 856-860.

[11]. Andred, Meiler M, Steiner K, et al. Characterization of high-power lithium-ion batteries by electrochemical Impedance spectroscopy. I. Experimental investigation[J]. Journal of Power Sources, 2011, 196 (12): 5334-5341.

[12]. Tian N, Wang Y, Chen J, et al. One-shot parameter identification of the Thevenin’s model for batteries: Methods and validation[J]. Journal of Energy Storage,2020,29:101282.

[13]. United States Idaho National Engineering & Environmental Laboratory,

Freedom CAR Battery Test Manual for Power Assist Hybrid Electric Vehicles, http://avt.inel.gov/battery/pdf/freedomcar_manual_04_15_03.pdf (2003).

[14]. Jin F; Yongling H; Guofu W. Comparison Study of Equivalent Circuit Model of Li-Ion Battery for Electrical Vehicles. Res. J.App l. Sci. Eng. Technol. 2013, 6, 3756–3759.

[15]. Feng T, Yang L, Zhao X, et al. Online identification of lithium-ion battery parameters based on an improved equivalent-circuit model and its implementation on battery state-of-power prediction[J]. Journal of Power Sources,2015,281:192-203.

[16]. Qian N, Yan Y B, Li W J, et al, Improving of Thevenin equivalent model for lithium iron phosphate Li-ion battery (In Chinses) [J]. Battery bimonthly, 2018, 48(4): 5.

[17]. Ding X F, Zhang D H, Cheng J W, et al. An improved Thevenin Model of Lithium-ion Battery with High Accuracy for Electric Vehicles[J]. Applied Energy, 2019, 254(15): 113615.

[18]. Dang X, Yan L, Xu K, et al. Open circuit voltage based state of charge estimation of lithium-ion battery using dual neural network fusion battery model[J]. Electrochimica Acta, 2016,188:356-366.

[19]. Wang Q K, He Y J, Shen J N, et al. A unified modeling framework for lithium-ion batteries: An artificial neural network based thermal coupled equivalent circuit model approach[J]. Energy, 2017, 138: 118-132

[20]. Li S, He H, Li J. Big data driven lithium-ion battery modeling method based on SDAE-ELM algorithm and data pre-processing technology [J] .Applied Energy, 2019, 242: 1259-1273.

[21]. Andred, Meiler M, Steiner K, et al. Characterization of high-power lithium-ion batteries by electrochemical impedance spectroscopy. II: Modelling [J]. Journal of Power Sources, 2011, 196 (12): 5349-5356.

[22]. Newman J, Tiedemann W. Porous-electrode theory with battery applications[J]. AIChE Journal, 1974, 21 (1):25-41.

[23]. Fuller T F, Doyle M, Newman J. Simulation and optimization of the dual lithium ion insertion cell [J]. Journal of the Electrochemical Society, 1993, 141 (1): 1-10.

[24]. Wang C Y, Gu W B, Liaw B Y. Micro-macroscopic coupled modeling of batteries and fuel cells: I. model development [J]. Journal of the Electrochemical Society, 1998, 145(10): 3407-3417.

[25]. Ning G, Popov B N. Cycle life modeling of lithium-ion batteries[J]. Journal of the Electrochemical Society, 2004,151 (10): A1584.

[26]. Bernardi D, Pawlikowski E, Newman J. A general energy balance for battery

systems[J]. Journal of the Electrochemical Society, 1985, 132 (1): 5-12.

[27]. Forgez C, Do D V, Friedrich G, et al. Thermal modeling of a cylindrical LiFePO4/Graphite lithium-ion battery[J]. Journal of Power Sources, 2010, 195 (9): 2961-2968.

[28]. Allafi W, Zhang C, Uddin K, et al. A lumped thermal model of lithium-ion battery cells considering radiative heat transfer[J]. Applied Thermal Engineering, 2018, 143:472-481.

[29]. Richardson R R, Zhao S, Howey D A. On-board monitoring of 2-D spatially-resolved temperatures in cylindrical lithium-ion batteries: Part I. Low-order thermal modelling[J]. Journal of Power Sources, 2016, 326: 377-388

[30]. Pan D, Guo H J, Tang S Q, et al. Evaluating the Accuracy of Electro-thermal Coupling Model in Lithium-ion Battery Via Altering Internal Resistance Acquisition Methods[J]. Journal of Power Sources, 2020, 463: 228174.

[31]. Chen M. B., Bai F. F., Song W. J., et al. A Multilayer Electro-thermal Model of Pouch Battery During Normal Discharge and Internal Short Circuit Process[J]. Applied Thermal Engineering, 2017, 120: 506-516.

[32]. A Review of Lithium-Ion Battery Fire Suppression - Scientific Figure on ResearchGate. Available from: https://www.researchgate.net/figure/The-principle-of-the-lithium-ion-battery-LiB-showing-the-intercalation-of-lithium-ions_fig1_344448023

[33]. Application Study on the Dynamic Programming Algorithm for Energy Management of Plug-in Hybrid Electric Vehicles - Scientific Figure on ResearchGate. Available from: https://www.researchgate.net/figure/The-Rint-battery-model_fig6_276177314

[34]. Overviewing Quality of Electric Vehicle Charging Stations' Service Evaluation Scientific Figure on ResearchGate. Available from: https://www.researchgate.net/figure/Thevenin-equivalent-model-of-battery-33_fig3_325286105

[35]. Classification of Electric modelling and Characterization methods of lithium ion batteries for vehicle applications - Scientific Figure on ResearchGate. Available from: https://www.researchgate.net/figure/Schematic-representation-of-the-PNGV-model_fig6_302964276

[36]. Study on the Characteristics of a High Capacity Nickel Manganese Cobalt Oxide (NMC) Lithium-Ion Battery An Experimental Investigation Scientific Figure on ResearchGate. Available from: https://www.researchgate.net/figure/2RC-circuit-battery-model_fig1_327310441

[37]. Kollmeyer, Philip; Vidal, Carlos; Naguib, Mina; Skells, Michael (2020), “LG 18650HG2 Li-ion Battery Data and Example Deep Neural Network xEV SOC

Estimator Script", Mendeley Data, V3, doi: 10.17632/cp3473x7xv.3

[38]. Bernardi D., Pawlikowski E., Newman J.. A General Energy Balance for Battery Systems[J]. Journal of The Electrochemical Society, 1985, 132(1): 5-12.

[39]. Kuai Y H, Electrothermal Coupling Modeling and Multi-state Joint Estimation for Lithium-ion Battery(in Chinese)[D]. Shangdong University, China, 2023.

[40]. Wu C, Sehab R, Akrad A, Morel C. Fault Diagnosis Methods and Fault Tolerant Control Strategies for the Electric Vehicle Powertrains. Energies. 2022; 15(13):4840

[41]. Advance in lithium-ion batteries: an overview - Scientific Figure on ResearchGate. Available from: https://www.researchgate.net/figure/The-comparison-plots-of-LIBs_fig3_37814213